Generalized Mathematical Modelling of a Novel Singularity-free Class of Six Degrees of Freedom Motion Platform

by

Abraham Weiss

B.Sc. - Technion - Israel Institute of Technology, 1990

B.A. - Open University, Israel, 1996

M.S. - University of Alabama, 2004

A thesis submitted to

the Faculty of Graduate and Postdoctoral Affairs

in partial fulfillment of

the requirements for the degree of

Doctor of Philosophy

Ottawa-Carleton Institute for

Mechanical and Aerospace Engineering

Department of

Mechanical and Aerospace Engineering

Carleton University

Ottawa, Ontario

November 2, 2010

The undersigned recommend to

the Faculty of Graduate Studies and Research

acceptance of the thesis

Generalized Mathematical Modelling of a Novel Singularity-free Class of Six Degrees of Freedom Motion Platform

submitted by **Abraham Weiss**

in partial fulfillment of the requirements for

the degree of Doctor of Philosophy

Dr. M.J.D. Hayes
Thesis Supervisor

Dr. R.G. Langlois
Thesis Supervisor

Dr. M.I. Yaras
Chair, Department of
Mechanical and Aerospace Engineering

Carleton University

November 2, 2010

Abstract

The current state-of-the-art simulation motion platforms are based on parallel manipulators known as Gough-Stewart platforms or hexapods. These have limited motion range in both translational and angular senses, and are subject to singularities. An alternative novel kinematic architecture, the Atlas platform, has been developed at Carleton University. The Atlas platform achieves six degree of freedom motion by mounting the Atlas spherical platform on top of an XYZ translation platform. The Atlas rotational stage comprises a sphere manipulated by three omnidirectional wheels. Each wheel imparts a prescribed velocity to the sphere through friction enabling it to rotate about any desired axis with unlimited angular displacement. This thesis investigates four main issues including: unified and generalized kinematics of a sphere actuated by n omnidirectional wheels; the dynamics of a sphere actuated by omnidirectional wheels; vibration induced by omnidirectional wheels on an actuated sphere; and a comparison between classes of omnidirectional wheels in the context of the Atlas platform.

The kinematic model for the system was derived using a zero-slip approach yielding a basic Jacobian. The model was then generalized to include any number and type of omnidirectional wheels treating the various wheel designs as geometric classes. Results show non-negligible corrections in both magnitude and direction of the resulting angular motion of the sphere. The equations of motion for the system were obtained taking into account several non-rigid effects. The non-smooth shape of the wheels was taken as a positional input for vibration analysis. Comparison between omnidirectional wheel types was made from the standpoint of vibration and transmission efficiency, with mixed results, using a numerical integration program developed in Matlab. The program, developed with numerical simulation in mind, was then used to investigate the effects of various parameters on the behaviour of the platform. Thus, it is parameterized to enable further research on various design parameters.

Acknowledgements

This work could not have been done without the support of several dear people whom I would like to acknowledge.

First and foremost, I would like to thank the loveliest of all, my wife Rissella, who was the reason I have pursued this degree to start with, and who will never be able to see or hear about another wheel in this lifetime. I would like to thank Yarden, Libby, and Eliad, my beloved children who had to suffer through my short attention span having seen my mind wandering off to other directions instead of where it should have been. May they one day read this thesis.

I am grateful to my parents who encouraged me and gave me the gift of learning throughout the years.

I want to acknowledge funding received through a NSERC PGS D scholarship, as well as funding from OGS and Carleton University.

Last but not least I would like to thank my two supervisors Prof. John Hayes, and Prof. Rob Langlois, who gave their time, patience, and expertise so that I would develop an understanding of the subject, and would be able to complete the work presented here.

List of Symbols

a_i	Radius of contact patch at contact point i
c_i	Effective damping coefficient of omnidirectional wheel i mounting
C_i	Effective spring coefficient of contact point i
E_s	Elastic modulus of the sphere
E_{w_i}	Elastic modulus of omnidirectional wheel i
E_i'	Equivalent elastic modulus of contact point i
$\vec{f_i}$	Friction force at contact point i
$\vec{F}_{ext}$	Total applied external force
$[I_s]$	Inertia tensor of sphere
$[I_w]$	Diagonal matrix with moments of inertia of the omnidirectional wheels
J	Jacobian Matrix
k_i	Effective spring coefficient of omnidirectional wheel i mounting
K_i	Effective spring coefficient of contact point i
K'	Effective spring coefficient of kinematic closure mounting
$\vec{l}_{r_i}$	Rolling resistance moment arm at contact point i
$\vec{l}_{s_i}$	Spin resistance moment arm at contact point i
m_i	Mass of omnidirectional wheel i
M_l	mass of linear platform
M_s	Mass of sphere
M_T	Total mass of the system
n	Number of Omnidirectional Wheels
$\vec{N_i}$	Normal force at contact point i
p_i	Pressure distribution at contact point i
$\vec{P}$	Translational platform driving force

q	Unit Quaternion Describing the Orientation of the Sphere
r_{b_i}	Base radius of omnidirectional wheel i
r_r	Radius of omnidirectional wheel's rollers
r_{w_i}	Radius of Omnidirectional Wheel i
$[r_w]$	Matrix with $\hat{r}_{w_i}$ as its columns
R	Radius of the Sphere
$\vec{R}_i$	Position Vector of Contact Point i
$\hat{R}_i$	Unit Vector in the Direction of Contact Point i
$[R_i]$	Matrix with $\hat{R}_i$ as its columns
$\vec{R}_l$	Position vector of translation platform
$\vec{R}_s$	Position vector of centre of sphere
R'_i	Equivalent radius at contact point i
S	Slip Assessment Indicator
S_i	Slip Ratio at Contact Point i
S_{a_i}	Linear Motion Parameter at Contact Point i
S_{b_i}	Linear Motion Parameter at Contact Point i
S_{c_i}	Linear Motion Parameter at Contact Point i
S_{d_i}	Linear Motion Parameter at Contact Point i
$\{T\}$	Column matrix of the omnidirectional wheels driving moments
$\vec{T}_{r_i}$	Rolling resistance at contact point i
$\vec{T}_{s_i}$	Spin resistance at contact point i
$[v]$	Matrix with $\hat{v}_i$ as its columns
$\hat{v}_i$	Unit Vector in the Actuation Direction at Contact Point i
$\hat{v}_{r_i}$	Unit Vector in the Free-Roll Direction at Contact Point i
$\vec{V}_i$	Velocity Induced by Omnidirectional Wheel i
$\vec{V}'_i$	Velocity of the Sphere at Contact Point i

δ_i	Deflection at contact point i
Δ_i	Deflection of omnidirectional wheel i at mounting point
η_i	Roundness ratio of omnidirectional wheel i
θ_{b_i}	Angular width of rollers of omnidirectional wheel i
θ_i	Orientation of omnidirectional wheel i
θ_{R_i}	Angular gap between rollers of omnidirectional wheel i
θ_{s_i}	Angular cycle between two rollers of omnidirectional wheel i
ι	Equivalent transfer ratio
κ	Maximal magnitude ratio
$[\mu]$	Matrix with mu_i at its diagonal
μ_i	Friction coefficient at contact point i
ν_s	Poisson ratio of the sphere
ν_{w_i}	Poisson ratio of omnidirectional wheel i
ξ	Transmission effectiveness
ω_n	Natural frequency
ω_i	Angular Speed of Omnidirectional Wheel i
$\vec{\Omega}$	Angular velocity vector of the sphere
$\hat{\Omega}_i$	Unit Induced Angular velocity by omnidirectional wheel i
$[\Omega]$	Matrix with $\hat{\Omega}_i$ as its columns

Contents

List of Figures

List of Tables

Chapter 1

Introduction

1.1 Overview

Conventional training simulator motion platforms commonly use a Gough-Stewart platform [1, 2], otherwise known as a hexapod, to provide motion cues. A hexapod is a mechanical system with six extensible legs in parallel connecting a moving platform to a relatively fixed base. Positions and orientations of the moving platform are manipulated with six degrees of freedom (6 DOF) by changing the lengths of the six prismatic legs. Figure 1.1 shows a typical example. Various configurations based on this architecture exist, and will be reviewed later in the literature review. These designs all attempt to expand the workspace of the manipulator, and to reduce singularities within the workspace. The reason for the limits and some singularities of the workspace of the parallel manipulators lies in the hardware limits of this type of motion platform; however, there are other areas that require improvement. These areas have to do mostly with the complicated kinematics of such platforms. The kinematics expressions are mathematically complex, and in most cases, require numerical solutions. In addition, the translational and rotational degrees-of-freedom are heavily coupled, a fact that further increases the complexity of the equations, and consequently increases the resources

Figure 1.1: CAE's version of a Gough-Stewart motion platform for a flight simulator [3].

required to evaluate them.

1.2 The Atlas Platform

The idea suggested and implemented in the Atlas platform aims to resolve all the aforementioned issues; namely, remove singularities from the interior of the reachable workspace, remove the rotational limits, and decouple the rotational and translational degrees-of-freedom. The new platform is broken down into two different mechanisms sitting one on top of the other; a translational platform and a rotational platform, as shown in Figure 1.2. The first is a simple, well-known, XYZ platform. The latter is a novel design, where a sphere rests on three wheels, and motion is provided with friction at the sphere-wheel interface. Different linear combinations of angular speeds of the wheels yield different angular velocity vectors for the sphere. This suggested new platform has the potential, under certain conditions

that need to be precisely defined, to open the workspace to become rotationally unlimited while eliminating interior singularities. Other benefits that can be derived from this design are the decoupling of the rotational degrees-of-freedom from the translational ones, and the compact analytical expressions resulting for the kinematics of the system. Friction wheels, while offering unlimited range of motion, resist motion in the direction normal to their rotation axis. Instead, omnidirectional wheels with free spinning passive castor rollers on their periphery, that minimize the resisting friction in the directions normal to their rotation, are used. Various omnidirectional wheel designs exist, each with its respective pros and cons discussed in more detail in Section 1.3.3.

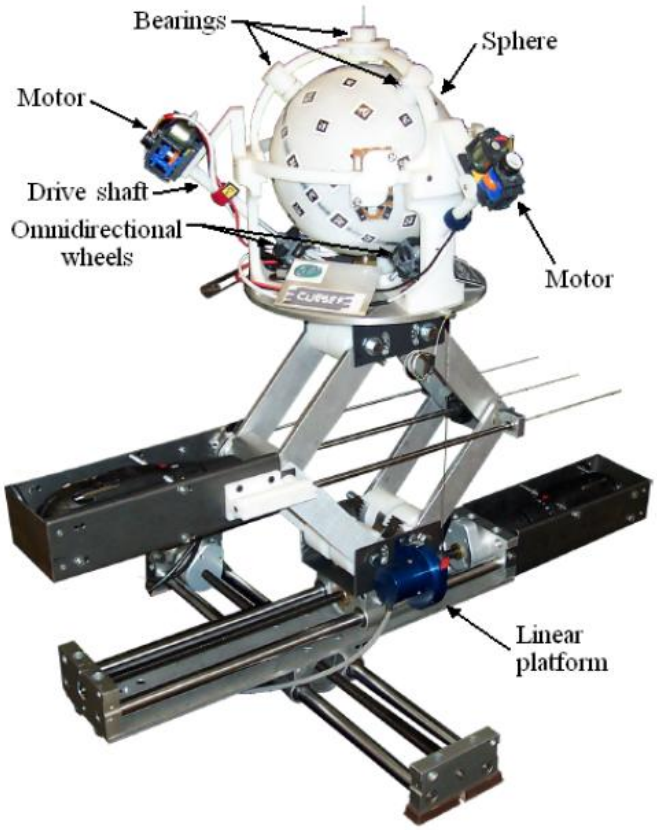

Figure 1.2: The Atlas demonstrator.

The original Atlas rotational stage shown in Figure 1.3 comprises a sphere mounted on

three dual-race omnidirectional wheels having contact points at the vertices of an equilateral triangle at an elevation angle of 40°. A generalization of the Atlas sphere idea is to have the omnidirectional wheels located at any position relative to the sphere. Omnidirectional wheels are wheels that have rollers on their periphery, which are free to rotate about an axis which is not parallel to the omnidirectional wheel primary rotation axis but is on a plane tangent to the wheel's perimeter. An example of an omnidirectional wheel is shown in Figure 1.4. These wheels may be actuated about their axis; thus providing tractive force at their contact point in the plane of the wheel. In its most intuitive form, combining three orthogonally-arranged omnidirectional wheels, enables actuation of the Atlas sphere about three orthogonal axes, each omnidirectional wheel acting like a friction wheel only in its actuation direction but without resisting motion in the transverse direction, unlike friction wheels. Proof of concept platforms have been constructed by the Carleton University Simulator Project (CUSP) team, and it has been shown qualitatively that the actuation method is feasible. However, to be able to put this conceptual design to practical use, a comprehensive understanding of the kinematics and dynamics of the platform must be achieved as well as overcoming engineering issues related to vibration and performance, such that an optimal platform, with respect to specific application design parameters, can be achieved.

1.3 Literature Review

To obtain a better background to the work presented in the thesis, a literature review of existing motion platforms was performed. In addition, since the suggested solution involves the interaction between a sphere and omnidirectional wheels, a survey of existing published work on the motion of a sphere and on omnidirectional wheel designs and applications followed. Finally, a survey of kinematic and dynamic formulations and methods was conducted as preliminary work to the development of the kinematics and dynamics of the suggested

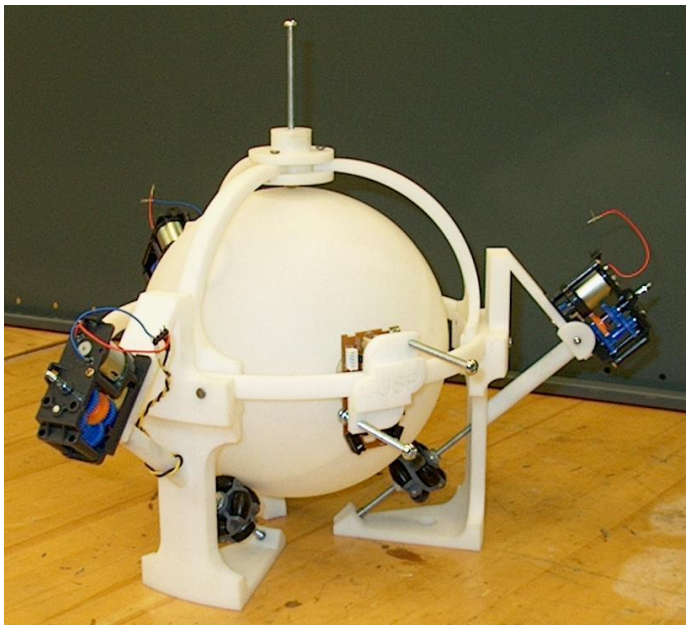

Figure 1.3: Atlas orientation platform.

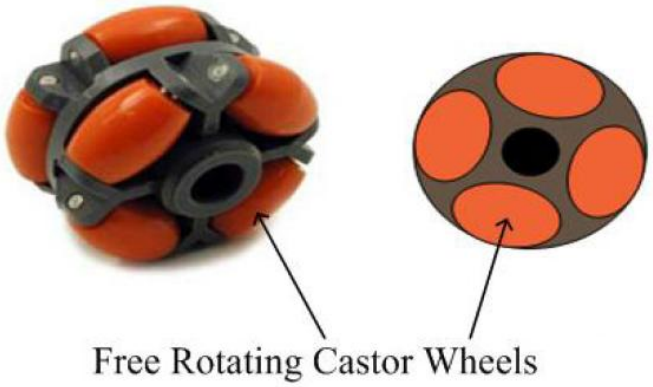

Figure 1.4: Example of an omnidirectional wheel.

platform. Thus, the literature review covers the following topics:

- motion platforms;
- motion of a sphere;
- omnidirectional wheels;
- kinematics; and
- dynamics.

1.3.1 On Holonomic Systems

The term 'holonomic' is used to describe the kinematic level of controllability of a mechanical system. Mathematically, a holonomic system is defined as one in which all constraints depend only on position coordinates and not on velocities. Another approach for looking at a holonomic system is one where the number of controllable degrees-of-freedom is equal to the total number of degrees-of-freedom. It is noted hereby that in this thesis the term 'holonomic' relates to the latter definition. That is, a holonomic system is one where the number of controllable degrees-of-freedom is equal to the total number of degrees-of-freedom.

1.3.2 Motion Platforms

Existing motion platform designs may be clearly divided into three categories: parallel manipulators, serial manipulators, and newer ideas that essentially recognize the inherent flaws of the more traditional designs and try new approaches to improve the performance of motion platforms.

Parallel Manipulators

Parallel manipulators are closed-loop mechanisms with the ability to accurately manipulate large loads. The current state-of-the-art in motion platforms, mentioned in Section 1.1, includes parallel manipulators known as Gough-Stewart platforms [1, 2], sometimes referred to as hexapods. Thorough analysis and synthesis of such systems is presented by Merlet [6], and a vast survey of the kinematics and design of parallel manipulators in flight simulator applications is presented by Advani [7]. A popular research direction in this field of parallel manipulators is dealing with various designs of the legs constraining the platforms. Research has considered variations that change the joint types and geometry of the legs, or the actuated joints, or both; see for example Hunt [8] and McCallion [9]. All these designs, in addition to having limited range of motion, also have their translational and rotational degrees-of-freedom coupled, i.e. their actuators influence both translation and rotation, or, alternatively stated, a single actuator impacts more than a single degree-of-freedom. From the standpoint of control, it is preferable to have a motion platform where three actuators control translation, and three other actuators control rotation independently. Such designs exist, still utilizing the hexapod configuration. Innocenti's approach [10], shown in Figure 1.5, has three links that share a common ball and socket joint, where controlling the lengths of the links determines the position of the centre of the joint without rotating the platform, and controlling the lengths of the three remaining legs determines the orientation of the platform.

A similar approach with slightly different implementation is presented by Bernier [11]. Another approach, suggested by Uchiyama [12], changes the configuration of the legs themselves, where some of the legs have only revolute joints such that some of the legs are controlled by changing their length and others by actuating a revolute joint to achieve decoupling of the translational and rotational degrees-of-freedom. Some variations of the concept exist,

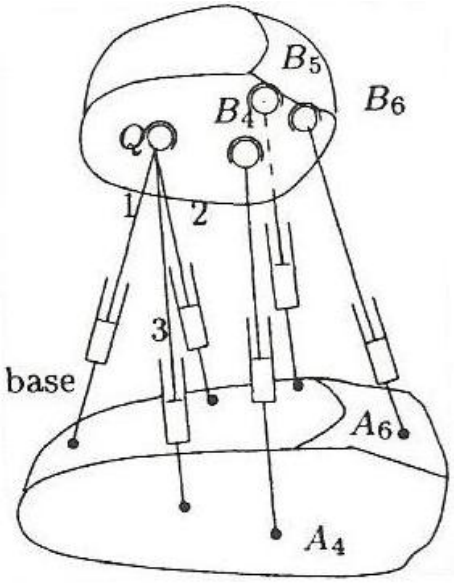

Figure 1.5: Decoupled translation and orientation in a hexapod configuration [10].

as presented by Zlatanov [13], Mianowski [14], and others. Although these platforms succeed in decoupling the translational degrees-of-freedom from the rotational ones, the limited range of motion issue remains.

Serial Manipulators

Since serial manipulators have a single point of contact with the payload, they are not as limiting as parallel manipulators from the standpoint of workspace and singularities. However, their major flaw, and the main reason why parallel manipulators are still dominating the motion platform market, is their payload to manipulator weight ratio. Because of the cantilever loading of the individual links, serial manipulators have a small payload to manipulator weight ratio compared to parallel manipulators of similar weight. The typical serial manipulator with 6 degrees-of-freedom has a payload to manipulator weight ratio of less than 1/10 to manipulate a mass [6]. This means that it takes a 10 ton manipulator to manipulate a 1 ton payload. Research in this field tries to improve this ratio.

Newer Ideas

Some ideas that are different from the traditional parallel or serial manipulators have recently appeared. One of these motion platform types may be classified as the hybrid type. That usually means placing a serial 3 DOF manipulator on top of a parallel 3 DOF manipulator. Such examples may be seen in [15, 16, 17] to name a few. These usually possess compromised performance between the serial manipulator and the parallel manipulator.

An interesting hybrid mobile robot is suggested by Moosavian [18] to allow handling heavy objects on a moving platform, having a serial arm mounted on a planar parallel platform. Some other attempts have been made to resolve some of the aforementioned issues. Yan et al. [19] suggest a platform that decouples the translational degrees-of-freedom from the rotational ones. This architecture relies on three actuators, each controlling two degrees-of-freedom - one translational and one rotational, where each leg has two prismatic and two rotational joints, all of which are passive as presented in Figure 1.6. However, singularities within the workspace, limited payload capacity, as well as a limited range of angular motion result.

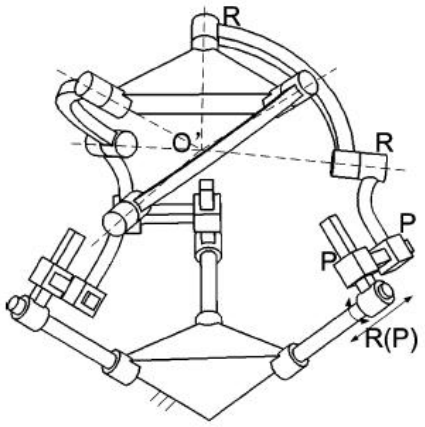

Figure 1.6: Decoupled translation and orientation through compound legs [19].

Unbounded rotational motion is achieved by the Eclipse II architecture [20], which is

essentially an active gimbal system. However, it is not singularity free and the kinematics are very complicated and require numerical solutions. A similar commercial platform is the Desdemona [21], which has a fully gimballed cabin for essentially unlimited angular motion on top of a 3 DOF system comprising two linear degrees-of-freedom and another rotational degree-of-freedom. Thus the rotational and translational motions are still coupled.

1.3.3 Motion of a Sphere

Since the Atlas platform is essentially a sphere actuated by omnidirectional wheels, it is a worthwhile activity to research the domain of actuated spheres. Generally, there are two applications for actuated spheres. These are joints and wheels for robotic applications. In the vast majority of cases, the sphere is utilized such that it is actuated only about a single axis while allowing passive degrees-of-freedom in the other directions. An interesting approach is used by Ferriere and Raucent [22], where a sphere is actuated for a single degree-of-freedom by means of a single omnidirectional wheel. Three such wheels may be utilized to drive a wheeled mobile robot in a holonomic fashion. Another idea involving actuation of a mobile robot using spheres is presented in [23], where a sphere is actuated using passive rollers mounted on an actuated ring. Again, the sphere is actuated only in one direction, where the benefit of using the sphere is for the free rolling in the non-actuated directions.

A similar application is described by West et al. [24] who show how to use a ball wheel for single degree-of-freedom actuation with the remaining degrees-of-freedom passive such that there is no slip. Three such ball wheels may be utilized similarly to omnidirectional wheels with rollers on their periphery to drive a wheeled mobile robot on a plane.

Two degrees-of-freedom are accomplished by Lauwers et al. [25] utilizing friction wheels to drive a single sphere for a very interesting single-sphere mobile robot, balanced by a pendulum. However, there are major losses in the system due to the use of simple friction

wheels rather than omnidirectional wheels. Attempting to obtain spherical motion is not only the domain of pure mechanical engineering mechanisms, but rather electromagnetic-based motion has also been considered. Such ideas were developed by Chirikjian et al. [26, 27] and Lee et al. [28], to name a few.

1.3.4 Omnidirectional Wheels

The majority of the research and development in the area of omnidirectional wheel actuation focuses on mobile robots. That is, the actuation of the robotic platform on a plane, taking advantage of the omnidirectional wheels to eliminate singularities in the workspace of the mobile robot and to achieve the ability to change direction with zero turning radius. Omnidirectional wheels are wheels that may be actuated in one direction, while allowing two passive degrees-of-freedom. These are the free spinning of the castor roller about its axis, and unconstrained rotation about an axis perpendicular to the point of contact. There are quite a few designs for omnidirectional wheels, and a few major applications for them that are explored in what follows.

Omnidirectional Wheel Design

The basic design of omnidirectional wheels is such that there are rollers around the periphery of the wheel. The axis of rotation of the rollers may be perpendicular to the axis of rotation of the wheel, as in a standard omnidirectional wheel, or at another angle. When the angle is $\pm 45^\circ$, the wheel is called a Mecanum wheel (or Swedish wheel). Regardless of the angle, all of these designs possess a basic inherent flaw: there must be gaps between the rollers, such that there may be either loss of contact, contact with a non-rolling structural surface, and vibration on the transition between rollers. Some attempts to resolve these problems are focused on adding races of rollers that interlace such that there is always contact with a

roller, though the contact point may change. Others attempt to minimize and smooth the gap as much as possible. An alternative approach is to use spherical omnidirectional wheels [22, 24].

A few attempts to solve the vibration issues caused by the inherent discontinuity of the omnidirectional wheel rollers were attempted starting with Mecanum-type wheels shown in Figure 1.7 [29]. An interesting feature of Mecanum wheels with an offset angle of $\pm 45^\circ$ is that they can generate motion normal to the rotation direction of the wheels, see for example Viboonchaicheep [30], Han [31], and Diegel et al. [32] for an alternate version of the Mecanum wheels idea.

Another attempt at solving the vibration issue is a double wheel drive, which maintains continuous contact, but changes the point of contact [22]. Another solution that utilizes the idea of the double wheel drive while eliminating the problem of a changing point of contact by decoupling the two omnidirectional wheels by means of two offset wheels that are not mounted on the same axis, is proposed. Instead, they are mounted on parallel axes, maintaining the offset between the rollers and being driven by a single actuator (Figure 1.8). That way, continuous contact is maintained, while the point of contact, although not the same, is on the same great circle, leading to decreased vibrations.

Finally, a solution that appears to be most promising, utilizes rollers that are of different diameters, which allows construction of an omnidirectional wheel that maintains continuous contact and does not change the point of contact, as suggested by Song et al. [33] (Figure 1.9).

Omnidirectional Wheel Applications

Most of the research involving omnidirectional wheels concentrates on wheeled mobile robots, where an extensive amount of literature already exists for the kinematics of mobile robots with standard wheels (see Alexander et al. [34], Low et al. [35] to name a few), and offset

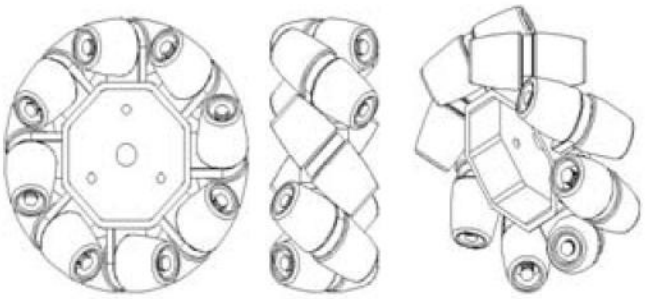

Figure 1.7: Mecanum-type wheel [29].

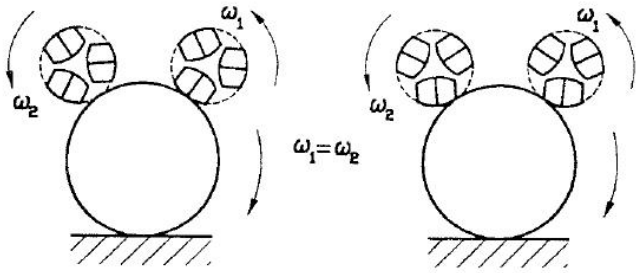

Figure 1.8: Two offset wheels mounted on different axes [22].

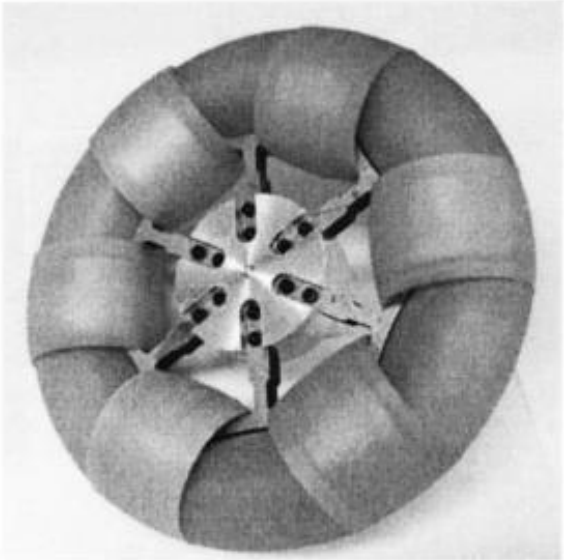

Figure 1.9: Continuous contact through variable diameter rollers [33].

castor wheels (see Yu et al. [36]). The work of West et al. [24] shows how to use a ball wheel for single DOF actuation with the remaining degrees-of-freedom passive such that there is no slip. Three such ball wheels may be utilized similarly to omnidirectional wheels with rollers on their periphery to drive a wheeled mobile robot on a plane. Similarly, Williams et al. [37], and Saha et al. [38] use three omnidirectional wheels to drive a mobile robot or vehicle on a plane.

Several configurations have been considered for omnidirectional mobile robots. A triangular configuration, where three omnidirectional wheels are located on the points of a triangle is considered in two identical papers [39, 40], as well as [37]. More exotic configurations include one where a chain-like construction is suggested for a crawler type mobile robot, and a six-wheel combination [42]. These are all examples of various omnidirectional wheel configurations for mobile robots moving on a flat surface. Other applications of omnidirectional wheels exist. In one case omnidirectional wheels are used for an odometer, where the free rolling is allowing another passive degree-of-freedom rather than actuating anything [43]. In [41], which is another variation on the application of omnidirectional wheels for actuation of mobile robots on a flat surface, four omnidirectional wheels are aligned on the four sides of a square, instead of the more common triangular setting where three omnidirectional wheels are set up on the three sides of an equilateral triangle.

In the case of the Atlas platform, the final arrangement of the driving omnidirectional wheels has not yet been optimized. In addition, despite the fact that different arrangements have been considered for the mobile robot case, there exists no publicly available research on optimization of the omnidirectional wheel arrangement from the standpoint of the number and relative positions of the wheels under any criterion.

Mecanum Wheels

As mentioned earlier, Mecanum wheels, where the rollers have a $\pm 45^{\circ}$ angle, are designed to generate smoother continuous contact. This however is a side effect of the original concept that allows a four-wheeled platform to have pure translational motion in the transverse direction [44]. Utilizing four Mecanum wheels, a ground vehicle becomes holonomic, and is capable of translating in any direction, as well as rotating as shown in Figure 1.10.

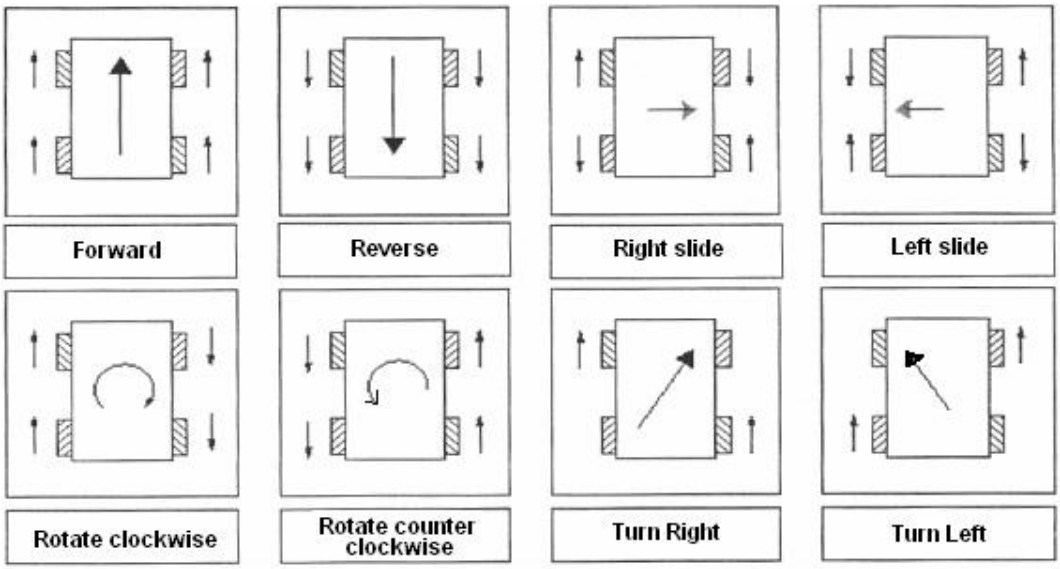

Figure 1.10: Mobile robot with Mecanum wheels motion examples [45].

The geometry and kinematics of a Mecanum wheel are investigated by Gfrerrer [46] with the emphasis on the effects of manufacturing, and wheel and rollers design. The single use of Mecanum wheels in the literature is in the field of mobile robotics, as presented earlier. The basic kinematics of such a mobile robot with four omnidirectional wheels is presented in [30]. Tlale et al. [47] add the treatment of dynamics and Shimada et al. [48] treat control issues for a similar four-wheeled robot.

Some published applications of such four-wheeled mobile robots include a robot for mobile haptic interface [31], and a floor cleaning robot [49, 50] among others. Indiveri [51] generalizes

the kinematics of mobile robots with Mecanum wheels to robots with n Mecanum wheels, with special attention given to the most basic configuration where $n = 3$. The latter is the single published paper on the kinematics of mobile robots with omnidirectional or Mecanum wheels where a generalization of the problem is treated.

1.3.5 Kinematics

Kinematics of the system means the relation between the motion inputs and motion outputs of the system; specifically, the relationship between the velocities of the actuators and velocities (translational and rotational) of the motion platform. The majority of the problems mentioned for existing motion platforms, are kinematic in nature. Workspace singularities, limited ranges of motion, coupling of the translational and rotational degrees-of-freedom, and computational complexity are all due to the kinematic architecture of these systems, and subsequently their kinematics.

While a generalized approach to finding the instantaneous screw based on velocities of three points on a rigid body exists [52, 53], it requires perfect knowledge of these velocities, i.e. three components of the velocity for each given point. Here, only two components of the velocity per contact point are known, namely the actuation direction and the zero-velocity in the radial direction of the sphere. Hence, the approach in [52, 53] may not be utilized as presented.

Since the Altas platform is actuated using a friction mechanism, avoiding slip at the contact points is essential to the design. While slip commonly is the result of kinetic considerations, attention must be paid to the existence of slip for kinematic reasons. That is, some kinematic configurations would result in slip at the contact points no matter what the forces and friction coefficients were. Prior to considering slip due to kinetic considerations, lack of kinematic slip is a necessary condition.

Three related fields; namely motion platforms, wheeled mobile robots, and wheeled mobile robots with omnidirectional wheels will be surveyed here. While the reason for surveying motion platform kinematics is obvious, the other two fields have to consider kinematic slip in the kinematic analysis and therefore were researched and presented here.

One basic goal of this thesis is generalization of the Atlas kinematics for application to optimization. Kinematic design optimization is the concern of many research publications, such as Stock et al. [54], Fattah et al. [55] for cable suspended platforms, and Merlet [56], to name a few.

Motion Platforms

While the kinematics of serial platforms have accepted methods and closed form solutions generated using the Denavit-Hartenberg formulation [57], kinematics of parallel motion platforms have more complex formulations [58] that usually require numerical solutions to be resolved due to the existence of multiple closed-loop kinematic chains unless the workspace is planar [59]. Most other references to kinematic architecture of motion platforms deal with parallel manipulators [6], specifically the Gough-Stewart platform, which has the inherent limitation of range of angular motion. Comprehensive survey of kinematic architectures of flight simulation motion platforms with emphasis on Gough-Stewart platforms was performed by Advani [7] in his Ph.D. thesis, which underscores the fact that all the considered platforms were essentially parallel manipulators. Significant research on determining the workspace of parallel platforms also exists (see for example Gosselin [60]).

Wheeled Mobile Robots

Most wheeled mobile robots are nonholonomic systems with three or more wheels. A classification survey of such systems was performed by Campion et al. [61], which presents various configurations of wheeled mobile robots, including some omnidirectional ones, utilizing either

offset castor wheels or what they refer to as Swedish wheels, which are essentially referred to here as omnidirectional wheels.

Omnidirectional mobile robots utilizing conventional wheels also exist, sometimes referred to as pseudo-holonomic omnidirectional mobile robots, where essentially all wheels have control of their orientation without angular limits [62]. Another omnidirectional robot using conventional wheels with redundant actuation is presented and analyzed by Yi and Kim [63].

Wheeled Mobile Robots with Omnidirectional Wheels

More interesting are the kinematics of wheeled mobile robots with omnidirectional wheels, since these are holonomic vehicles and are closer in terms of approach and thus treatment to the problem of actuating a sphere using omnidirectional wheels than any of the previous applications. There is no generalized method for these applications, and each case is treated separately.

A triangular configuration, where three omnidirectional wheels are located on the points of a triangle is considered in [39] and [40] as mentioned earlier. Their approach is comparing the linear velocity vector of the platform and its rotation speed with the three velocity vectors induced by the omnidirectional wheels. A similar approach is taken by Angeles [52] for a similar configuration.

This basic three omnidirectional wheels in a triangular arrangement configuration is common also where research is geared more toward control and path planning as the basic holonomic mobile robot as opposed to the more standard nonholonomic configurations utilizing standard wheels, see for example Kanjanawanaishkul et al. [64]. This approach works for the specific case of a robot rolling on a plane having three omnidirectional wheels, in a specific configuration, but is not general. A square configuration is suggested in [41].

More exotic configurations include one where a chain-like construction is suggested for a crawler type mobile robot [42], and a six-wheel combination. Song et al. [33, 65] look

at a mobile robot with steerable omnidirectional wheels, where the kinematics are treated similarly to the three-wheeled robot; only here, each omnidirectional wheel has four degrees-of-freedom, instead of three.

1.3.6 Dynamics and Vibration

Much of the material for this topic can be found in advanced-level dynamics textbooks, such as Ginsberg [66], Baruh [67], and Greenwood [68]. These books present advanced methods for the development of the equations of motion for a system. Common methods such as Newton-Euler, Hamilton, Lagrange, and d'Alembert are well documented and covered in such textbooks, where more obscure and less known methods, such as Gibbs-Appell Equations, Jourdain's principle, and Kane's Equations are less documented, though they have been in use for at least several decades.

The specific topic of the motion of a disc on a surface and of a sphere on a surface is covered in some textbooks such as Baruh [67] that deals with the problem of a disc rolling on a surface using Lagrange's equations, and Neimark [69] that deals specifically with a sphere rolling on an absolutely rough surface (no friction limit), using the Newton-Euler Method. This latter textbook, also suggests that the Gibbs-Appell method may be very suitable for the development of the equations of motion for nonholonomic systems as also suggested in [70]. However, the particular motions in the case of a cylinder actuated by a wheel and the case of a sphere actuated by three wheels are holonomic, providing that kinematic slip is avoided.

In the sphere case, the complete angular motion of the sphere could be described using three generalized coordinates. The solution proposed in this thesis utilizes three independent actuating omnidirectional wheels. Therefore, the number of degrees-of-freedom is equal to the number of generalized coordinates. Hence, the problem is holonomic, even though it may

not seem so at first glance. It is concluded that a more specific search for a similar problem needs to be conducted.

The specific platform in this thesis became a possibility only recently when omnidirectional wheels were introduced. Prior to that it was not possible to create such a kinematic architecture. Hence, there is not much literature on the dynamics of such a configuration. The slip issue has more coverage in the literature. Papers such as [71] discuss the topic of slip in mobile robots, where the concern is slip between wheels and a flat surface. The same idea is discussed and developed by Williams et al. [37], where two models for evaluating the friction force between the omnidirectional wheels and the ground are presented. The development of the dynamics in this case uses the Newton-Euler method for evaluating the forces and accelerations.

Some of these ideas for actuation using omnidirectional wheels have been developed either at the kinematic level or at the dynamic level. It is noted though, that the treatment is always for a holonomic mobile robot with 3 degrees-of-freedom moving on a plane. This differs from the proposed platform in three ways. First, the suggested problem has 6 degrees-of-freedom. Second, the motion handled by the omnidirectional wheels is purely rotational. Finally, the moving platform is not the platform attached to the wheels, but, using the mobile robot analogy, a reference plane which is the sphere.

In addition to the dynamics and the development of the equations of motion, vibration is a wide topic, which is covered by many textbooks such as Rao [72] and Shabana [73], which treat linear systems having one through several degrees-of-freedom. More advanced textbooks such as Shabana [74] deal with continuous non-rigid systems. Other texts such as Nayfeh [75] treat the issue of nonlinear systems.

In the case of the Atlas sphere, attention needs to be paid to what happens at the contact points between the sphere and the omnidirectional wheels. Although the bodies involved may be assumed rigid, it is essential to maintain high normal forces at the contact

points to avoid kinetic slip. These high forces lead to deflections at the contact points that affect the kinematics and dynamics of the system. Most texts and papers dealing with the contact point interactions treat the issue mostly from the standpoint of stresses and strains which are structural concerns. However, some of the analyses may be utilized for the current application. A major source in the field is the textbook by Johnson [76] utilizing the Hertzian contact pressure model [77].

1.4 Project Definition

The Atlas platform [4, 5] described above is a novel concept for an orientation motion platform. The proposed project is to establish a complete mathematical framework for the spherical Atlas actuation concept from the standpoint of kinematics, dynamics, and vibration. The formulation allows investigation of various possible designs where the rotational platform is based on a sphere actuated by omnidirectional wheels.

Thorough examination of the kinematics and dynamics of the Atlas platform requires that it be posed in a general way. A generalization of the concept at hand would be to examine the concept of actuating a sphere using omnidirectional wheels. This way, the number of omnidirectional wheels, their types, their relative sizes, their position and orientation, and their shape, become kinematic design parameters. In addition, dynamic design parameters such as stiffness of the sphere and omnidirectional wheel mounts, friction coefficients, position of the centre of mass, and others may be explored to achieve complete understanding of the novel kinematic architecture suggested.

This thesis presents a complete kinematic analysis of such a system, addressing the design issues mentioned above, as well as the very important slip issue. In addition, the dynamics of the system are addressed, and non-ideal conditions, such as contact flexibility, and non-ideal shape of the wheels, are investigated. A numerical simulation program has been developed

to integrate the dynamic equations of motion of the non-ideal system that allows for the investigation of the effects of various design parameters, such as location and orientation of the omnidirectional wheels, stiffness of the sphere, position of the centre of mass of the sphere relative to its geometric centre, friction coefficients, and other parameters on performance of the Atlas platform. The result is a generalized unified treatment of the kinematics and dynamics of a sphere actuated by omnidirectional wheels.

1.5 Significance and Contributions of this Thesis

1.5.1 Significance

The work in this thesis is built on novel concepts in terms of kinematic architecture and actuation methods of simulation motion platforms, and the results mean the removal of angular displacement limitations and a class of singularities from the current state of the art motion platforms. The results may be used by the simulation community, but other applications that may require such unlimited angular motion, such as gyroscope calibration, optical sensor mounts, and other pointing applications may find them beneficial.

The actuation method, though already used in the planar mobile robot industry and in some limited-space motor vehicle applications (such as a forklift in a crowded warehouse [78], wheelchairs [79], etc.), can be applied to a wider range of applications that require spherical motion.

1.5.2 Contributions

The mathematical modelling and analysis of this kinematic architecture of motion platform are novel. The kinematics of such a system suggests further advantages in terms of the kinematic expressions that can be solved analytically in closed form. Major overall contri-

butions to knowledge include the development and application of kinematic and dynamic formulations for the motion of a sphere actuated by omnidirectional or Mecanum wheels as well as analyses suggesting best practice for their use in the design and operation of the Atlas motion platform.

Some of the results presented in this thesis have been presented at international conferences and in archival journals [81, 82, 83, 84, 85]. Specific novel contributions of the thesis include the following.

1. First general kinematics model for a sphere actuated with three active degrees-of-freedom.

2. Method for determining the angular velocity of a sphere based on partial information of velocities of points on the sphere.

3. First treatment of kinematics of dual-race and triple-race omnidirectional wheels. Despite the relatively wide use of dual-race omnidirectional wheels in the mobile robots field, they were always assumed to be single-race. This work analyzes the kinematics of the dual-race omnidirectional wheels, yielding correction matrices and estimates of the error of the single-race assumption that turns out to be more significant than previously assumed.

4. Complete kinematics model for a sphere actuated by n omnidirectional wheels of any type, including slip estimation and equivalent points.

5. Complete dynamics and vibration model for a 6 DOF motion platform with a sphere actuated by omnidirectional wheels as its rotational subsystem.

6. Application of the suggested models for the purpose of analyzing and comparing two similar systems with different omnidirectional wheel types from the vibration standpoint.

Chapter 2

Kinematics

The kinematics of the Atlas platform is an especially significant contribution of this work. A sphere is actuated by omnidirectional wheels using friction, thus avoiding joints that limit the motion of the platform. This, in turn, allows for a singularity-free workspace with unlimited rotation about any axis. In this chapter, conditions on the position and orientation of the actuating omnidirectional wheels will be developed such that the theoretical benefits of the design will be feasible. Although proof of concept investigation was previously performed using one arbitrary selection of omnidirectional wheel type, position, and orientation [5]; thorough research is required as to the effects of these parameters on the kinematics of the platform.

Essential to the design of Atlas is that kinematic slip be avoided at all contact points between omnidirectional wheels and the sphere. Kinematic slip is a velocity difference between corresponding contacting points on the sphere and omnidirectional wheel due to kinematics alone, i.e., regardless of kinetic reasons such as insufficient friction limits at the contact point necessary to avoid slip. Avoiding kinematic slip is a necessary condition to avoid slip completely at the contact points. Once this is achieved, kinetic slip due to insufficient normal forces at the contact points needs to be investigated.

A complete kinematic model for a sphere actuated by omnidirectional wheels will be developed here for the general case. The kinematics of dual-race and triple-race omnidirectional wheels will be treated for the first time for any application, with emphasis made on highlighting the correction required for models that work with single-race kinematics and the error in using a single-race kinematic model for a dual-race application. The issue of driving a sphere using omnidirectional wheels is therefore completely generalized here allowing for any particular configuration to be analyzed from the standpoint of workspace, singularities, slip at contact points, as well as both forward and inverse kinematics. Even though the Atlas platform is a parallel design, the resulting kinematics have a closed form analytical expression which significantly reduces the computational requirements for any controller implementation.

2.1 The Generalized Problem

A generalization of the Atlas platform kinematics problem is to define the orienting platform as a sphere actuated by omnidirectional wheels positioned at n arbitrary contact points and arranged in arbitrary orientations. Thus, the Atlas platform is a specific case of the generalized problem, where $n = 3$. The theoretical kinematics problem then becomes one of finding a geometrical configuration for the omnidirectional wheels such that the slip due to kinematic issues is zero. To develop the kinematics of the platform, a general configuration is assumed, and an inertial coordinate frame is positioned at the geometric centre of the sphere as illustrated in Figure 2.1. The kinematic slip is defined as the difference between the linear velocity vector $\tilde{\mathbf{V}}_\mathbf{i}$ induced by the actuating wheel i at its contact point with the sphere and the velocity vector of the same contact point $\tilde{\mathbf{V}}'_\mathbf{i}$ on the sphere. It must be emphasized here that the no-kinematic slip condition is a necessary but not sufficient condition for achieving zero slip in the system. It is a necessary condition since not meeting this condition means

that the velocities of two bodies at a contact point are different, thus slip is imminent. It is not sufficient, since the contact forces, specifically the friction force, that evolve at a contact point may exceed the friction limit of the contacting surfaces, thus creating slip due to kinetic reasons.

The translational motion, generated with an XYZ gantry or some other means of translational actuation, is completely decoupled from the rotational motion of the sphere, thus the velocity of the geometric centre of the sphere is simply the velocity dictated by the gantry. Relative translational motion resulting from imperfections will be treated as an overlaying perturbation in the subsequent chapter dealing with dynamics and vibration (Chapter 3). The resulting rectilinear motion is straightforward and well understood, and will not be further discussed. Since an omnidirectional wheel allows free rolling in the direction perpendicular to the actuation direction, the no-slip requirement for this direction does not apply. The omnidirectional wheels are initially treated as ideal, meaning that the location and geometry of the contact point is assumed to be constant. The change in location of the contact point due to omnidirectional wheel design, such as dual-race omnidirectional wheels will be addressed subsequently.

All mathematical developments presented here are referenced to the inertial coordinate frame illustrated in Figure 2.1. The position vectors of the i^{th} contact point is indicated by $\tilde{\mathbf{R}}_\mathbf{i}$, and $\tilde{\mathbf{\Omega}}$ is the angular velocity of the sphere. The contact point velocity on the sphere side of the sphere/omnidirectional wheel interface is therefore

$$\tilde{\mathbf{V}}'_\mathbf{i} = \tilde{\mathbf{\Omega}} \times \tilde{\mathbf{R}}_\mathbf{i} \quad , \tag{2.1}$$

where subscript i refers to a specific omnidirectional wheel, where $i \in \{1, 2, ..., n\}$. The velocity of the contact point on the omnidirectional wheel side, can be broken into two components: one in the actuation direction, V_i, and the other in the direction of the free-roll

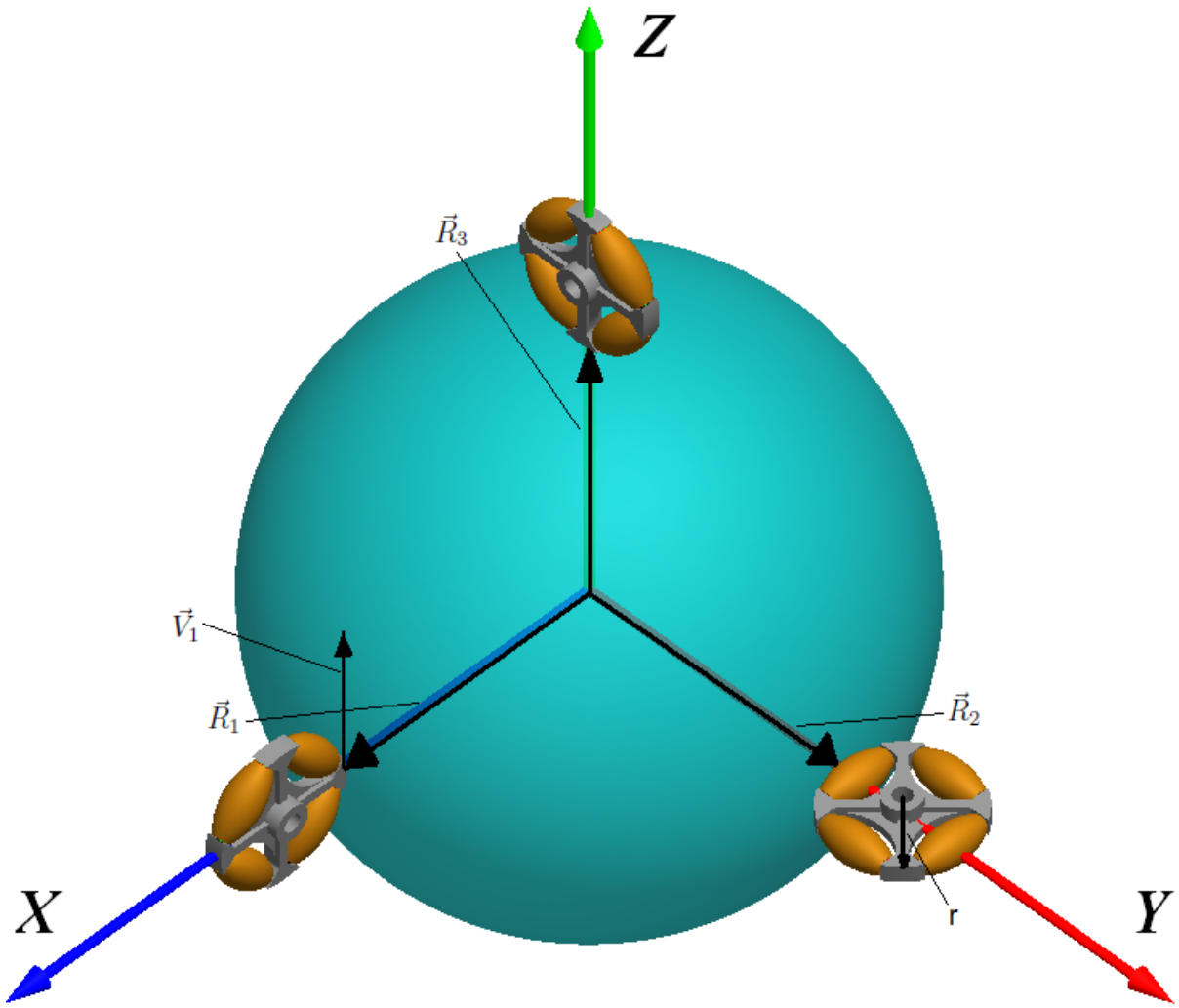

Figure 2.1: Inertial coordinate frame with origin at the geometric centre of the sphere.

of the castors, V_{ri}:

$$\tilde{\mathbf{V}}_\mathbf{i} = V_i \hat{\mathbf{v}}_\mathbf{i} + V_{ri} \hat{\mathbf{v}}_\mathbf{ri} \quad , \tag{2.2}$$

where $\hat{\mathbf{v}}_\mathbf{i}$ is a unit vector in the actuation direction, and $\hat{\mathbf{v}}_\mathbf{ri}$ is a unit vector in the free-roll direction. These two directions are orthogonal by design, such that

$$\hat{\mathbf{v}}_\mathbf{i} \cdot \hat{\mathbf{v}}_\mathbf{ri} = 0 \quad . \tag{2.3}$$

The no-slip requirement may now be restated as:

$$(\tilde{\boldsymbol{\Omega}} \times \tilde{\mathbf{R}}_\mathbf{i}) \cdot \hat{\mathbf{v}}_\mathbf{i} = V_i \quad , \tag{2.4}$$

or, alternatively stated in words, the magnitude of the velocity of a sphere contact point with the omnidirectional wheel in the actuation direction is required to be the same as the one on the omnidirectional wheel in the same direction, thereby eliminating slip. Equation 2.4 can be rearranged using vector product relations as:

$$(\tilde{\boldsymbol{\Omega}} \times \tilde{\mathbf{R}}_\mathbf{i}) \cdot \hat{\mathbf{v}}_\mathbf{i} = (\tilde{\mathbf{R}}_\mathbf{i} \times \hat{\mathbf{v}}_\mathbf{i}) \cdot \tilde{\boldsymbol{\Omega}} = V_i \quad . \tag{2.5}$$

Since the magnitude of all position vectors is the radius of the sphere, R, the position vectors of the contact points can be written as

$$\tilde{\mathbf{R}}_\mathbf{i} = R \hat{\mathbf{R}}_\mathbf{i} \quad , \tag{2.6}$$

where $\hat{\mathbf{R}}_\mathbf{i}$ is a unit vector in the direction of contact point i from the sphere centre. Equa-

tion 2.5 can then be rewritten as

$$(\hat{\mathbf{R}}_\mathbf{i} \times \hat{\mathbf{v}}_\mathbf{i}) \cdot \tilde{\mathbf{\Omega}} = \frac{V_i}{R} \quad . \tag{2.7}$$

Now, since the actuation velocity of the omnidirectional wheel may be expressed as:

$$V_i \hat{\mathbf{v}}_\mathbf{i} = \tilde{\omega}_\mathbf{i} \times \tilde{\mathbf{r}}_\mathbf{i} \quad , \tag{2.8}$$

where $\tilde{\omega}_\mathbf{i}$ is the angular velocity of omnidirectional wheel i and $\tilde{\mathbf{r}}_\mathbf{i}$ is the vector emanating from the omnidirectional wheel's centre to its contact point with the sphere. The contact point actuation velocity can be expressed in terms of the magnitudes of $\tilde{\omega}_\mathbf{i}$ and $\tilde{\mathbf{r}}_\mathbf{i}$ as:

$$V_i = \omega_i r_i \quad . \tag{2.9}$$

Hence, Equation 2.7 may be reexpressed as

$$(\hat{\mathbf{R}}_\mathbf{i} \times \hat{\mathbf{v}}_\mathbf{i}) \cdot \tilde{\mathbf{\Omega}} = \frac{r_i}{R} \omega_i \quad . \tag{2.10}$$

Next the unit induced angular velocities , $\hat{\mathbf{\Omega}}_\mathbf{i}$, are defined to be

$$\hat{\mathbf{\Omega}}_\mathbf{i} = \hat{\mathbf{R}}_\mathbf{i} \times \hat{\mathbf{v}}_\mathbf{i} \tag{2.11}$$

and used to simplify Equation 2.10, yielding

$$\hat{\mathbf{\Omega}}_\mathbf{i} \cdot \tilde{\mathbf{\Omega}} = \frac{r_i}{R} \omega_i \quad . \tag{2.12}$$

Equation 2.12 defines a relationship between $\tilde{\mathbf{\Omega}}$, the angular velocity of the sphere, and ω_i, the magnitudes of the actuation angular velocities of the omnidirectional wheels, which define

the kinematics of the system. Thus, for n contact points, the following matrix equation in component form is obtained:

$$\begin{bmatrix} \hat{\boldsymbol{\Omega}}_{\mathbf{1}}^{\mathbf{T}} \\ \hat{\boldsymbol{\Omega}}_{\mathbf{2}}^{\mathbf{T}} \\ \hat{\boldsymbol{\Omega}}_{\mathbf{3}}^{\mathbf{T}} \\ . \\ . \\ \hat{\boldsymbol{\Omega}}_{\mathbf{n}}^{\mathbf{T}} \end{bmatrix} \tilde{\boldsymbol{\Omega}} = \frac{1}{R} \begin{bmatrix} r_1 & 0 & 0 & . & . & . \\ 0 & r_2 & 0 & . & . & . \\ 0 & 0 & r_3 & . & . & . \\ . & . & . & . & . & . \\ . & . & . & . & . & . \\ . & . & . & . & . & r_n \end{bmatrix} \begin{Bmatrix} \omega_1 \\ \omega_2 \\ \omega_3 \\ . \\ . \\ \omega_n \end{Bmatrix} \quad . \tag{2.13}$$

The relationship in Equation 2.13 is valid as long as there is a solution to this system of n equations. Three cases are next considered: $n < 3$; $n = 3$; and $n > 3$.

2.1.1 The $n < 3$ Case

In the case where $n < 3$, there are fewer omnidirectional wheel angular velocity inputs than rotational degrees-of-freedom. Thus, while slip-free conditions may exist, singularities in the workspace must also exist since the system is nonholonomic, that is, there are fewer controls than degrees-of-freedom. This case is not suitable for a 3 DOF orientation platform, and is not discussed further.

2.1.2 The $n = 3$ Case

In this case, the system of equations reduces to:

$$\begin{bmatrix} \hat{\boldsymbol{\Omega}}_{\mathbf{1}}^{\mathbf{T}} \\ \hat{\boldsymbol{\Omega}}_{\mathbf{2}}^{\mathbf{T}} \\ \hat{\boldsymbol{\Omega}}_{\mathbf{3}}^{\mathbf{T}} \end{bmatrix} \tilde{\boldsymbol{\Omega}} = \frac{1}{R} \begin{bmatrix} r_1 & 0 & 0 \\ 0 & r_2 & 0 \\ 0 & 0 & r_3 \end{bmatrix} \begin{Bmatrix} \omega_1 \\ \omega_2 \\ \omega_3 \end{Bmatrix} \tag{2.14}$$

and in this case the requirement for no-slip is that the matrix

$$\begin{bmatrix} \hat{\mathbf{\Omega}}_\mathbf{1}^\mathbf{T} \\ \hat{\mathbf{\Omega}}_\mathbf{2}^\mathbf{T} \\ \hat{\mathbf{\Omega}}_\mathbf{3}^\mathbf{T} \end{bmatrix} \tag{2.15}$$

be non-singular. To satisfy this, it is required that the three unit vectors $\hat{\mathbf{\Omega}}_\mathbf{i}$ be linearly independent. In this case, the system will have zero slip, and the kinematics of the system are given by:

$$\tilde{\mathbf{\Omega}} = \frac{1}{R} \begin{bmatrix} \hat{\mathbf{\Omega}}_\mathbf{1}^\mathbf{T} \\ \hat{\mathbf{\Omega}}_\mathbf{2}^\mathbf{T} \\ \hat{\mathbf{\Omega}}_\mathbf{3}^\mathbf{T} \end{bmatrix}^{-1} \begin{bmatrix} r_1 & 0 & 0 \\ 0 & r_2 & 0 \\ 0 & 0 & r_3 \end{bmatrix} \begin{Bmatrix} \omega_1 \\ \omega_2 \\ \omega_3 \end{Bmatrix} \tag{2.16}$$

or in Jacobian form:

$$\tilde{\mathbf{\Omega}} = \mathbf{J}\tilde{\omega} \tag{2.17}$$

where

$$\tilde{\omega} = \begin{Bmatrix} \omega_1 & \omega_2 & \omega_3 \end{Bmatrix}^T \tag{2.18}$$

and

$$\mathbf{J} = \frac{1}{R} \begin{bmatrix} \hat{\mathbf{\Omega}}_\mathbf{1}^\mathbf{T} \\ \hat{\mathbf{\Omega}}_\mathbf{2}^\mathbf{T} \\ \hat{\mathbf{\Omega}}_\mathbf{3}^\mathbf{T} \end{bmatrix}^{-1} \begin{bmatrix} r_1 & 0 & 0 \\ 0 & r_2 & 0 \\ 0 & 0 & r_3 \end{bmatrix} \quad . \tag{2.19}$$

Note that $\tilde{\mathbf{\Omega}}$ here is 3×1 array whose elements are the angular velocity magnitudes of the three omnidirectional wheels. Since the Jacobian of the system is constant once the configuration has been determined, acceleration-level kinematics can be derived by differentiation of Equation 2.19 yielding:

$$\dot{\tilde{\mathbf{\Omega}}} = \mathbf{J}\dot{\tilde{\omega}} \quad . \tag{2.20}$$

Obtaining the expression for the orientation of the platform, however, is not as simple. To accomplish that, quaternions or Euler parameters are the natural choice since the unbounded and singularity-free nature of the design calls for a singularity-free representation. Thus, integration of the quaternionic differential equation [80]

$$\dot{q} = \frac{1}{2}\Omega \circ q \tag{2.21}$$

is required, where q is the unit quaternion describing the orientation of the system, and $\Omega \circ q$ is a quaternionic product. Integration of this equation yields the quaternion describing the orientation of the sphere in terms of Euler parameters. Finally, the inverse kinematics of the system relating the required omnidirectional wheel speeds to the desired sphere angular velocity is obtained using the inverse of the Jacobian

$$\mathbf{J}^{-1} = R \begin{bmatrix} \frac{1}{r_1} & 0 & 0 \\ 0 & \frac{1}{r_2} & 0 \\ 0 & 0 & \frac{1}{r_3} \end{bmatrix} \begin{bmatrix} \hat{\mathbf{\Omega}}_\mathbf{1}^\mathbf{T} \\ \hat{\mathbf{\Omega}}_\mathbf{2}^\mathbf{T} \\ \hat{\mathbf{\Omega}}_\mathbf{3}^\mathbf{T} \end{bmatrix} \tag{2.22}$$

such that

$$\tilde{\omega} = \mathbf{J}^{-1}\tilde{\mathbf{\Omega}} \quad . \tag{2.23}$$

2.1.3 The $n > 3$ Case

The motivation for performing the analysis for the $n > 3$ case is twofold: first, generalizing the problem to seek other potential solutions that may allow for improved designs; and second, as will be presented later, some omnidirectional wheels, such as triple-race omnidirectional wheels may have more than a single contact point per wheel, and having three of these implies having more than three contact points with the sphere.

The case where $n > 3$ results in an overdetermined set of equations. This case usually requires approximation, typically using a least squares approach because solutions do not exist in general. Rewriting Equation 2.13 in matrix notation, results in

$$\left[\boldsymbol{\Omega}^{\mathbf{T}}\right] \tilde{\boldsymbol{\Omega}} = \frac{1}{R} [r] \, \tilde{\omega} \quad , \tag{2.24}$$

where

$$\left[\boldsymbol{\Omega}^{\mathbf{T}}\right] = \begin{bmatrix} \hat{\boldsymbol{\Omega}}_{\mathbf{1}}^{\mathbf{T}} \\ \hat{\boldsymbol{\Omega}}_{\mathbf{2}}^{\mathbf{T}} \\ \hat{\boldsymbol{\Omega}}_{\mathbf{3}}^{\mathbf{T}} \\ . \\ . \\ \hat{\boldsymbol{\Omega}}_{\mathbf{n}}^{\mathbf{T}} \end{bmatrix} \quad , \tag{2.25}$$

and

$$[r] = \begin{bmatrix} r_1 & 0 & 0 \\ 0 & r_2 & 0 \\ 0 & 0 & r_3 \end{bmatrix} \quad . \tag{2.26}$$

While the forward kinematics of the system are expressed as an overdetermined set of equations, the inverse kinematics is straightforward. Knowing the desired angular velocity vector allows easily calculating the input angular velocities required to obtain the desired output:

$$\tilde{\omega} = R\,[r]^{-1}\left[\mathbf{\Omega}^T\right]\tilde{\mathbf{\Omega}} \quad . \tag{2.27}$$

As mentioned earlier, the forward kinematics may not be obtained, that is, there is no solution to the system through kinematics alone. The outcome would depend on the kinetics of the system, that is, taking the forces, moments, masses and inertia of the system components into account to obtain the system's behaviour. To obtain a sense of the behaviour of the system from kinematics alone, and to enable comparison between various configurations with more than three actuating wheels, one may resort to approximation. The solution to the forward kinematics in the least square sense, yields:

$$\tilde{\mathbf{\Omega}}_{\mathbf{ls}} \approx \frac{1}{R}\{[\mathbf{\Omega}]\left[\mathbf{\Omega}^T\right]\}^{-1}[\mathbf{\Omega}]\,[r]\,\tilde{\omega} \quad , \tag{2.28}$$

where

$$[\mathbf{\Omega}] = \left[\mathbf{\Omega}^T\right]^{\mathrm{T}} \quad . \tag{2.29}$$

This can be abbreviated as:

$$\tilde{\mathbf{\Omega}}_{\mathbf{ls}} \approx \mathbf{J}_{\mathbf{ls}}\tilde{\omega} \quad , \tag{2.30}$$

where the Jacobian for the least squares approximation is:

$$\mathbf{J}_{\mathbf{ls}} = \frac{1}{R}\{[\mathbf{\Omega}]\left[\mathbf{\Omega}^T\right]\}^{-1}[\mathbf{\Omega}]\,[r] \tag{2.31}$$

The Jacobian exists if the columns of $\left[\mathbf{\Omega}^T\right]$ are linearly independent, or alternatively, if the rows of $[\mathbf{\Omega}]$ are linearly independent. Since $\hat{\Omega}_i$ are unit vectors, the Jacobian does not exist only if all $\hat{\Omega}_i$ point in the same (or reverse) directions.

Slip

To evaluate the slip at the contact points, it is necessary to compare the contact point velocity on the sphere to the contact point velocity on the omnidirectional wheel. It is important to remember that using the least square approximation method does not yield the actual slip at the contact point. To obtain that, kinetics need to be considered. However, utilizing such approximation would provide with a tool that may give a measure of the slip involved at the best case scenario. Thus, it would allow comparing various designs quantitatively.

It was shown previously that the contact point velocity on the omnidirectional wheel is:

$$\tilde{\mathbf{V}}_\mathbf{i} = \omega_i r_i \hat{v}_i \tag{2.32}$$

and the corresponding contact point velocity on the sphere is:

$$\tilde{\mathbf{V}}'_\mathbf{i} = \tilde{\mathbf{\Omega}}_\mathbf{ls} \times \tilde{\mathbf{R}}_\mathbf{i} \quad . \tag{2.33}$$

Thus, the velocity difference in the actuating direction is

$$\Delta V_i = |\tilde{\mathbf{V}}_\mathbf{i}| - \tilde{\mathbf{V}}'_\mathbf{i} \cdot \hat{v}_i \quad . \tag{2.34}$$

The slip ratio can be defined as:

$$S_i \equiv \frac{\Delta V_i}{|\tilde{\mathbf{V}}_\mathbf{i}|} = 1 - \frac{\tilde{\mathbf{V}}'_\mathbf{i} \cdot \hat{v}_i}{|\tilde{\mathbf{V}}_\mathbf{i}|} \quad . \tag{2.35}$$

An overall slip assessment indicator is defined to be

$$S = \sqrt{\sum_{i=1}^{n} S_i^2} \quad , \tag{2.36}$$

where the minimal value for S is desired.

In the general case, it is clear that having more than three omnidirectional wheels driving the sphere leads to slip and energy loss, since the system is overdetermined. Thus, assigning arbitrary angular velocities to the wheels would yield slip in the general case. However, a larger number of omnidirectional wheels may be utilized without slip if the velocities of the redundant omnidirectional wheels are coordinated such that their slip ratios will all be zero, resulting in a master-slave system, where three omnidirectional wheels determine the angular velocity of the sphere and the remaining wheels match their speeds such that slip is zero. To obtain that, three omnidirectional wheels need to be selected such that they meet the criteria set out for the $n = 3$ case, such that the resulting sphere angular velocity is evaluated, then the required velocities at the remaining contact points are obtained resulting in zero slip. Although there is no kinematic benefit from such a master-slave system, benefits that stem from dynamics, vibration, and stress considerations may exist. Since omnidirectional wheels must have some gaps between their rollers, there are areas where loss of contact may occur; thus having a second omnidirectional wheel covering the same degree-of-freedom allows compensating for this problem as detailed in Section 3.2.3.

2.2 Omnidirectional Wheel Types and Their Effect on the Kinematics

2.2.1 Single-race Omnidirectional Wheels

The most basic omnidirectional wheel has a single race of rollers. As presented in the introduction, the Atlas platform requires three omnidirectional wheels to achieve a singularity-free workspace that allows for angular motion about any axis. The following two examples of kinematic configurations will serve as benchmarks, and will be revisited with the various wheel types covered here.

The Orthogonal Case

The following example shows an architecture that satisfies the necessary condition stated in Equation 2.15 , and indeed yields zero kinematic slip. Figure 2.2 shows the architecture suggested. For simplicity, and without loss of generality, the global coordinate frame was chosen as shown in the figure. That, in turn, allows all calculations to be performed directly in the global coordinate frame.

Here, the sphere has a radius R, and each of the omnidirectional wheels has a radius r. Thus, the position vectors of the three contact points are:

$$\begin{aligned} \vec{R}_1 &= R\hat{\imath} \quad ; \\ \vec{R}_2 &= R\hat{\jmath} \quad ; \\ \vec{R}_3 &= R\hat{k} \quad . \end{aligned} \tag{2.37}$$

The position vectors of the contact points with respect to the omnidirectional wheels's centres

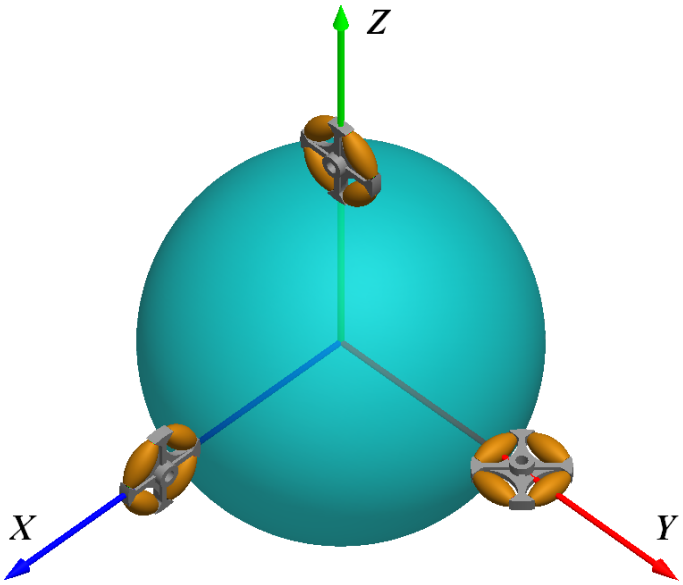

Figure 2.2: Kinematic architecture for the orthogonal case.

of rotation are:

$$\begin{aligned} \vec{r}_1 &= -r\hat{\imath} \quad ; \\ \vec{r}_2 &= -r\hat{\jmath} \quad ; \\ \vec{r}_3 &= -r\hat{k} \quad . \end{aligned} \tag{2.38}$$

The angular velocities of the omnidirectional wheels are:

$$\begin{aligned} \vec{\omega}_1 &= \omega_1\hat{\jmath} \quad ; \\ \vec{\omega}_2 &= \omega_2\hat{k} \quad ; \\ \vec{\omega}_3 &= \omega_3\hat{\imath} \quad . \end{aligned} \tag{2.39}$$

Therefore the velocities they induce on the sphere at the contact points are:

$$\begin{aligned} \vec{V}_1 &= \vec{\omega}_1 \times \vec{r}_1 = \omega_1 r \hat{k} \quad ; \\ \vec{V}_2 &= \vec{\omega}_2 \times \vec{r}_2 = \omega_2 r \hat{\imath} \quad ; \\ \vec{V}_3 &= \vec{\omega}_3 \times \vec{r}_3 = \omega_3 r \hat{\jmath} \quad . \end{aligned} \tag{2.40}$$

These velocities create the three components of angular velocity of the sphere:

$$\begin{aligned} \hat{\Omega}_1 &= \hat{\imath} \times \hat{k} = -\hat{\jmath} \quad ; \\ \hat{\Omega}_2 &= \hat{\jmath} \times \hat{\imath} = -\hat{k} \quad ; \\ \hat{\Omega}_3 &= \hat{k} \times \hat{\jmath} = -\hat{\imath} \quad . \end{aligned} \tag{2.41}$$

It is clear now, that these are mutually orthogonal, since:

$$\begin{aligned} \hat{\Omega}_1 \cdot \hat{\Omega}_2 &= 0 \quad ; \\ \hat{\Omega}_1 \cdot \hat{\Omega}_3 &= 0 \quad ; \\ \hat{\Omega}_2 \cdot \hat{\Omega}_3 &= 0 \quad . \end{aligned} \tag{2.42}$$

This could alternatively be shown directly by evaluating the Jacobian of the system as:

$$\mathbf{J} = \frac{r}{R} \begin{bmatrix} 0 & -1 & 0 \\ 0 & 0 & -1 \\ -1 & 0 & 0 \end{bmatrix}^{-1} = \frac{r}{R} \begin{bmatrix} 0 & 0 & -1 \\ -1 & 0 & 0 \\ 0 & -1 & 0 \end{bmatrix} \tag{2.43}$$

and noting that rows are linearly independent as required by the theory presented.

The Atlas Sphere

Atlas motion platform demonstrators, constructed to date, have the three omnidirectional wheels arranged on the edges of an equilateral triangle with an elevation angle of 40°. To generalize the symmetric configuration, an arbitrary elevation angle θ will be used. The configuration is presented in Figure 2.3.

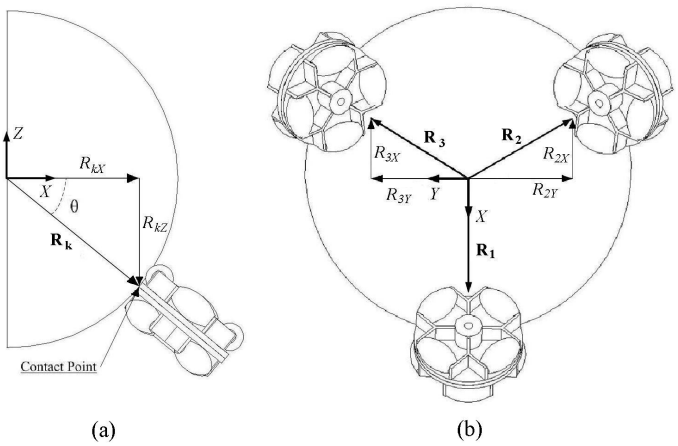

Figure 2.3: Kinematic architecture for the Atlas sphere case [86].

In this case, the omnidirectional wheel position vectors are:

$$\begin{aligned}
\vec{R}_1 &= R(\cos\theta\hat{\imath} - \sin\theta\hat{k}) \quad ; \\
\vec{R}_2 &= R(-\frac{1}{2}\cos\theta\hat{\imath} + \frac{\sqrt{3}}{2}\cos\theta\hat{\jmath} - \sin\theta\hat{k}) \quad ; \\
\vec{R}_3 &= R(-\frac{1}{2}\cos\theta\hat{\imath} - \frac{\sqrt{3}}{2}\cos\theta\hat{\jmath} - \sin\theta\hat{k}) \quad . \qquad (2.44)
\end{aligned}$$

The contact point velocities are given by:

$$\begin{aligned}
\vec{V}_1 &= \omega_1 r\hat{\jmath} \quad ; \\
\vec{V}_2 &= \omega_2 r(-\frac{\sqrt{3}}{2}\hat{\imath} - \frac{1}{2}\hat{\jmath}) \quad ; \\
\vec{V}_3 &= \omega_3 r(\frac{\sqrt{3}}{2}\hat{\imath} - \frac{1}{2}\hat{\jmath}) \quad . \qquad (2.45)
\end{aligned}$$

as shown in [86]. These yield:

$$\begin{aligned}
\hat{\Omega}_1 &= (\cos\theta\hat{\imath} - \sin\theta\hat{k}) \times \hat{\jmath} = (\sin\theta\hat{\imath} + \cos\theta\hat{k}) \quad ; \\
\hat{\Omega}_2 &= (-\frac{1}{2}\cos\theta\hat{\imath} + \frac{\sqrt{3}}{2}\cos\theta\hat{\jmath} - \sin\theta\hat{k}) \times (-\frac{\sqrt{3}}{2}\hat{\imath} - \frac{1}{2}\hat{\jmath}) \\
&= (-\frac{1}{2}\sin\theta\hat{\imath} + \frac{\sqrt{3}}{2}\sin\theta\hat{\jmath} + \cos\theta\hat{k}) \quad ; \\
\hat{\Omega}_3 &= (-\frac{1}{2}\cos\theta\hat{\imath} - \frac{\sqrt{3}}{2}\cos\theta\hat{\jmath} - \sin\theta\hat{k}) \times (\frac{\sqrt{3}}{2}\hat{\imath} - \frac{1}{2}\hat{\jmath}) \\
&= (-\frac{1}{2}\sin\theta\hat{\imath} - \frac{\sqrt{3}}{2}\sin\theta\hat{\jmath} + \cos\theta\hat{k}) \quad . \qquad (2.46)
\end{aligned}$$

Hence,

$$\begin{bmatrix} \hat{\Omega}_1^T \\ \hat{\Omega}_2^T \\ \hat{\Omega}_3^T \end{bmatrix} = \begin{bmatrix} \sin\theta & 0 & \cos\theta \\ -\frac{1}{2}\sin\theta & \frac{\sqrt{3}}{2}\sin\theta & \cos\theta \\ -\frac{1}{2}\sin\theta & -\frac{\sqrt{3}}{2}\sin\theta & \cos\theta \end{bmatrix} \quad . \qquad (2.47)$$

The determinant of this matrix will yield zero for:

$$\frac{3\sqrt{3}}{2}\sin^2\theta\cos\theta = 0 \qquad (2.48)$$

and so, the only singularities would be for $\theta = 0$ and $\theta = \pm 90°$. For all other cases, the Jacobian can be evaluated. In this case,

$$\mathbf{J} = \frac{r}{R}\begin{bmatrix} \sin\theta & 0 & \cos\theta \\ -\frac{1}{2}\sin\theta & \frac{\sqrt{3}}{2}\sin\theta & \cos\theta \\ -\frac{1}{2}\sin\theta & -\frac{\sqrt{3}}{2}\sin\theta & \cos\theta \end{bmatrix}^{-1} \qquad (2.49)$$

thereby defining the direct relationship between omnidirectional wheel speeds and sphere angular velocity without kinematic slip.

Figure 2.4: A dual-race omnidirectional wheel [86].

2.2.2 Dual-race Omnidirectional Wheels and Shifting Contact Points

In the preceding discussion, the omnidirectional wheels were assumed to be perfectly round; while in reality, it is impossible to have a perfectly round omnidirectional wheel as illustrated in Figure 1.4. A simple solution to the discontinuity problem caused by the basic design of omnidirectional wheels is utilizing a dual-race omnidirectional wheel as shown in Figure 2.4. While the kinematics for the Atlas platform have been developed in the previous section for perfectly round omnidirectional wheels, here that basic assumption is removed. Instead, one of the more common solutions to the contact discontinuity problem, the use of dual race omnidirectional wheels will be treated. The dual race design aligns the rollers in two parallel races, such that exactly when a roller on one race loses contact with the rolling surface, the roller on the other race makes contact at the same point in time, thus maintaining roller contact at all times.

Figure 2.5 shows an imprint of a dual-race omnidirectional wheel, in use in the Atlas demonstrator, on a flat surface. Attention is drawn to the fact that shifting one of the two parallel races to align with the other yields a continuous straight line. This design indeed solves the contact gap problem, but introduces a new one: there is no longer a single point of contact. Rather, there are two alternating points of contact on the sphere. This change in location of the contact point on the sphere alters the system's kinematics and, as a result, modifications to the kinematic model are necessary to improve the accuracy of the system kinematic and dynamic models. This is important for subsequent use in model-based control.

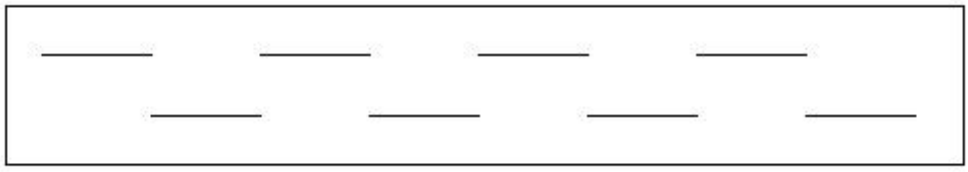

Figure 2.5: The imprint of a dual-race omnidirectional wheel on a flat surface.

Refined Kinematics Model

As presented earlier, the underlying concept in obtaining the kinematics for the sphere is to obtain a relationship between $\vec{\Omega}$, the angular velocity vector of the sphere, and $\omega_{\mathbf{i}}$, the angular speeds of the three omnidirectional wheels, that would account for zero kinematic slip between the sphere and the omnidirectional wheels. The condition is met by requiring that the projection of the velocities of the sphere at all contact points in the actuation direction of the omnidirectional wheel be the same; or, expressed mathematically,

$$(\tilde{\mathbf{\Omega}} \times \tilde{\mathbf{R}}_{\mathbf{i}}) \cdot \hat{v}_i = V_i \quad . \tag{2.50}$$

This condition results in the relationship

$$\tilde{\mathbf{\Omega}} = \mathbf{J}\tilde{\omega} \tag{2.51}$$

where

$$\mathbf{J} = \frac{1}{R} \begin{bmatrix} \hat{\mathbf{\Omega}}_{\mathbf{1}}^{\mathbf{T}} \\ \hat{\mathbf{\Omega}}_{\mathbf{2}}^{\mathbf{T}} \\ \hat{\mathbf{\Omega}}_{\mathbf{3}}^{\mathbf{T}} \end{bmatrix}^{-1} \begin{bmatrix} r_1 & 0 & 0 \\ 0 & r_2 & 0 \\ 0 & 0 & r_3 \end{bmatrix} \quad . \tag{2.52}$$

In the case of dual-race omnidirectional wheels, the position vector $\tilde{\mathbf{R}}_{\mathbf{i}}$ of the contact points alternates between two locations. Six contact points (two per omnidirectional wheel)

$\tilde{\mathbf{R}}_{\mathbf{ij}}$ are identified where the first index marks the omnidirectional wheel and the second index marks the point of contact of a specific race on the wheel. This results in eight different combinations of possible simultaneous contact points:

$$\begin{array}{llll} R_{11} & R_{21} & R_{31} & ; \\ R_{11} & R_{21} & R_{32} & ; \\ R_{11} & R_{22} & R_{31} & ; \\ R_{11} & R_{22} & R_{32} & ; \\ R_{12} & R_{21} & R_{31} & ; \\ R_{12} & R_{21} & R_{32} & ; \\ R_{12} & R_{22} & R_{31} & ; \\ R_{12} & R_{22} & R_{32} & . \end{array}$$

Now, since $\hat{v}_i$ remains the same as with the single-race case, the only change to $\hat{\Omega}_i$ is due to the change from $\hat{R}_i$ to $\hat{R}_{ij}$, thus

$$\hat{\Omega}_{ij} = \hat{R}_{ij} \times \hat{v}_i \tag{2.53}$$

and so, we obtain eight Jacobians for the eight combinations above:

$$\mathbf{J}_{lmn} = \frac{1}{R} \begin{bmatrix} \hat{\mathbf{\Omega}}^{\mathbf{T}}_{\mathbf{1l}} \\ \hat{\mathbf{\Omega}}^{\mathbf{T}}_{\mathbf{2m}} \\ \hat{\mathbf{\Omega}}^{\mathbf{T}}_{\mathbf{3n}} \end{bmatrix}^{-1} \begin{bmatrix} r_1 & 0 & 0 \\ 0 & r_2 & 0 \\ 0 & 0 & r_3 \end{bmatrix} ...l, m, n = 1, 2 \tag{2.54}$$

where the indices l, m, and n determine the race in contact with the sphere on omnidirectional wheels 1, 2, and 3 respectively. Determining l, m, and n could be performed directly using sensors, or by simply integrating the angular velocities of each omnidirectional wheel

independently, such that:

$$\phi_i = \int_0^t \omega_i dt \tag{2.55}$$

and for $2N$ rollers per omnidirectional wheel, the indices may simply be calculated, using the integer floor values, as

$$l = \text{floor}\left[\frac{\text{N}\phi_1}{\pi} \mod 2\right] + 1 \quad , \tag{2.56}$$

$$m = \text{floor}\left[\frac{\text{N}\phi_2}{\pi} \mod 2\right] + 1 \quad , \tag{2.57}$$

$$n = \text{floor}\left[\frac{\text{N}\phi_3}{\pi} \mod 2\right] + 1 \quad . \tag{2.58}$$

This approach would require first evaluating the indices l, m, and n, and then calculating the angular velocity of the sphere, using the appropriate Jacobian.

As mentioned above, the two benchmark examples used for the single-race case are utilized to illustrate the differences between the kinematic behaviour of the dual-race omnidirectional wheels and the single-race ones. These are both architectures that satisfy the necessary no-slip condition. Just as shown earlier, the sphere has a radius R, and each of the omnidirectional wheels has a radius r. However, the contact point details are now those of a dual-race omnidirectional wheel and are presented in Figure 2.6.

There is a deviation of $\pm\Delta\theta$ from the ideal contact point used in the evaluation of the Jacobian of the ideal case. It is clear from Figure 2.6 that

$$\sin\Delta\theta = \frac{\frac{d}{2}}{R + r_r} = \frac{d}{2(R + r_r)} \quad . \tag{2.59}$$

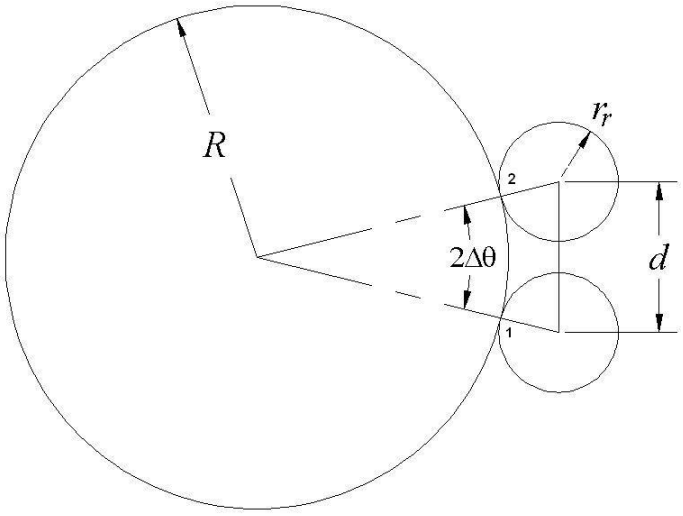

Figure 2.6: The actual contact points on the Atlas sphere.

Thus,

$$\cos\Delta\theta = \sqrt{1-\sin^2\Delta\theta} = \frac{1}{2(R+r_r)}\sqrt{4(R+r_r)^2-d^2} \quad . \tag{2.60}$$

Utilizing these relations, it is clear that for any arbitrary angle θ,

$$\begin{aligned} \sin(\theta \pm \Delta\theta) &= \frac{1}{2(R+r_r)}(\sqrt{4(R+r_r)^2-d^2}\sin\theta \pm d\cos\theta) \quad , \\ \cos(\theta \pm \Delta\theta) &= \frac{1}{2(R+r_r)}(\sqrt{4(R+r_r)^2-d^2}\cos\theta \mp d\sin\theta) \quad . \end{aligned} \tag{2.61}$$

The Orthogonal Case with Dual-race Omnidirectional Wheels

Figure 2.2 shows a case where the omnidirectional wheels are mutually orthogonal. Thus, the position vectors of the three contact points for the ideal case are, as shown in the single-race case:

$$\vec{R}_1 = R\hat{\imath} \quad ; \; \vec{R}_2 = R\hat{\jmath} \quad ; \; \vec{R}_3 = R\hat{k} \quad . \tag{2.62}$$

However, accounting for the angular deviation from the ideal contact point (in the case of dual-race wheels), the position vectors become

$$\begin{aligned}
\vec{R}_{11} &= R(\cos\Delta\theta\hat{\imath} + \sin\Delta\theta\hat{\jmath}) = \frac{R}{2(R+r_r)}(\sqrt{4(R+r_r)^2 - d^2}\hat{\imath} + d\hat{\jmath}) \quad ; \\
\vec{R}_{12} &= R(\cos\Delta\theta\hat{\imath} - \sin\Delta\theta\hat{\jmath}) = \frac{R}{2(R+r_r)}(\sqrt{4(R+r_r)^2 - d^2}\hat{\imath} - d\hat{\jmath}) \quad ; \\
\vec{R}_{21} &= R(\cos\Delta\theta\hat{\jmath} + \sin\Delta\theta\hat{k}) = \frac{R}{2(R+r_r)}(\sqrt{4(R+r_r)^2 - d^2}\hat{\jmath} + d\hat{k}) \quad ; \\
\vec{R}_{22} &= R(\cos\Delta\theta\hat{\jmath} - \sin\Delta\theta\hat{k}) = \frac{R}{2(R+r_r)}(\sqrt{4(R+r_r)^2 - d^2}\hat{\jmath} - d\hat{k}) \quad ; \\
\vec{R}_{31} &= R(\sin\Delta\theta\hat{\imath} + \cos\Delta\theta\hat{k}) = \frac{R}{2(R+r_r)}(d\hat{\imath} + \sqrt{4(R+r_r)^2 - d^2}\hat{k}) \quad ; \\
\vec{R}_{32} &= R(-\sin\Delta\theta\hat{\imath} + \cos\Delta\theta\hat{k}) = \frac{R}{2(R+r_r)}(-d\hat{\imath} + \sqrt{4(R+r_r)^2 - d^2}\hat{k}) \quad .
\end{aligned} \tag{2.63}$$

The direction cosines of the omnidirectional wheel contact point velocities in the actuation directions are, as shown earlier

$$\begin{aligned}
\hat{v}_1 &= \hat{k} \quad ; \\
\hat{v}_2 &= \hat{\imath} \quad ; \\
\hat{v}_3 &= \hat{\jmath} \quad .
\end{aligned} \tag{2.64}$$

Using these relations in Equation 2.2.2, yields

$$\begin{aligned}
\hat{\Omega}_{11} &= \frac{1}{2(R+r_r)}(d\hat{\imath} - \sqrt{4(R+r_r)^2 - d^2}\hat{\jmath}) \quad ; \\
\hat{\Omega}_{12} &= \frac{1}{2(R+r_r)}(-d\hat{\imath} - \sqrt{4(R+r_r)^2 - d^2}\hat{\jmath}) \quad ; \\
\hat{\Omega}_{21} &= \frac{1}{2(R+r_r)}(d\hat{\jmath} - \sqrt{4(R+r_r)^2 - d^2}\hat{k}) \quad ; \\
\hat{\Omega}_{22} &= \frac{1}{2(R+r_r)}(-d\hat{\jmath} - \sqrt{4(R+r_r)^2 - d^2}\hat{k}) \quad ; \\
\hat{\Omega}_{31} &= \frac{1}{2(R+r_r)}(-\sqrt{4(R+r_r)^2 - d^2}\hat{\imath} + d\hat{k}) \quad ; \\
\hat{\Omega}_{32} &= \frac{1}{2(R+r_r)}(-\sqrt{4(R+r_r)^2 - d^2}\hat{\imath} - d\hat{k}) \quad .
\end{aligned} \tag{2.65}$$

Finally, the inverse Jacobian becomes

$$\mathbf{J}^{-1}_{lmn} = \frac{\sqrt{4(R+r_r)^2 - d^2}}{2(R+r_r)}\mathbf{J}^{-1}_{id} + \frac{Rd}{2r(R+r_r)}\begin{bmatrix} (-1)^{l+1} & 0 & 0 \\ 0 & (-1)^{m+1} & 0 \\ 0 & 0 & (-1)^{n+1} \end{bmatrix} \quad , \tag{2.66}$$

where $\mathbf{J}_{id}$ is the Jacobian for the ideal case:

$$\mathbf{J}^{-1}_{id} = \frac{R}{r}\begin{bmatrix} 0 & -1 & 0 \\ 0 & 0 & -1 \\ -1 & 0 & 0 \end{bmatrix} \quad . \tag{2.67}$$

The orthogonal case is presented for discussion as it is convenient to study the essential difference between the single-race and dual-race omnidirectional wheels. The first term in Equation 2.66 indicates a slight reduction of the magnitude of $\vec{\Omega}$ in the original direction,

while the second term reveals a more significant change in direction.

The Atlas Platform

The second benchmark, has the configuration of the Atlas spherical motion platform where the three omnidirectional wheels are arranged on the edges of an equilateral triangle with an elevation angle of θ, as illustrated in Figure 2.3. In this case

$$\begin{aligned}
\vec{R}_1 &= R(\cos\theta\hat{\imath} - \sin\theta\hat{k}) \quad ; \\
\vec{R}_2 &= R(-\frac{1}{2}\cos\theta\hat{\imath} + \frac{\sqrt{3}}{2}\cos\theta\hat{\jmath} - \sin\theta\hat{k}) \quad ; \\
\vec{R}_3 &= R(-\frac{1}{2}\cos\theta\hat{\imath} - \frac{\sqrt{3}}{2}\cos\theta\hat{\jmath} - \sin\theta\hat{k}) \quad . \qquad (2.68)
\end{aligned}$$

Accounting for the change in the contact points, the new position vectors may be expressed as

$$\begin{aligned}
\vec{R}_{11} &= R(\cos(\theta - \Delta\theta)\hat{\imath} - \sin(\theta - \Delta\theta)\hat{k}) \quad ; \\
\vec{R}_{12} &= R(\cos(\theta + \Delta\theta)\hat{\imath} - \sin(\theta + \Delta\theta)\hat{k}) \quad ; \\
\vec{R}_{21} &= R(-\frac{1}{2}\cos(\theta - \Delta\theta)\hat{\imath} + \frac{\sqrt{3}}{2}\cos(\theta - \Delta\theta)\hat{\jmath} - \sin(\theta - \Delta\theta)\hat{k}) \quad ; \\
\vec{R}_{22} &= R(-\frac{1}{2}\cos(\theta + \Delta\theta)\hat{\imath} + \frac{\sqrt{3}}{2}\cos(\theta + \Delta\theta)\hat{\jmath} - \sin(\theta + \Delta\theta)\hat{k}) \quad ; \\
\vec{R}_{31} &= R(-\frac{1}{2}\cos(\theta - \Delta\theta)\hat{\imath} - \frac{\sqrt{3}}{2}\cos(\theta - \Delta\theta)\hat{\jmath} - \sin(\theta - \Delta\theta)\hat{k}) \quad ; \\
\vec{R}_{32} &= R(-\frac{1}{2}\cos(\theta + \Delta\theta)\hat{\imath} - \frac{\sqrt{3}}{2}\cos(\theta + \Delta\theta)\hat{\jmath} - \sin(\theta + \Delta\theta)\hat{k}) \quad . \qquad (2.69)
\end{aligned}$$

The direction cosines of the omnidirectional wheel contact point velocities in the actuation

directions are, as presented earlier

$$\begin{aligned} \hat{v}_1 &= \hat{j} \quad ; \\ \hat{v}_2 &= -\frac{\sqrt{3}}{2}\hat{\imath} - \frac{1}{2}\hat{j} \quad ; \\ \hat{v}_3 &= \frac{\sqrt{3}}{2}\hat{\imath} - \frac{1}{2}\hat{j} \quad . \end{aligned} \tag{2.70}$$

Utilizing the relations shown in Equations 2.61, 2.69, 2.70 in Equation 2.2.2, the expressions for the unit vectors identifying the directions of the sphere's angular velocity components

induced by the individual omnidirectional wheels are

$$
\begin{aligned}
\hat{\Omega}_{11} &= \frac{1}{2(R+r_r)}[(\sqrt{4(R+r_r)^2-d^2}\sin\theta - d\cos\theta)\hat{\imath} \\
&+ (\sqrt{4(R+r_r)^2-d^2}\cos\theta + d\sin\theta)\hat{k}] \quad ; \\
\hat{\Omega}_{12} &= \frac{1}{2(R+r_r)}[(\sqrt{4(R+r_r)^2-d^2}\sin\theta + d\cos\theta)\hat{\imath} \\
&+ (\sqrt{4(R+r_r)^2-d^2}\cos\theta - d\sin\theta)\hat{k}] \quad ; \\
\hat{\Omega}_{21} &= \frac{1}{2(R+r_r)}[-\frac{1}{2}(\sqrt{4(R+r_r)^2-d^2}\sin\theta - d\cos\theta)\hat{\imath} \\
&+ \frac{\sqrt{3}}{2}(\sqrt{4(R+r_r)^2-d^2}\sin\theta - d\cos\theta)\hat{\jmath} \\
&+ (\sqrt{4(R+r_r)^2-d^2}\cos\theta + d\sin\theta)\hat{k}] \quad ; \\
\hat{\Omega}_{22} &= \frac{1}{2(R+r_r)}[-\frac{1}{2}(\sqrt{4(R+r_r)^2+d^2}\sin\theta + d\cos\theta)\hat{\imath} \\
&+ \frac{\sqrt{3}}{2}(\sqrt{4(R+r_r)^2+d^2}\sin\theta + d\cos\theta)\hat{\jmath} \\
&+ (\sqrt{4(R+r_r)^2-d^2}\cos\theta - d\sin\theta)\hat{k}] \quad ; \\
\hat{\Omega}_{31} &= \frac{1}{2(R+r_r)}[-\frac{1}{2}(\sqrt{4(R+r_r)^2-d^2}\sin\theta - d\cos\theta)\hat{\imath} \\
&- \frac{\sqrt{3}}{2}(\sqrt{4(R+r_r)^2-d^2}\sin\theta - d\cos\theta)\hat{\jmath} \\
&+ (\sqrt{4(R+r_r)^2-d^2}\cos\theta + d\sin\theta)\hat{k}] \quad ; \\
\hat{\Omega}_{32} &= \frac{1}{2(R+r_r)}[-\frac{1}{2}(\sqrt{4(R+r_r)^2+d^2}\sin\theta + d\cos\theta)\hat{\imath} \\
&- \frac{\sqrt{3}}{2}(\sqrt{4(R+r_r)^2-d^2}\sin\theta + d\cos\theta)\hat{\jmath} \\
&+ (\sqrt{4(R+r_r)^2-d^2}\cos\theta - d\sin\theta)\hat{k}] \quad .
\end{aligned}
\tag{2.71}
$$

Finally, the inverse Jacobian becomes:

$$\mathbf{J}^{-1}_{lmn} = \frac{R}{r}\frac{\sqrt{4(R+r_r)^2-d^2}}{2(R+r_r)}\begin{bmatrix} \sin\theta & 0 & \cos\theta \\ -\frac{1}{2}\sin\theta & \frac{\sqrt{3}}{2}\sin\theta & \cos\theta \\ -\frac{1}{2}\sin\theta & -\frac{\sqrt{3}}{2}\sin\theta & \cos\theta \end{bmatrix}$$
$$+ \quad \frac{R}{r}\frac{d}{2(R+r_r)}\begin{bmatrix} (-1)^l\cos\theta & 0 & (-1)^{l+1}\sin\theta \\ (-1)^{m+1}\frac{1}{2}\cos\theta & (-1)^m\frac{\sqrt{3}}{2}\cos\theta & (-1)^{m+1}\sin\theta \\ (-1)^{n+1}\frac{1}{2}\cos\theta & (-1)^{n+1}\frac{\sqrt{3}}{2}\cos\theta & (-1)^{n+1}\sin\theta \end{bmatrix} \quad . \tag{2.72}$$

The inverse Jacobian for the ideal system is:

$$\mathbf{J}^{-1} = \frac{R}{r}\begin{bmatrix} \sin\theta & 0 & \cos\theta \\ -\frac{1}{2}\sin\theta & \frac{\sqrt{3}}{2}\sin\theta & \cos\theta \\ -\frac{1}{2}\sin\theta & -\frac{\sqrt{3}}{2}\sin\theta & \cos\theta \end{bmatrix} \quad . \tag{2.73}$$

For the dual row system the inverse Jacobian is:

$$\mathbf{J}^{-1}_{lmn} = \frac{\sqrt{4(R+r_r)^2-d^2}}{2(R+r_r)}\mathbf{J}^{-1} + \frac{R}{r}\mathbf{\Delta J'} \tag{2.74}$$

where $\mathbf{J}^{-1}$ is the inverse of the Jacobian for the ideal case and $\mathbf{\Delta J'}$ is the correction component for the contact point change, such that

$$\mathbf{\Delta J'} = \frac{d}{2(R+r_r)}\begin{bmatrix} (-1)^l\cos\theta & 0 & (-1)^{l+1}\sin\theta \\ (-1)^{m+1}\frac{1}{2}\cos\theta & (-1)^m\frac{\sqrt{3}}{2}\cos\theta & (-1)^{m+1}\sin\theta \\ (-1)^{n+1}\frac{1}{2}\cos\theta & (-1)^{n+1}\frac{\sqrt{3}}{2}\cos\theta & (-1)^{n+1}\sin\theta \end{bmatrix} \quad . \tag{2.75}$$

This last term is the only one required to be re-evaluated as it is the only one that may vary

in time. The Jacobian of the system is therefore

$$\mathbf{J}_{lmn} = (\mathbf{J}^{-1} + \frac{R}{r}\mathbf{\Delta J}')^{-1} \quad . \tag{2.76}$$

Evaluating the Error Correction: Some Numerical Results

Some numerical examples have been studied in order to demonstrate the importance of the suggested correction to the Jacobian. The program developed for this purpose evaluates the resulting angular velocity vector for a few sets of time-varying inputs, for both the original Jacobian developed for the ideal case, and for the corrected Jacobian suggested in this section. The magnitude and the direction of the resulting angular velocity vectors are evaluated and compared for both cases. The reference platform for the numerical experiment is an Atlas platform as described in the previous section, with an elevation angle of 40°, and the following design parameters:

$$R = 15 \text{ cm},\ r_r = 4.85 \text{ mm},\ d = 12.5 \text{ mm},\ r = 25 \text{ mm},\ 2N = 16.$$

The input is the set of angular speeds of the three omnidirectional wheels, prescribed to illustrate a variety of cases. The inputs are described in Table 2.1.

The prescribed input was selected to demonstrate cases with various ratios among the omnidirectional wheels's angular speeds. The first step was intended for creating a slight misalignment such that the experiment had a starting point where not all omnidirectional wheels were in the same phase.

Figure 2.7 shows the orientation error [°] of the angular velocity vector $\vec{\Omega}$ of the sphere and the error [%] in the magnitude of $\vec{\Omega}$. The orientation error is defined as the angle between

Table 2.1: Prescribed omnidirectional wheel inputs.

time [s]	ω_1 [rad/s]	ω_2 [rad/s]	ω_3 [rad/s]
0	1	0	0
0.1	1	1	1
1	1	2	2
2	2	1	1
3	2	1	2
4	0	0	1
5	1	0	0
6	0	1	0
7	1	2	3
8	2	1	3
9	1	3	2
10	2	3	1
11	3	1	2
12	3	2	1
13	0	0	0

the two resulting angular velocity vectors:

$$\epsilon = \cos^{-1}\left(\frac{\tilde{\mathbf{\Omega}}_{\mathbf{id}} \cdot \tilde{\mathbf{\Omega}}}{|\tilde{\mathbf{\Omega}}_{\mathbf{id}}||\tilde{\mathbf{\Omega}}|}\right) \tag{2.77}$$

where $\vec{\Omega}_{id}$ is the resultant angular velocity vector for the ideal single-row case. It is clear from the results that there are both magnitude and direction errors that are generally non-zero. The magnitude error peaks at 3.8%, for the selected input set. The angular deviation, which is the angle between the angular velocity vector of the sphere, calculated using the augmented Jacobian, and the angular velocity vector of the sphere calculated using the ideal-case Jacobian, as demonstrated in Equation 2.77 is also generally non-zero, and peaks at an angle of 3.2°. The zero case only exists when the prescribed angular speeds of all three omnidirectional wheels are the same, which translates to a rotation about the Z-axis of the sphere, as long as all omnidirectional wheels are touching with the same race. The initial intentional misalignment was used to prevent this unique case, and demonstrate the more

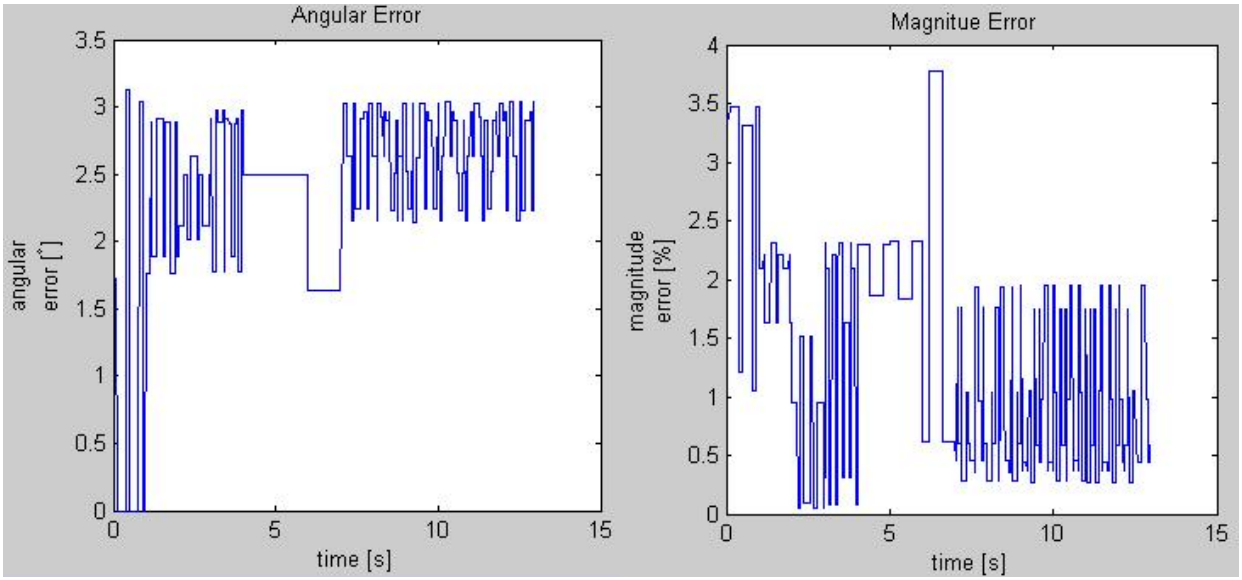

Figure 2.7: Errors in angle and magnitude of the sphere angular velocity vector.

general case for which the augmented Jacobian presented above was developed.

A closer look at Equations 2.66 and 2.72 from the examples reveals that one can generalize the Jacobian of a system comprising of three identical dual-row omnidirectional wheels:

$$\mathbf{J}_{lmn}^{-1} = \frac{R}{r}\frac{1}{2(R+r_r)}\left\{\sqrt{4(R+r_r)^2-d^2}\begin{bmatrix}\hat{\Omega}_1^T\\ \hat{\Omega}_2^T\\ \hat{\Omega}_3^T\end{bmatrix} - d\begin{bmatrix}(-1)^l\hat{R}_1^T\\ (-1)^m\hat{R}_2^T\\ (-1)^n\hat{R}_3^T\end{bmatrix}\right\} \quad ...l,m,n=1,2 \quad . \tag{2.78}$$

Since $\hat{R}_i$ is orthogonal to $\hat{\Omega}_i$ by definition, the only way to avoid the directional error of $\vec{\Omega}$ is to set $d=0$, thereby reducing the solution to a single row.

The dual-race omnidirectional wheel solution addresses the problem of obtaining continuous contact with the sphere; however, it introduces a shift in the location of the contact points on the sphere, thereby introducing complications in the kinematics of the system that are shown to produce significant errors both in magnitude and in direction of the angular

velocity vector of the sphere as detailed in [81], and thus possibly control issues.

This problem could theoretically be avoided by splitting the dual-row omnidirectional wheels, having the two rows mounted on separate races that touch on antipodal points [1] on the sphere. Antipodal points on the sphere would have the same velocity in the actuation direction. For a contact point $\tilde{\mathbf{R}}_\mathbf{1}$ with actuation direction $\hat{v}_1$ we have the velocity $\tilde{\mathbf{V}}_\mathbf{1} = \tilde{\mathbf{\Omega}} \times \tilde{\mathbf{R}}_\mathbf{1}$. It is clear that for the point located on the same great circle but angularly offset by 180°, $\tilde{\mathbf{R}}_\mathbf{2} = -\tilde{\mathbf{R}}_\mathbf{1}$ and the velocity $\tilde{\mathbf{V}}_\mathbf{2} = \tilde{\mathbf{\Omega}} \times \tilde{\mathbf{R}}_\mathbf{2} = -\tilde{\mathbf{\Omega}} \times \tilde{\mathbf{R}}_\mathbf{1} = -\tilde{\mathbf{V}}_\mathbf{1}$ that is, the same magnitude but opposite in direction. Thus, setting the actuation direction to be $\hat{v}_2 = -\hat{v}_1$, results in an equivalent second row at $\tilde{\mathbf{R}}_\mathbf{2}$ enslaved to the omnidirectional wheel at $\tilde{\mathbf{R}}_\mathbf{1}$. All that is left is to arrange the omnidirectional wheels such that the rollers are synchronized between the two races, a relatively easy task since the actuation speeds for both wheels are identical and they could, in principle, be actuated by the same motor.

Another attempt to combine the benefits of the single and dual row designs, driven by intuition, is to have triple-race omnidirectional wheels, as shown in Figure 2.8. Here, the two external races touch the sphere at the same time, alternating with the centre race. The idea is to create an equivalent or effective contact point that is exactly centred in between the two external races, hence generating continuous contact with the sphere in the same effective contact point.

Utilizing three dual-race omnidirectional wheels, instead of single-race ones, changes the kinematics due to the shift of contact points when shifting between the two races of each omnidirectional wheel occurs, as presented in [81]. However, the problem remains one with $n = 3$, since at any instance there are exactly three effective contact points.

[1] points that lie on the same great circle and are diametrically opposed.

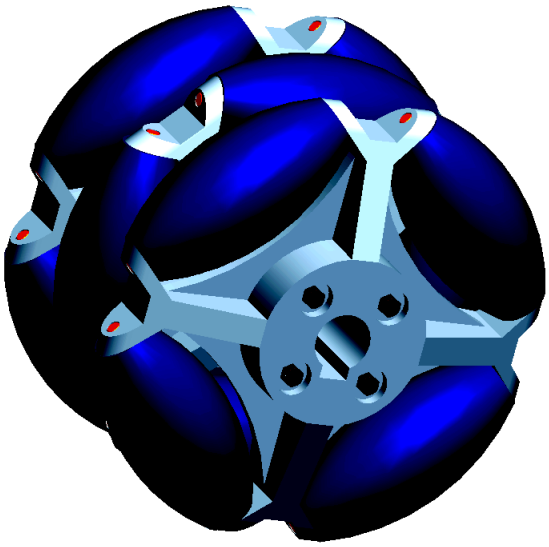

Figure 2.8: A triple-race omnidirectional wheel.

2.2.3 Triple-race Omnidirectional Wheels

Utilizing three triple-race omnidirectional wheels, however, is a completely different case. Triple-race omnidirectional wheels alternate between one point of contact when the centre race is in contact with the sphere, and two points of contact when the two outer races are in contact with the sphere simultaneously. This in turn, creates numerous combinations, where anywhere between three and six contact points (i.e., $n = 3, 4, 5, 6$) could exist at any given time, and where all combinations would be encountered during typical operation. However, this case has simplifying constraints, since any two simultaneous contact points belonging to a single omnidirectional wheel, share the same r, ω, and $\hat{v}$. This allows for the simplification

of the equations. In the worst case scenario, where $n = 6$, the kinematics are given by

$$\begin{bmatrix} \hat{\Omega}_{11}^T \\ \hat{\Omega}_{12}^T \\ \hat{\Omega}_{21}^T \\ \hat{\Omega}_{22}^T \\ \hat{\Omega}_{31}^T \\ \hat{\Omega}_{32}^T \end{bmatrix} \tilde{\boldsymbol{\Omega}} = \frac{1}{R} \begin{bmatrix} r_1 & 0 & 0 & 0 & 0 & 0 \\ 0 & r_1 & 0 & 0 & 0 & 0 \\ 0 & 0 & r_2 & 0 & 0 & 0 \\ 0 & 0 & 0 & r_2 & 0 & 0 \\ 0 & 0 & 0 & 0 & r_3 & 0 \\ 0 & 0 & 0 & 0 & 0 & r_3 \end{bmatrix} \begin{Bmatrix} \omega_1 \\ \omega_1 \\ \omega_2 \\ \omega_2 \\ \omega_3 \\ \omega_3 \end{Bmatrix} \tag{2.79}$$

where

$$\hat{\Omega}_{ij} = \hat{R}_{ij} \times \hat{v}_i \tag{2.80}$$

and $\hat{R_{ij}}$ is a unit vector in the direction of the contact point j of omnidirectional wheel i.

As presented above, this kind of overdetermined equation set is usually solved with an approximation method. However, using such an approach leads to a solution that is missing the point of the design: to achieve motion that is equivalent to that induced by the contact point of the centre race. It should be expected that any set of two equations belonging to the same omnidirectional wheel will yield a result in the same direction as the equivalent result for the single-race case. While this may be accomplished by utilizing the results from the single-race analysis, the equations are still over constrained. Solutions can only be approximated, which implies that the slip-free condition cannot be satisfied. Thus, without being able to achieve slip-free conditions, the kinetics of the system must be taken into consideration, and the true motion cannot be determined using kinematics alone.

Rearranging the terms in Equation 2.79, yields another way to look at the problem:

$$\begin{bmatrix} \hat{\Omega}_{11}^T & -\frac{r_1}{R} & 0 & 0 \\ \hat{\Omega}_{12}^T & -\frac{r_1}{R} & 0 & 0 \\ \hat{\Omega}_{21}^T & 0 & -\frac{r_2}{R} & 0 \\ \hat{\Omega}_{22}^T & 0 & -\frac{r_2}{R} & 0 \\ \hat{\Omega}_{31}^T & 0 & 0 & -\frac{r_3}{R} \\ \hat{\Omega}_{32}^T & 0 & 0 & -\frac{r_3}{R} \end{bmatrix} \begin{Bmatrix} \Omega_x \\ \Omega_y \\ \Omega_z \\ \omega_1 \\ \omega_2 \\ \omega_3 \end{Bmatrix} = \vec{0} \quad . \tag{2.81}$$

This representation allows, once again, examining a given design. In order to obtain a nontrivial solution, it is required for the determinant of the matrix in Equation 2.81 to be zero. Once this is established, there could be sets of allowable solutions $\{\tilde{\mathbf{\Omega}}, \tilde{\omega}\}$ that yield slip-free conditions.

Gaussian elimination further simplifies the equations, yielding:

$$\begin{bmatrix} \hat{\Omega}_{11}^T & -\frac{r_1}{R} & 0 & 0 \\ \hat{\Omega}_{12}^T - \hat{\Omega}_{11}^T & 0 & 0 & 0 \\ \hat{\Omega}_{21}^T & 0 & -\frac{r_2}{R} & 0 \\ \hat{\Omega}_{22}^T - \hat{\Omega}_{21}^T & 0 & 0 & 0 \\ \hat{\Omega}_{31}^T & 0 & 0 & -\frac{r_3}{R} \\ \hat{\Omega}_{32}^T - \hat{\Omega}_{31}^T & 0 & 0 & 0 \end{bmatrix} \begin{Bmatrix} \Omega_x \\ \Omega_y \\ \Omega_z \\ \omega_1 \\ \omega_2 \\ \omega_3 \end{Bmatrix} = \vec{0} \quad . \tag{2.82}$$

Rows 1, 3, and 5 of the coefficient matrix of Equation 2.82 are clearly linearly independent with respect to each other, and with respect to rows 2, 4, and 6. All that remains is to

ensure that the determinant of the smaller (3x3) matrix

$$\begin{bmatrix} \hat{\Omega}_{12}^T - \hat{\Omega}_{11}^T \\ \hat{\Omega}_{22}^T - \hat{\Omega}_{21}^T \\ \hat{\Omega}_{32}^T - \hat{\Omega}_{31}^T \end{bmatrix} \tag{2.83}$$

is zero. Remembering that $\hat{\Omega}_{ij} = \hat{R}_{ij} \times \hat{v}_i$, the rows of the matrix in Equation 2.83 may be rewritten as:

$$\hat{\Omega}_{i2} - \hat{\Omega}_{i1} = (\hat{R}_{i2} - \hat{R}_{i1}) \times \hat{v}_i \quad . \tag{2.84}$$

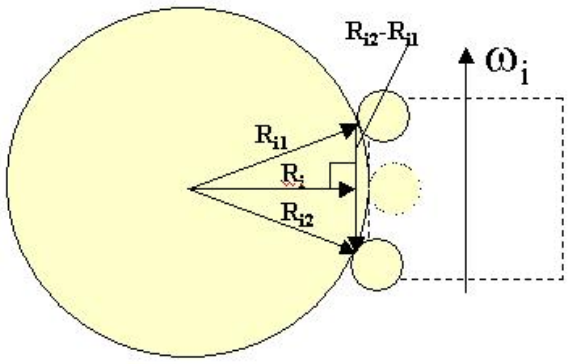

Figure 2.9: Contact point geometry when two races touch the sphere simultaneously.

From the geometry of the problem, illustrated in Figure 2.9, it is observed that the resultant vector $\hat{R}_{i2} - \hat{R}_{i1}$ is perpendicular to both $\hat{v}_i$ and $\hat{R}_i$. Thus, it is concluded that the result of Equation 2.84 is a vector in the direction of $\hat{R}_i$. Hence, the matrix above can be rewritten as:

$$\begin{bmatrix} \hat{R}_1^T \\ \hat{R}_2^T \\ \hat{R}_3^T \end{bmatrix} \quad . \tag{2.85}$$

The no-slip condition now becomes a requirement on the position vectors of the effective contact points to be linearly dependent. Finally, combining this requirement with the no-slip requirement on the centre row combination, which was shown to be that the matrix

$$\begin{bmatrix} \hat{\Omega}_1^T \\ \hat{\Omega}_2^T \\ \hat{\Omega}_3^T \end{bmatrix} \tag{2.86}$$

be non-singular; denotes the need for $\hat{R}_i$ to be linearly dependent while $\hat{\Omega}_i$ are linearly independent.

Once again, the two benchmark examples used for the single-race case are utilized to illustrate the differences between the kinematic behaviour of the triple-race omnidirectional wheels and the single-race ones. These are both architectures that satisfy the necessary no-slip condition for the single-race case. However, it is shown here that the additional requirements are not met; thus these configurations no longer yield no-slip conditions. These two benchmark examples are then followed with an example that does meet the new criteria, and finally, an example with six separate omnidirectional wheels is presented illustrating both the evaluation of the slip factor and the master-slave approach.

The Orthogonal Case

The following example examines the benchmark architecture, illustrated in Figure 2.2 and presented earlier for single-race and dual-race omnidirectional wheels, that satisfies the necessary condition for these cases, and indeed yields zero kinematic slip. While this architecture is fairly simple, it provides a good benchmark to demonstrate the principles, and point out the problems without the need for cumbersome expressions. For simplicity, and without loss of generality, the global coordinate frame is the one in Figure 2.2. This allows all calculations

to be performed directly in the global coordinate frame.

The sphere has radius R, and each of the omnidirectional wheels has radius r. Thus, the position vectors of the three contact points are:

$$\tilde{\mathbf{R}}_{\mathbf{1}} = R\hat{\imath} \; ; \quad \tilde{\mathbf{R}}_{\mathbf{2}} = R\hat{\jmath} \; ; \quad \tilde{\mathbf{R}}_{\mathbf{3}} = R\hat{k} \tag{2.87}$$

and the position vectors of the contact points with respect to the omnidirectional wheel centres of rotation are:

$$\tilde{\mathbf{r}}_{\mathbf{1}} = -r\hat{\imath} \; ; \quad \tilde{\mathbf{r}}_{\mathbf{2}} = -r\hat{\jmath} \; ; \quad \tilde{\mathbf{r}}_{\mathbf{3}} = -r\hat{k} \quad . \tag{2.88}$$

The angular velocities of the omnidirectional wheels are:

$$\tilde{\omega}_{\mathbf{1}} = \omega_1\hat{\jmath} \; ; \quad \tilde{\omega}_{\mathbf{2}} = \omega_2\hat{k} \; ; \quad \tilde{\omega}_{\mathbf{3}} = \omega_3\hat{\imath} \tag{2.89}$$

and therefore the velocities they induce on the sphere at the contact points are

$$\begin{aligned} \tilde{\mathbf{V}}_{\mathbf{1}} &= \tilde{\omega}_{\mathbf{1}} \times \tilde{\mathbf{r}}_{\mathbf{1}} = \omega_1 r\hat{k} \quad , \\ \tilde{\mathbf{V}}_{\mathbf{2}} &= \tilde{\omega}_{\mathbf{2}} \times \tilde{\mathbf{r}}_{\mathbf{2}} = \omega_2 r\hat{\imath} \quad , \\ \tilde{\mathbf{V}}_{\mathbf{3}} &= \tilde{\omega}_{\mathbf{3}} \times \tilde{\mathbf{r}}_{\mathbf{3}} = \omega_3 r\hat{\jmath} \quad , \end{aligned} \tag{2.90}$$

respectively. These velocities create the three components of angular velocity of the sphere:

$$\hat{\mathbf{\Omega}}_{\mathbf{1}} = \hat{\imath} \times \hat{k} = -\hat{\jmath} \; ; \quad \hat{\mathbf{\Omega}}_{\mathbf{2}} = \hat{\jmath} \times \hat{\imath} = -\hat{k} \; ; \quad \hat{\mathbf{\Omega}}_{\mathbf{3}} = \hat{k} \times \hat{\jmath} = -\hat{\imath} \quad . \tag{2.91}$$

It is clear now that these are mutually orthogonal, since

$$\hat{\mathbf{\Omega}}_\mathbf{i} \cdot \hat{\mathbf{\Omega}}_\mathbf{j} = 0 \quad ...i \neq j \qquad . \tag{2.92}$$

This could alternatively be shown directly by evaluating the Jacobian of the system as:

$$\mathbf{J} = \frac{r}{R}\begin{bmatrix} 0 & -1 & 0 \\ 0 & 0 & -1 \\ -1 & 0 & 0 \end{bmatrix}^{-1} = \frac{r}{R}\begin{bmatrix} 0 & 0 & -1 \\ -1 & 0 & 0 \\ 0 & -1 & 0 \end{bmatrix} \tag{2.93}$$

noting that the rows are linearly independent as required for the single-row case. It is obvious, however, that this case does not simultaneously fulfill the requirement for $n = 6$.

The Atlas Sphere

The second benchmark configuration is the Atlas sphere presented earlier in Section 3.2.1. To generalize the equilateral configuration, an arbitrary elevation angle θ will be used. The configuration is presented in Figure 2.3.

In this case

$$\begin{aligned} \tilde{\mathbf{R}}_\mathbf{1} &= R(\cos\theta\hat{\imath} - \sin\theta\hat{k}) \qquad , \\ \tilde{\mathbf{R}}_\mathbf{2} &= R(-\frac{1}{2}\cos\theta\hat{\imath} - \frac{\sqrt{3}}{2}\cos\theta\hat{\jmath} - \sin\theta\hat{k}) \qquad , \\ \tilde{\mathbf{R}}_\mathbf{3} &= R(-\frac{1}{2}\cos\theta\hat{\imath} + \frac{\sqrt{3}}{2}\cos\theta\hat{\jmath} - \sin\theta\hat{k}) \qquad , \end{aligned} \tag{2.94}$$

and the contact point velocities are

$$\begin{aligned}
\tilde{\mathbf{V}}_{\mathbf{1}} &= -\omega_1 r\hat{\jmath} \quad , \\
\tilde{\mathbf{V}}_{\mathbf{2}} &= \omega_2 r(-\frac{\sqrt{3}}{2}\hat{\imath} + \frac{1}{2}\hat{\jmath}) \quad , \\
\tilde{\mathbf{V}}_{\mathbf{3}} &= \omega_3 r(\frac{\sqrt{3}}{2}\hat{\imath} + \frac{1}{2}\hat{\jmath}) \quad ,
\end{aligned} \tag{2.95}$$

as shown in [86]. These yield:

$$\begin{bmatrix} \hat{\mathbf{\Omega}}_{\mathbf{1}}^{\mathbf{T}} \\ \hat{\mathbf{\Omega}}_{\mathbf{2}}^{\mathbf{T}} \\ \hat{\mathbf{\Omega}}_{\mathbf{3}}^{\mathbf{T}} \end{bmatrix} = \begin{bmatrix} -\sin\theta & 0 & -\cos\theta \\ \frac{1}{2}\sin\theta & \frac{\sqrt{3}}{2}\sin\theta & -\cos\theta \\ \frac{1}{2}\sin\theta & -\frac{\sqrt{3}}{2}\sin\theta & -\cos\theta \end{bmatrix} \quad . \tag{2.96}$$

The determinant of this matrix will be zero for

$$\frac{3\sqrt{3}}{2}\sin^2\theta\cos\theta = 0 \quad . \tag{2.97}$$

So, the only singularities would be for $\theta = 0$ and $\theta = \pm 90°$. For all other cases, the Jacobian can be evaluated. In this case,

$$\mathbf{J} = \frac{r}{R}\begin{bmatrix} -\sin\theta & 0 & -\cos\theta \\ \frac{1}{2}\sin\theta & \frac{\sqrt{3}}{2}\sin\theta & -\cos\theta \\ \frac{1}{2}\sin\theta & -\frac{\sqrt{3}}{2}\sin\theta & -\cos\theta \end{bmatrix}^{-1} = \frac{r}{3R}\begin{bmatrix} -2\csc\theta & \csc\theta & \csc\theta \\ 0 & \sqrt{3}\csc\theta & -\sqrt{3}\csc\theta \\ -\sec\theta & -\sec\theta & -\sec\theta \end{bmatrix} \quad . \tag{2.98}$$

Thereby showing the direct relationship between omnidirectional wheel speeds and sphere angular velocity without kinematic slip for the single-row case. It is obvious once again that this case does not simultaneously fulfill the requirement for $n = 6$.

The Collinear Case

An example that conforms to both conditions of the triple-race case can easily be constructed.

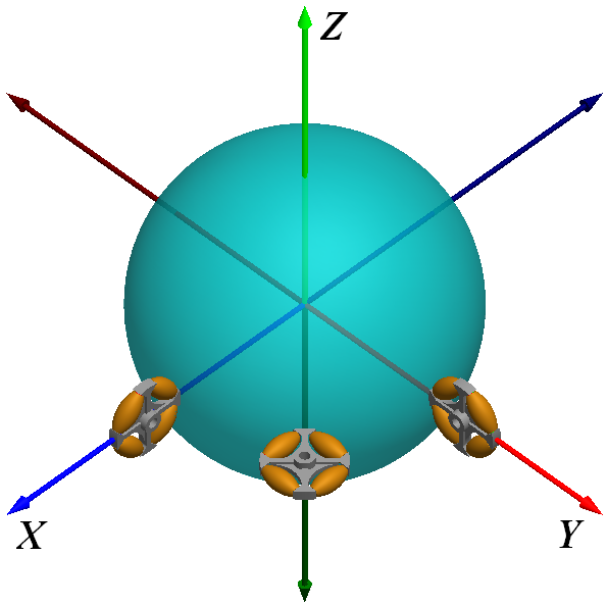

Figure 2.10: A configuration that allows for slip-free conditions.

In the configuration shown in Figure 2.10 we have:

$$\hat{R}_1 = \hat{\imath}\ ; \quad \hat{R}_2 = \frac{\sqrt{2}}{2}\hat{\imath} + \frac{\sqrt{2}}{2}\hat{\jmath}\ ; \quad \hat{R}_3 = \hat{\jmath} \tag{2.99}$$

$$\hat{\Omega}_1 = \hat{\jmath}\ ; \quad \hat{\Omega}_2 = \hat{k}\ ; \quad \hat{\Omega}_3 = \hat{\imath} \quad . \tag{2.100}$$

It is clear that the three induced angular velocities are linearly independent, while all position unit vectors lie in the XY plane, thus being linearly dependent.

Orthogonal Case with Six Omnidirectional Wheels

This example examines a case where six omnidirectional wheels are employed. First, arbitrary values for the speeds of the omnidirectional wheels will be assigned and the slip factor will be evaluated; then the same scenario will be investigated using the master-slave concept.

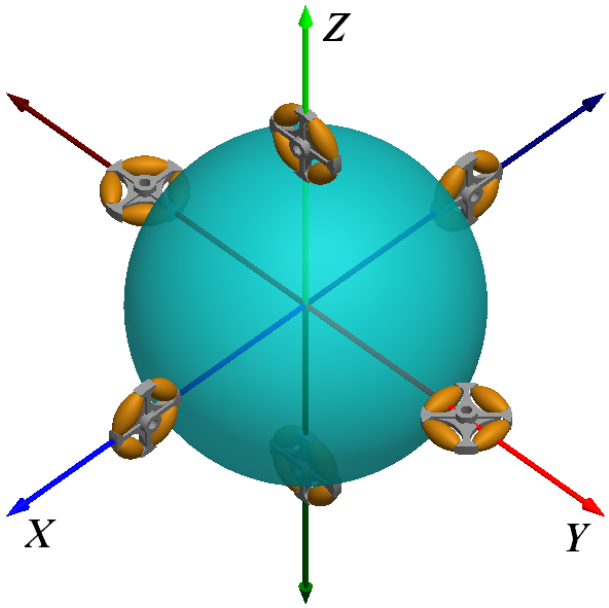

Figure 2.11: Kinematic architecture for the orthogonal case with six omnidirectional wheels.

Here, the position vectors of the six contact points, as shown in Figure 2.11 are:

$$\begin{aligned} \tilde{\mathbf{R}}_1 = R\hat{\imath}\ , \quad \tilde{\mathbf{R}}_2 = R\hat{\jmath}\ , \quad \tilde{\mathbf{R}}_3 = R\hat{k}\ , \\ \tilde{\mathbf{R}}_4 = -R\hat{\imath}\ , \quad \tilde{\mathbf{R}}_5 = -R\hat{\jmath}\ , \quad \tilde{\mathbf{R}}_6 = -R\hat{k}\ , \end{aligned} \tag{2.101}$$

and the position vectors of the contact points with respect to the omnidirectional wheel centres of rotation are:

$$\begin{aligned} \tilde{\mathbf{r}}_1 = -r\hat{\imath}; \quad \tilde{\mathbf{r}}_2 = -r\hat{\jmath}; \quad \tilde{\mathbf{r}}_3 = -r\hat{k} \\ \tilde{\mathbf{r}}_4 = r\hat{\imath}; \quad \tilde{\mathbf{r}}_5 = r\hat{\jmath}; \quad \tilde{\mathbf{r}}_6 = r\hat{k} \quad . \end{aligned} \tag{2.102}$$

The angular velocities of the omnidirectional wheels are:

$$\tilde{\omega}_{\mathbf{1}} = \omega_1 \hat{\jmath}; \quad \tilde{\omega}_{\mathbf{2}} = \omega_2 \hat{k}; \quad \tilde{\omega}_{\mathbf{3}} = \omega_3 \hat{\imath}$$
$$\tilde{\omega}_{\mathbf{4}} = \omega_4 \hat{\jmath}; \quad \tilde{\omega}_{\mathbf{5}} = \omega_5 \hat{k}; \quad \tilde{\omega}_{\mathbf{6}} = \omega_6 \hat{\imath} \quad . \tag{2.103}$$

Therefore the velocities they induce on the sphere at the contact points are:

$$\begin{aligned}
\tilde{\mathbf{V}}_{\mathbf{1}} &= \tilde{\omega}_{\mathbf{1}} \times \tilde{\mathbf{r}}_{\mathbf{1}} = \omega_1 r \hat{k} \quad ; \\
\tilde{\mathbf{V}}_{\mathbf{2}} &= \tilde{\omega}_{\mathbf{2}} \times \tilde{\mathbf{r}}_{\mathbf{2}} = \omega_2 r \hat{\imath} \quad ; \\
\tilde{\mathbf{V}}_{\mathbf{3}} &= \tilde{\omega}_{\mathbf{3}} \times \tilde{\mathbf{r}}_{\mathbf{3}} = \omega_3 r \hat{\jmath} \quad ; \\
\tilde{\mathbf{V}}_{\mathbf{4}} &= \tilde{\omega}_{\mathbf{4}} \times \tilde{\mathbf{r}}_{\mathbf{4}} = -\omega_4 r \hat{k} \quad ; \\
\tilde{\mathbf{V}}_{\mathbf{5}} &= \tilde{\omega}_{\mathbf{5}} \times \tilde{\mathbf{r}}_{\mathbf{5}} = -\omega_5 r \hat{\imath} \quad ; \\
\tilde{\mathbf{V}}_{\mathbf{6}} &= \tilde{\omega}_{\mathbf{6}} \times \tilde{\mathbf{r}}_{\mathbf{6}} = -\omega_6 r \hat{\jmath} \quad .
\end{aligned} \tag{2.104}$$

These velocities create the six components of angular velocity of the sphere:

$$\begin{aligned}
\hat{\mathbf{\Omega}}_{\mathbf{1}} &= \hat{\imath} \times \hat{k} = -\hat{\jmath} \quad ; \\
\hat{\mathbf{\Omega}}_{\mathbf{2}} &= \hat{\jmath} \times \hat{\imath} = -\hat{k} \quad ; \\
\hat{\mathbf{\Omega}}_{\mathbf{3}} &= \hat{k} \times \hat{\jmath} = -\hat{\imath} \quad ; \\
\hat{\mathbf{\Omega}}_{\mathbf{4}} &= -\hat{\imath} \times -\hat{k} = -\hat{\jmath} \quad ; \\
\hat{\mathbf{\Omega}}_{\mathbf{5}} &= -\hat{\jmath} \times -\hat{\imath} = -\hat{k} \quad ; \\
\hat{\mathbf{\Omega}}_{\mathbf{6}} &= -\hat{k} \times -\hat{\jmath} = -\hat{\imath} \quad .
\end{aligned} \tag{2.105}$$

Thus, we have:

$$\left[\boldsymbol{\Omega}^{\mathbf{T}}\right] = \begin{bmatrix} 0 & -1 & 0 \\ 0 & 0 & -1 \\ -1 & 0 & 0 \\ 0 & -1 & 0 \\ 0 & 0 & -1 \\ -1 & 0 & 0 \end{bmatrix} \tag{2.106}$$

and the Jacobian becomes:

$$\mathbf{J_{ls}} = \frac{r}{R} \begin{bmatrix} 0 & 0 & -0.5 & 0 & 0 & -0.5 \\ -0.5 & 0 & 0 & -0.5 & 0 & 0 \\ 0 & -0.5 & 0 & 0 & -0.5 & 0 \end{bmatrix} \quad . \tag{2.107}$$

This leads to the slip factor for the i^{th} wheel being:

$$S_i = \frac{1}{2}\left(1 - \frac{\omega_{((i+2) \bmod 6)+1}}{\omega_i}\right) \quad i = 1, 2, ..., 6 \quad . \tag{2.108}$$

Thus, the only way to obtain zero slip at all points requires:

$$\omega_{((i+2) \bmod 6)+1} = \omega_i \quad \forall i \tag{2.109}$$

In other words, to enslave omnidirectional wheels $4, 5$, and 6 to omnidirectional wheels $1, 2$, and 3 or vice versa. Any other angular velocity combination would yield non-zero slip. For example, consider

$$\omega_1 = \omega_2 = \omega_3 = 1, \quad \omega_4 = \omega_5 = \omega_6 = 1.5 \tag{2.110}$$

resulting in a slip factor of $S = 0.52$.

2.2.4 Mecanum Wheels

Mecanum wheels, also known as Swedish wheels or Ilonators after their Swedish inventor [44], are similar to single-race omnidirectional wheels only the rollers have a 45° angle relative to the rotation axis of the wheel, as shown in Figure 1.7. Such a design allows for a smoother interface between the rollers and the sphere, thus potentially reducing induced vibration. Since the axes of the rollers and the rotation axis of the wheel are no longer orthogonal, the effects of the rollers's spin needs to be considered in the kinematics of the system. Thus, the kinematics will be modified to include rollers at any angle, generalizing the previous expressions even further. As in the standard omnidirectional wheel case, the contact point velocity on the sphere side of the sphere/omnidirectional wheel interface is

$$\tilde{\mathbf{V}}'_{\mathbf{i}} = \tilde{\boldsymbol{\Omega}} \times \tilde{\mathbf{R}}_{\mathbf{i}} \tag{2.111}$$

where subscript i refers to a specific omnidirectional wheel. The velocity of the contact point on the omnidirectional wheel side, is once again broken into two components: one in the actuation direction, and the other in the direction of the free-roll of the castors

$$\tilde{\mathbf{V}}_{\mathbf{i}} = V_i \hat{\mathbf{v}}_{\mathbf{i}} + V_{ri} \hat{\mathbf{v}}_{\mathbf{ri}} \quad . \tag{2.112}$$

However, unlike the standard case, the $\hat{\mathbf{v}}_{\mathbf{ri}}$ direction is not orthogonal to the actuation direction, but may be expressed as

$$\hat{\mathbf{v}}_{\mathbf{ri}} = \cos\alpha \hat{\mathbf{v}}_{\mathbf{i}} + \sin\alpha \hat{\mathbf{v}}_{\mathbf{ni}} \tag{2.113}$$

where $\hat{\mathbf{v}}_{\mathbf{ni}}$ is a direction normal to the actuation direction, and α is the offset angle of the rollers, as illustrated in Figure 2.12.

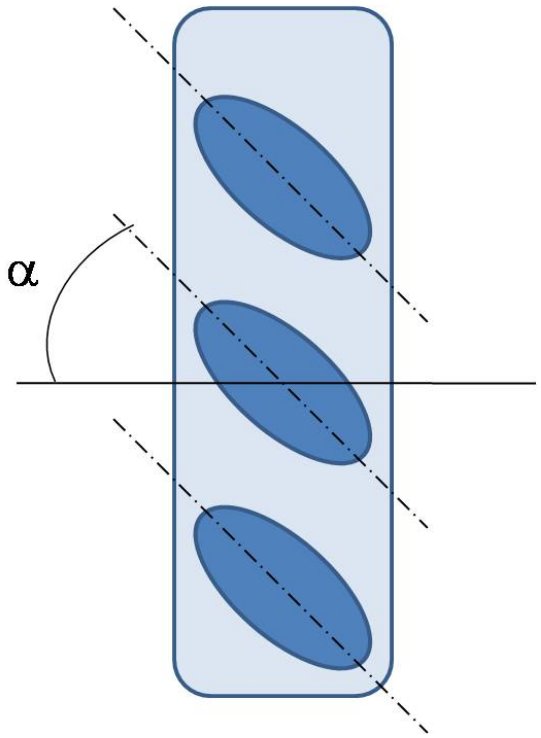

Figure 2.12: Mecanum wheel rollers offset angle.

The no-slip requirement then becomes

$$(\tilde{\mathbf{\Omega}} \times \tilde{\mathbf{R}}_{\mathbf{i}}) \cdot \hat{\mathbf{v}}_{\mathbf{i}} = (\tilde{\mathbf{R}}_{\mathbf{i}} \times \hat{\mathbf{v}}_{\mathbf{i}}) \cdot \tilde{\mathbf{\Omega}} = \tilde{\mathbf{V}}_{\mathbf{i}} \cdot \hat{\mathbf{v}}_{\mathbf{i}} \tag{2.114}$$

thus,

$$R\hat{\Omega}_i \cdot \tilde{\mathbf{\Omega}} = \omega_i r_i + V_{ri} \cos\alpha \quad . \tag{2.115}$$

In the normal direction the relationship is

$$(\tilde{\mathbf{\Omega}} \times \tilde{\mathbf{R}}_{\mathbf{i}}) \cdot \hat{\mathbf{v}}_{\mathbf{ni}} = (\tilde{\mathbf{R}}_{\mathbf{i}} \times \hat{\mathbf{v}}_{\mathbf{ni}}) \cdot \tilde{\mathbf{\Omega}} = V_{ri} \sin\alpha \quad . \tag{2.116}$$

Combining the latter two equations yields

$$R\hat{\Omega}_i \cdot \tilde{\mathbf{\Omega}} = \omega_i r_i + \frac{R}{\tan\alpha}(\hat{R}_i \times \hat{v}_{ni}) \cdot \tilde{\mathbf{\Omega}} \quad . \tag{2.117}$$

Finally, for each contact point:

$$(\hat{\Omega}_i + \frac{1}{\tan\alpha}\hat{v}_i) \cdot \tilde{\mathbf{\Omega}} = \frac{r_i}{R}\omega_i \quad . \tag{2.118}$$

Therefore, for three contact points, the kinematics may be expressed as,

$$\begin{bmatrix} \hat{\mathbf{\Omega}}_\mathbf{1}^\mathbf{T} + \frac{1}{\tan\alpha}\hat{\mathbf{v}}_\mathbf{1}^\mathbf{T} \\ \hat{\mathbf{\Omega}}_\mathbf{2}^\mathbf{T} + \frac{1}{\tan\alpha}\hat{\mathbf{v}}_\mathbf{2}^\mathbf{T} \\ \hat{\mathbf{\Omega}}_\mathbf{3}^\mathbf{T} + \frac{1}{\tan\alpha}\hat{\mathbf{v}}_\mathbf{3}^\mathbf{T} \end{bmatrix} \tilde{\mathbf{\Omega}} = \frac{1}{R}\begin{bmatrix} r_1 & 0 & 0 \\ 0 & r_2 & 0 \\ 0 & 0 & r_3 \end{bmatrix} \begin{Bmatrix} \omega_1 \\ \omega_2 \\ \omega_3 \end{Bmatrix} \tag{2.119}$$

or in Jacobian form

$$\tilde{\mathbf{\Omega}} = \mathbf{J}\tilde{\omega} \quad , \tag{2.120}$$

where

$$\mathbf{J} = \frac{1}{R}\begin{bmatrix} \hat{\mathbf{\Omega}}_\mathbf{1}^\mathbf{T} + \frac{1}{\tan\alpha}\hat{\mathbf{v}}_\mathbf{1}^\mathbf{T} \\ \hat{\mathbf{\Omega}}_\mathbf{2}^\mathbf{T} + \frac{1}{\tan\alpha}\hat{\mathbf{v}}_\mathbf{2}^\mathbf{T} \\ \hat{\mathbf{\Omega}}_\mathbf{3}^\mathbf{T} + \frac{1}{\tan\alpha}\hat{\mathbf{v}}_\mathbf{3}^\mathbf{T} \end{bmatrix}^{-1} \begin{bmatrix} r_1 & 0 & 0 \\ 0 & r_2 & 0 \\ 0 & 0 & r_3 \end{bmatrix} \quad . \tag{2.121}$$

Equation 2.121 is a more general version of Equation 2.19 and converges to it for $\alpha = 90°$ which is the case for the standard omnidirectional wheels in use for developing Equation 2.19.

Since the most common Mecanum wheels utilize an offset angle of $\alpha = 45°$, the following

two benchmark examples will use 45° to demonstrate the effect. However, the expressions will first be developed generally. For the angle $\alpha = 45°$, $\frac{1}{\tan\alpha} = 1$, thus, combining with the choice of three identical omnidirectional wheels with radius r, the expression becomes

$$\mathbf{J} = \frac{r}{R} \begin{bmatrix} \hat{\mathbf{\Omega}}_\mathbf{1}^\mathbf{T} + \hat{\mathbf{v}}_\mathbf{1}^\mathbf{T} \\ \hat{\mathbf{\Omega}}_\mathbf{2}^\mathbf{T} + \hat{\mathbf{v}}_\mathbf{2}^\mathbf{T} \\ \hat{\mathbf{\Omega}}_\mathbf{3}^\mathbf{T} + \hat{\mathbf{v}}_\mathbf{3}^\mathbf{T} \end{bmatrix}^{-1} \quad . \tag{2.122}$$

The Orthogonal Case

Here, as previously presented, the configuration is shown in Figure 2.2. In addition, the actuation directions and unit induced angular velocity vectors were shown to be

$$\begin{aligned} \hat{v}_1 &= \hat{k} \quad , \\ \hat{v}_2 &= \hat{\imath} \quad , \\ \hat{v}_3 &= \hat{\jmath} \quad , \end{aligned} \tag{2.123}$$

and

$$\begin{aligned} \hat{\Omega}_1 &= -\hat{\jmath} \quad , \\ \hat{\Omega}_2 &= -\hat{k} \quad , \\ \hat{\Omega}_3 &= -\hat{\imath} \quad , \end{aligned} \tag{2.124}$$

respectively. Thus,

$$\begin{aligned}
\hat{\Omega}_1 + \cot\alpha\hat{v}_1 &= -\hat{\jmath} + \cot\alpha\hat{k} \quad , \\
\hat{\Omega}_2 + \cot\alpha\hat{v}_2 &= -\hat{k} + \cot\alpha\hat{\imath} \quad , \\
\hat{\Omega}_3 + \cot\alpha\hat{v}_3 &= -\hat{\imath} + \cot\alpha\hat{\jmath} \quad . \qquad (2.125)
\end{aligned}$$

The no-slip condition is

$$\det \begin{bmatrix} 0 & -1 & \cot\alpha \\ \cot\alpha & 0 & -1 \\ -1 & \cot\alpha & 0 \end{bmatrix} \neq 0 \quad . \qquad (2.126)$$

Thus, the expression for the no-slip condition is

$$\frac{1}{\tan^3\alpha} - 1 \neq 0 \quad , \qquad (2.127)$$

which corresponds to the condition that $\alpha \neq 45°$. However, the Mecanum wheel has an offset angle of $\alpha = 45°$, and so the necessary condition is not met, and slip is unavoidable. This essentially means that the Jacobian is not valid because if there exists slip in the system there is no way to predict, by means of kinematics alone, the linear velocity imposed by an omnidirectional wheel at a contact point on the sphere. Two more extreme angles would be $\alpha = 0°$ which indicates an omnidirectional wheel where the actuation axis and the rollers axes are parallel, which yields a zero Jacobian, as expected; and the $\alpha = 90°$ case, which indicates a standard omnidirectional wheel, and converges into the Jacobian developed for that particular case.

Looking at the rows of the inverse of the Jacobian as vectors, as presented in Figure 2.13 one can observe that the no-slip condition shifts from depending on the unit induced angu-

lar velocity vectors being linearly independent, to shifted vectors comprised from the unit induced angular velocity vectors and the direction of the contact point velocity shifted by α. This, in turn, changes the angle between each two of the three vectors from the orthogonal 90° case to an angle of 120° case. The only arrangement for such an angular relation is in a plane; thus, the 45° shift of the orthogonal case (as highlighted in the left portion of Figure 2.13), flattens the row vectors of the matrix into a plane thereby making them linearly independent, as highlighted in the right portion of Figure 2.13.

For the general case with arbitrary offset angle $\alpha \neq 45°$ the Jacobian becomes

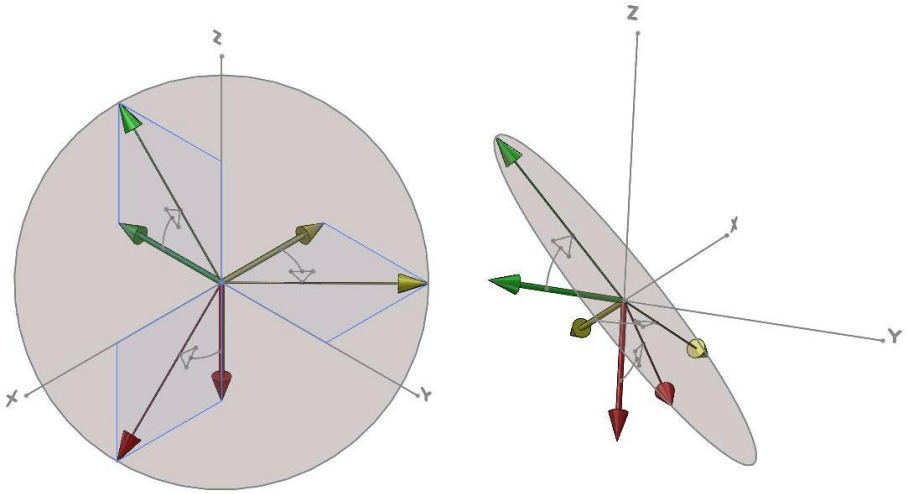

Figure 2.13: Shifted row vectors (left) align into a single plane in space (right) to form Jacobian singularity.

$$\mathbf{J} = \frac{r}{R(1-\tan^3\alpha)} \begin{bmatrix} \tan^2\alpha & \tan\alpha & \tan^3\alpha \\ \tan^3\alpha & \tan^2\alpha & \tan\alpha \\ \tan\alpha & \tan^3\alpha & \tan^2\alpha \end{bmatrix} . \tag{2.128}$$

The Atlas Sphere

As before, the Altas sphere kinematic architecture is shown in Figure 2.3. The actuation directions and unit induced angular velocity vectors were shown to be

$$\begin{aligned} \hat{v}_1 &= \hat{\jmath} \quad , \\ \hat{v}_2 &= -\frac{\sqrt{3}}{2}\hat{\imath} - \frac{1}{2}\hat{\jmath} \quad , \\ \hat{v}_3 &= \frac{\sqrt{3}}{2}\hat{\imath} - \frac{1}{2}\hat{\jmath} \quad , \end{aligned} \tag{2.129}$$

and

$$\begin{aligned} \hat{\Omega}_1 &= \sin\theta\hat{\imath} + \cos\theta\hat{k} \quad , \\ \hat{\Omega}_2 &= -\frac{1}{2}\sin\theta\hat{\imath} + \frac{\sqrt{3}}{2}\sin\theta\hat{\jmath} + \cos\theta\hat{k} \quad , \\ \hat{\Omega}_3 &= -\frac{1}{2}\sin\theta\hat{\imath} - \frac{\sqrt{3}}{2}\sin\theta\hat{\jmath} + \cos\theta\hat{k} \quad , \end{aligned} \tag{2.130}$$

respectively. The no-slip requirement becomes

$$\det \begin{bmatrix} \sin\theta & \cot\alpha & \cos\theta \\ -\frac{1}{2}\sin\theta - \frac{\sqrt{3}}{2\tan\alpha} & \frac{\sqrt{3}}{2}\sin\theta - \frac{1}{2\tan\alpha} & \cos\theta \\ -\frac{1}{2}\sin\theta + \frac{\sqrt{3}}{2\tan\alpha} & -\frac{\sqrt{3}}{2}\sin\theta - \frac{1}{2\tan\alpha} & \cos\theta \end{bmatrix} \neq 0 \tag{2.131}$$

and the expression for the no-slip condition becomes

$$\frac{3\sqrt{3}}{2}\cos\theta(\sin^2\theta + \cot^2\alpha) \neq 0 \quad . \tag{2.132}$$

This results in the same cases as in the original Atlas sphere architecture, where the determinant is zero only if $\theta = 90^\circ$ or if $\theta = 0^\circ$ and $\alpha = 90^\circ$ simultaneously, which is exactly an

Atlas sphere with regular omnidirectional wheels. The Jacobian for this system becomes

$$\mathbf{J} = \frac{r}{R}\begin{bmatrix} \sin\theta & \cot\alpha & \cos\theta \\ -\frac{1}{2}\sin\theta - \frac{\sqrt{3}}{2\tan\alpha} & \frac{\sqrt{3}}{2}\sin\theta - \frac{1}{2\tan\alpha} & \cos\theta \\ -\frac{1}{2}\sin\theta + \frac{\sqrt{3}}{2\tan\alpha} & -\frac{\sqrt{3}}{2}\sin\theta - \frac{1}{2\tan\alpha} & \cos\theta \end{bmatrix}^{-1} \quad . \tag{2.133}$$

Once again, it is clear that the resulting Jacobian converges into the Jacobian obtained for standard omnidirectional wheels, for the case where $\alpha = 90^\circ$, as expected.

2.3 Kinematics Summary

In this kinematics chapter, a general approach was developed to examine the kinematics of a sphere actuated by omnidirectional wheels. The approach was used to examine various design architectures. The effects of the number of omnidirectional wheels in use was closely examined, and a general Jacobian for the case was developed:

$$\begin{bmatrix} \hat{\Omega}_1^T \\ \hat{\Omega}_2^T \\ \hat{\Omega}_3^T \\ . \\ . \\ \hat{\Omega}_n^T \end{bmatrix} \tilde{\mathbf{\Omega}} = \frac{1}{R}\begin{bmatrix} r_1 & 0 & 0 & . & . & . \\ 0 & r_2 & 0 & . & . & . \\ 0 & 0 & r_3 & . & . & . \\ . & . & . & . & . & . \\ . & . & . & . & . & . \\ . & . & . & . & . & r_n \end{bmatrix} \begin{Bmatrix} \omega_1 \\ \omega_2 \\ \omega_3 \\ . \\ . \\ \omega_n \end{Bmatrix} \quad . \tag{2.134}$$

This general relation was analyzed and it was concluded that in the general sense, three omnidirectional wheels yield a singularity-free no-slip system in terms of applicable kinematics,

where the kinematics become:

$$\tilde{\boldsymbol{\Omega}} = \frac{1}{R} \begin{bmatrix} \hat{\boldsymbol{\Omega}}_{\mathbf{1}}^{\mathbf{T}} \\ \hat{\boldsymbol{\Omega}}_{\mathbf{2}}^{\mathbf{T}} \\ \hat{\boldsymbol{\Omega}}_{\mathbf{3}}^{\mathbf{T}} \end{bmatrix}^{-1} \begin{bmatrix} r_1 & 0 & 0 \\ 0 & r_2 & 0 \\ 0 & 0 & r_3 \end{bmatrix} \begin{Bmatrix} \omega_1 \\ \omega_2 \\ \omega_3 \end{Bmatrix} \quad . \tag{2.135}$$

Additionally, various omnidirectional wheel types were considered, where single-race, dual-race, and triple-race wheels were discussed and compared. Finally, Mecanum wheels were considered and a modified, more general version for the kinematics of a sphere actuated by three omnidirectional wheels was developed

$$\begin{bmatrix} \hat{\boldsymbol{\Omega}}_{\mathbf{1}}^{\mathbf{T}} + \frac{1}{\tan\alpha}\hat{\mathbf{v}}_{\mathbf{1}}^{\mathbf{T}} \\ \hat{\boldsymbol{\Omega}}_{\mathbf{2}}^{\mathbf{T}} + \frac{1}{\tan\alpha}\hat{\mathbf{v}}_{\mathbf{2}}^{\mathbf{T}} \\ \hat{\boldsymbol{\Omega}}_{\mathbf{3}}^{\mathbf{T}} + \frac{1}{\tan\alpha}\hat{\mathbf{v}}_{\mathbf{3}}^{\mathbf{T}} \end{bmatrix} \tilde{\boldsymbol{\Omega}} = \frac{1}{R} \begin{bmatrix} r_1 & 0 & 0 \\ 0 & r_2 & 0 \\ 0 & 0 & r_3 \end{bmatrix} \begin{Bmatrix} \omega_1 \\ \omega_2 \\ \omega_3 \end{Bmatrix} \quad , \tag{2.136}$$

which embodies both Mecanum wheels and standard omnidirectional wheels in a single expression. This representation allows examining new cases of omnidirectional wheels where the shift angle of the rollers may be different from the standard angles of 45° and 90° available currently.

Chapter 3

Dynamics and Vibration

Obtaining general equations of motion for a platform comprising a sphere actuated by omnidirectional wheels, assuming all components are rigid, is a first step towards understanding the dynamics of the system. However, as mentioned earlier, omnidirectional wheels are not ideal by design; that is, they are never ideally round. Other issues that may arise are the rigidity of their mounts and the contact rigidity. Moreover, various types of omnidirectional wheels exist composed of various materials, and having various geometric shapes. All these need to be taken into consideration when constructing the dynamic model and deriving the equations of motion of the system. The model developed in this work takes into account the effects of the shape of the omnidirectional wheels, the stiffness of their mounting, and the deflection of the sphere at the contact point. The overall mechanical system is analyzed as a combination of a completely rigid system, with a subsystem of springs and dampers to represent the non-rigid elements, while the shape of the wheel is treated as positional input.

This chapter will present the model and the corresponding equations of motion for the system. A Matlab program was written to integrate the equations numerically. Sample results will be presented and discussed to show the basic dynamic behaviour of the system for the purpose of verification and validation. The program was developed as a simulation

tool that is suitable for allowing more thorough research and analysis of the effects of various design parameters on the system's performance. The analysis of all possible design parameters and their effects on all performance indicators is a vast project; thus, a representative analysis will be presented in the following chapter.

3.1 System Model

3.1.1 Omnidirectional Wheel Shape

In Chapter 2, kinematic relationships were developed for the ideal case where the omnidirectional wheels were assumed to be perfectly round and there was no relative motion between the sphere's geometric centre and the omnidirectional wheels. In addition to the assumption that the omnidirectional wheels and the sphere are rigid, it had also been assumed that the rotational platform is rigidly attached to the translational platform. In order to obtain the equations of motion for a more realistic platform the kinematics must first be modified to include these departures from the ideal case. First, removing the assumption of a perfectly round omnidirectional wheel, means:

$$r_{w_i} = r_{w_i}(\theta_i) \tag{3.1}$$

thus,

$$\dot{r}_{w_i} = \dot{\theta}_i r'_{w_i} \tag{3.2}$$

$$\ddot{r}_{w_i} = \dot{\theta}_i^2 r''_{w_i} + \ddot{\theta}_i r'_{w_i} \quad , \tag{3.3}$$

where r_{w_i} is the distance from the centre of omnidirectional wheel i to its contact point with the sphere, and θ_i is a cyclical coordinate of the orientation of omnidirectional wheel i,

$r'_{w_i} = \frac{\mathrm{d}r_{w_i}}{\mathrm{d}\theta_i}$, and $r''_{w_i} = \frac{\mathrm{d}^2 r_{w_i}}{\mathrm{d}\theta_i^2}$. The actual shape of the omnidirectional wheel has a significant effect on the effective contact radius; however, the radius of the sphere itself also affects the effective contact radius r_{w_i}.

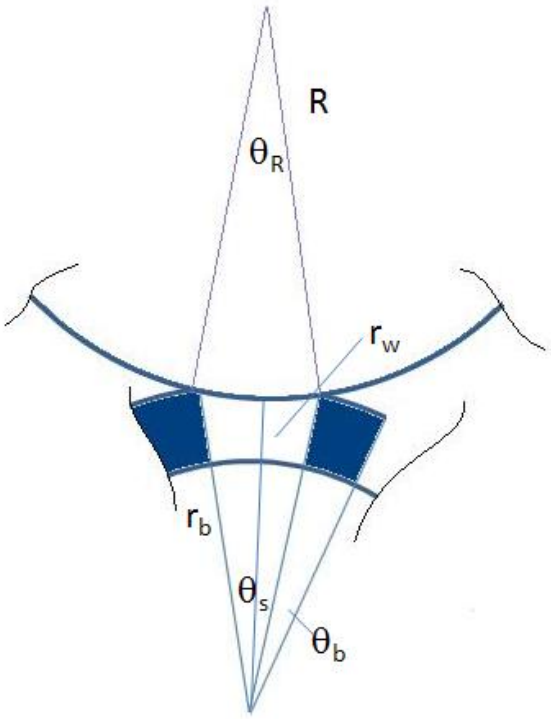

Figure 3.1: Contact area between omnidirectional wheel and sphere.

Figure 3.1 shows the contact area between an omnidirectional wheel and the sphere, illustrating the gaps between the rollers. Here, r_b is the maximal radius of the omnidirectional wheel, θ_b is the angular distance between two consecutive rollers, θ_s is the angular size of the gap between two consecutive rollers, both measured about the centre of the omnidirectional wheel, and θ_R is the same gap measured about the centre of the sphere. From geometric considerations, it is apparent that:

$$\sin\frac{\theta_{R_i}}{2} = \frac{r_{b_i}}{R_i}\sin\frac{\theta_{s_i}}{2} \quad . \tag{3.4}$$

The difference between the maximal and minimal distances between the centres of the sphere and the omnidirectional wheel is

$$\Delta r_{w_i} = (R + r_{b_i}) - [(R\cos\frac{\theta_{R_i}}{2}) + (r_{b_i}\cos\frac{\theta_{s_i}}{2})] \quad . \tag{3.5}$$

Thus,

$$\Delta r_{w_i} = R(1 - \cos\frac{\theta_{R_i}}{2}) + r_{b_i}(1 - \cos\frac{\theta_{s_i}}{2}) \quad , \tag{3.6}$$

where Δr_{w_i} is defined by the relation

$$r_{w_i} = r_{b_i} - \Delta r_{w_i} \quad . \tag{3.7}$$

Finally, combining with the constant radius r_{b_i} of the roller area:

$$\begin{aligned} 0 < \theta_i < \theta_{s_i} \quad r_{w_i} &= r_{b_i} - \Delta r_{w_i}\sin(2\pi\frac{\theta_i}{\theta_{s_i}}) \\ \theta_{s_i} \leq \theta_i \leq \theta_{s_i} + \theta_{b_i} \quad r_{w_i} &= r_{b_i} \end{aligned} \tag{3.8}$$

where for n_i rollers,

$$\theta_{s_i} + \theta_{b_i} = \frac{2\pi}{n_i} \quad . \tag{3.9}$$

Defining the roundness ratio η_i as

$$\eta_i = \frac{\theta_{s_i}}{\theta_{s_i} + \theta_{b_i}} \tag{3.10}$$

provides a means to classify omnidirectional wheels as follows:

- $\eta = 0$ - perfectly round wheel;
- $\eta = 1$ - wheel with continuous contact, such as Mecanum wheels; and
- $0 < \eta < 1$ - omnidirectional wheel with gaps between the rollers where smaller η means smaller gaps.

Thus, Equation 3.8 becomes

$$\begin{aligned} \eta_i &= 0; \quad r_{w_i} = r_{b_i} \\ \eta_i &\neq 0; \quad r_{w_i} = r_{b_i} - \Delta r_{w_i} \sin(\frac{n_i \theta_i}{\eta_i}) \quad . \end{aligned} \tag{3.11}$$

This model essentially presents the main cause for vibration in the system. It should be noted that the effects of the omnidirectional wheel's radius changes are small compared with the radius itself (less than 0.5% for a reasonably bad case), and thus the impact on the Jacobian and the angular motion resulting is negligible. However, its impact on the translational vibratory motion is significant. Since this is the main source for vibration it is there, in the translational motion of the centre of the sphere, that the model is used.

3.1.2 Sphere-Omnidirectional Wheel Interface

The interface between the omnidirectional wheels and the sphere is treated here as non-rigid. Thus, each contact point is modelled as a combination of a spring and a viscous damper. The non-rigid assumption, in turn, results in each contact point becoming a contact patch that is spread over more than a single point. The implications are that, in addition to radial deflection, there may be two additional resisting moments occurring: rolling resistance and spin resistance. Rolling resistance may be caused due to shifts in the position of the equivalent normal force over a contact patch from the line connecting the centres of the sphere and omnidirectional wheel involved. Spin resistance is due to friction.

Radial Deflection

The radial deflection is modelled as a combination of a spring with linear stiffness K_i and viscous damping of C_i. The importance of these coefficients is their contribution to isolation of the internal parts of the sphere from vibration. The main source of vibration in the system is the imperfect shape of the omnidirectional wheels as they roll in contact with the sphere. Since each contact point is not really connected to the others, its effect on the position of the effective centre of the deformed sphere is assumed independent of the other contact point deflections. Thus, the radial motion of each contact point is analyzed independent of the other contact points, and their contributions to the overall translation of the centre of the sphere is then vectorially summed to obtain the overall translation of the centre of the sphere.

Hertzian Contact Model

Since radial deflection depends on what happens at the contact point, a contact model must be considered. A widely accepted model for this purpose is the Hertzian model [76, 77]. The following analysis for the resisting moments is independent of the model of choice, yet an implementation of the Hertzian model is shown as an example. The Hertzian model suggests that the contact patch is circular. In that case, for a normal force N_i at contact point i, the pressure distribution p_i is:

$$p_i = p_{0_i}\sqrt{1 - \left(\frac{r}{a_i}\right)^2} \tag{3.12}$$

where r is a local coordinate representing the distance of the point in the contact patch from the centre of the contact patch, a is the radius of the contact patch, and is a function of the

equivalent radius $R_i^{'}$ and the equivalent elasticity modulus $E_i^{'}$ [76] detailed below such that

$$a_i = \left(\frac{3N_i R_i^{'}}{4E_i^{'}} \right)^{\frac{1}{3}} \quad , \tag{3.13}$$

and p_{0_i} is the maximal pressure at the centre of the patch,

$$p_{0_i} = \frac{3N_i}{2\pi a_i^2} \quad . \tag{3.14}$$

For this case, the deflection at contact point i is

$$\delta_i = \left(\frac{9N_i^2}{16R_i^{'}E_i^{'2}} \right)^{\frac{1}{3}} \quad . \tag{3.15}$$

The values of $E_i^{'}$ and $R_i^{'}$ are:

$$E_i^{'} = \frac{E_s E_{w_i}}{E_s(1-\nu_{w_i}^2) + E_{w_i}(1-\nu_s^2)} \tag{3.16}$$

and

$$R_i^{'} = \frac{Rr_i}{R+r_i} \quad , \tag{3.17}$$

where E_s and E_{w_i} are Young's moduli of the sphere and omnidirectional wheel i respectively, and ν_s and ν_{w_i} are the corresponding Poisson ratios.

Rolling Resistance

If the equivalent normal force corresponding to the pressure distribution within a contact patch is not located at the corresponding theoretically ideal rigid body contact point, then the normal force would not pass through the geometric centre of the sphere, and therefore

create a moment resisting the rolling motion. This, in turn, will affect the moment equations, both for the sphere and for the omnidirectional wheels. Various models exist to evaluate the length of the moment arm l_{r_i}. However, it must be included as a contribution to the moment equations of the sphere and the omnidirectional wheels:

$$\vec{T}_{r_i} = \vec{l}_{r_i} \times \vec{N}_i \quad i = 1, 2, 3 \tag{3.18}$$

where $\vec{T}_{r_i}$ is the rolling resistance moment at contact point i and $\vec{l}_{r_i}$ is the position of the equivalent normal force with respect to the rigid body contact point.

Thus, the magnitude of the rolling resistance for a single contact point i is:

$$T_{r_i} = -N_i l_{r_i} \quad i = 1, 2, 3 \tag{3.19}$$

where l_{r_i} is the effective roll moment arm of contact point i, and may be evaluated through either theoretical or experimental models.

The full vector expression of the rolling resistance is therefore:

$$\vec{T}_{r_i} = -N_i l_{r_i} \frac{\vec{\Omega} \cdot \hat{\Omega}_i}{|\vec{\Omega} \cdot \hat{\Omega}_i|} \hat{\Omega}_i \quad i = 1, 2, \qquad . \tag{3.20}$$

As an illustrative example, the Hertzian model will be used to obtain l_{r_i}. Since the Hertzian model calls for a symmetric distribution of the normal force, the equivalent contact point is at the rigid body contact point, therefore, the normal force passes through the geometric centre of the sphere, and so we obtain:

$$T_{r_i} = 0 \quad i = 1, 2, 3 \tag{3.21}$$

and clearly,

$$l_{r_i} = 0 \quad i = 1, 2, 3 \qquad . \tag{3.22}$$

This result is due to the fact that the Hertzian model is completely symmetrical. This may not necessarily be the realistic case, where possibly $l_{r_i} \neq 0$. However, the moment arm length is limited by the radius of the contact patch. Since l_{r_i} is essentially the centre of pressure offset, it depends on the viscoelastic properties of the interface between the sphere and the omnidirectional wheel, and varies with properties, speed of rotation, temperature, and other parameters. Practically, this moment arm can be obtained by rolling resistance tests. For demonstration, l_{r_i} will be taken to be $l_{r_i} = a_i$ as long as the angular velocity is non-zero.

Spin Resistance

Omnidirectional wheels allow actuation about one axis while providing practically no resistance in a direction perpendicular to the actuation direction. However, they have no mechanism that eliminates resistance in the spin direction. This is due to the assumption that the contact occurs at a point. Once the contact point becomes a contact patch, this assumption is no longer valid, and some spin resistance must exist. While specific models for evaluating this component may be considered, it can be modelled as a contribution to the moment equation:

$$T_{s_i} = \iint_{S_i} \mu_i N_i(r, \theta) \, \mathrm{d}S_i \quad i = 1, 2, 3 \tag{3.23}$$

where T_{s_i} is the spin resistance moment at contact point i, the normal force at the contact point N_i becomes a distributed pressure $N_i(r, \theta)$ over the contact patch S_i, where r and θ are local coordinates at the contact patch surface. The coefficients of dry friction at the

contact points are μ_i. As mentioned earlier, various models exist for the evaluation of the distributed normal pressure $N_i(r, \theta)$ and the contact patch shape S_i.

As far as the higher level dynamic model of the platform is concerned, the magnitude of the spin resistance when the angular velocity is non-zero may be modelled as:

$$T_{s_i} = \mu_i N_i l_{s_i} \quad i = 1, 2, 3 \tag{3.24}$$

where l_{s_i} is the effective spin lever of contact point i, and may be evaluated through either theoretical or experimental models.

The full vector expression of the spin resistance would therefore be:

$$\vec{T}_{s_i} = \mu_i N_i l_{s_i} \frac{\vec{\Omega} \cdot \vec{R}_i}{|\vec{\Omega} \cdot \vec{R}_i|} \hat{R}_i \quad i = 1, 2, 3 \quad . \tag{3.25}$$

Note that due to this definition of the resisting components

$$\vec{T}_{s_i} \cdot \vec{T}_{r_i} = 0 \quad i = 1, 2, 3 \quad . \tag{3.26}$$

Once more, the Hertzian model will be used to obtain l_{s_i}. Spin is the rotation about an axis that connects the geometric centres of the sphere and an omnidirectional wheel through the contact point. When the contact point becomes a contact patch, spin is accompanied by friction, which is proportional to the normal force at the point. Although the resultant friction force may be zero, the friction produces a moment resisting the spin motion:

$$T_{s_i} = \iint_{c.p.} \mu_i p_i r \mathrm{d}S = \int_0^{2\pi} \int_0^{a_i} \mu_i p_i r^2 \mathrm{d}r \mathrm{d}\theta \quad . \tag{3.27}$$

Utilizing Equation 3.12 and applying the integral limits, we obtain:

$$T_{s_i} = \frac{3\pi}{16}\mu_i N_i \left(\frac{3N_i R_i^{'}}{4E_i^{'}}\right)^{\frac{1}{3}} \quad . \tag{3.28}$$

The direction of the spin resistance is opposite that of the spin direction at the contact point, thus,

$$\vec{T}_{s_i} = -\frac{3\pi}{16}\mu_i N_i \left(\frac{3N_i R_i^{'}}{4E_i^{'}}\right)^{\frac{1}{3}} \frac{\vec{\Omega}\cdot\vec{R}_i}{|\vec{\Omega}\cdot\vec{R}_i|}\hat{R}_i \tag{3.29}$$

therefore,

$$l_{s_i} = \frac{3\pi}{16}\left(\frac{3N_i R_i^{'}}{4E_i^{'}}\right)^{\frac{1}{3}} \quad i = 1,2,3 \quad . \tag{3.30}$$

The total spin resistance is therefore:

$$\vec{T}_s = \sum_{i=1}^{3} \vec{T}_{s_i} \quad . \tag{3.31}$$

3.1.3 Omnidirectional Wheel-Linear Platform Interface

Another important interface is the one between the linear platform and the omnidirectional wheels. The reaction forces between the omnidirectional wheels and the sphere affect the mounting point of the omnidirectional wheel onto the linear platform. The mounting point, which is attached to the omnidirectional wheel's centre, is modelled as non-rigid. Each mounting point is modelled as having stiffness coefficient k_i, and viscous damping coefficient c_i.

Combining the effects of the shape of the omnidirectional wheels, the sphere-omnidirectional wheel contact interface, and the omnidirectional wheel-linear platform interface, with the

rigid body dynamics makes up the model for the system that allows investigation of the dynamics of the system as well as vibration issues.

The model for the contact point area is illustrated in Figure 3.2. It takes the linear platform's motion (S_{c_i} in the illustration) as a motion input into the sphere. The motion input into the sphere is a combination of the linear motion of the centre of the omnidirectional wheel and the distance to the effective contact point between the sphere and the omnidirectional wheel. All contact points are treated using the same model. Next, the parameters $S_{a_i}, S_{b_i}, S_{c_i}$ need to be mapped into the parameters in the context of the Atlas platform.

$$\begin{aligned} S_{a_i} &= \vec{R}_s \cdot \hat{r}_{w_i} \quad , \\ S_{b_i} &= \vec{R}_l \cdot \hat{r}_{w_i} + \Delta_i \quad , \\ S_{c_i} &= \vec{R}_l \cdot \hat{r}_{w_i} \quad , \\ S_{d_i} &= const. \quad , \end{aligned} \tag{3.32}$$

where $\vec{R}_s$ is the position of the centre of the sphere, $\vec{R}_l$ is the position of the translational platform, Δ_i is the local deflection of the attachment point of the omnidirectional wheel to the linear platform, and S_{d_i} is a constant distance definition of the kinematic closure of the system, $S_{d_i} > 2R$. The exact magnitude is determined by the geometric details and design of the system, and does not impact the results. To obtain vibration information, we observe

$$\Delta\vec{R} = \vec{R}_s - \vec{R}_l \quad , \tag{3.33}$$

where $\Delta\vec{R}$ is the displacement of the effective centre of the sphere from the geometric centre of a perfect sphere. One can observe that

$$\vec{R}_l \cdot \hat{r}_{w_i} + \Delta_i + r_{w_i} + \delta_i = \vec{R}_s \cdot \hat{r}_{w_i} \tag{3.34}$$

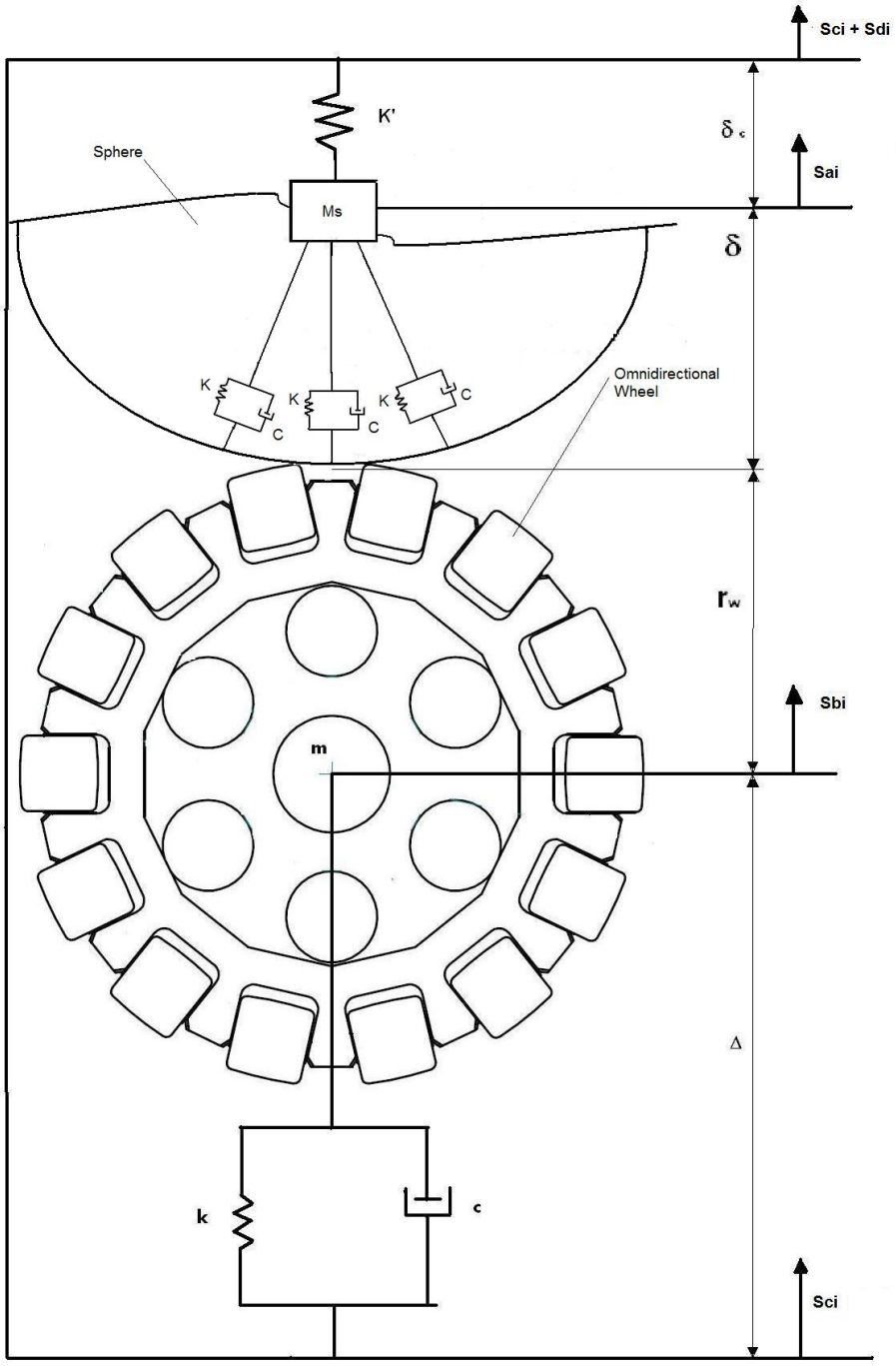

Figure 3.2: Model for contact point.

and kinematic closure equations maintain:

$$\Delta_i + r_{w_i} + \delta_i + \delta_{c_i} = Z_c \quad \text{, and} \tag{3.35}$$

$$\dot{\Delta}_i + \dot{r}_{w_i} + \dot{\delta}_i + \dot{\delta}_{c_i} = 0 \quad . \tag{3.36}$$

3.2 Equations of Motion

Utilizing the assumptions and relations described in the previous sections, combined with the kinematic relations, Equations 3.37 - 3.44 below are obtained using the Newton-Euler dynamic formulation. Since the focus of the thesis is on concept, not application, some details are generalized. Specifically, the translational motion implementation is treated as a black box controlled by three independent forces along its main axes. In addition, form closure is assumed without detail on the exact locations of support, since this is an implementation detail. The internal structure of the sphere is also application dependent and therefore not specified or structurally modelled.

Equations of motion were derived using a Newtonian approach. The system is broken down into two subsystems: the sphere and the linear platform (which includes everything but the sphere).

First, the force equation for the sphere is:

$$\vec{F}_{ext} + \sum_{i=1}^{3} \vec{N}_i + \sum_{i=1}^{3} \vec{f}_i = M_s(\ddot{\vec{R}}_s) \quad , \tag{3.37}$$

where M_s is the mass of the sphere, R_s is the position of the centre of the sphere, $\vec{F}_{ext}$ is an external compressive force applied to the sphere to ensure zero slip, $\vec{N}_i$ and $\vec{f}_i$ are the normal and frictional forces at contact point i respectively.

The force equation for the linear platform is:

$$\vec{P} - \sum_{i=1}^{3} \vec{N}_i - \sum_{i=1}^{3} \vec{f}_i \;=\; (M_l + \sum_{i=1}^{3} m_i)\ddot{\vec{R}}_l \quad , \tag{3.38}$$

where M_l is the mass of the linear platform, m_i is the mass of omnidirectional wheel i, $\vec{P}$ is the force applied to the linear platform, and R_l is the position vector of the mass centre of the linear platform. The moment equation of each omnidirectional wheel i about its geometric centre is:

$$T_i - f_i r_{w_i} - T_{r_i} \;=\; I_{w_i}\dot{\omega}_i \quad , \tag{3.39}$$

where T_i is the actuation moment of omnidirectional wheel i. This equation is a scalar equation, and is valid for each of the omnidirectional wheels in the system. In the case where there are three omnidirectional wheels, there are three equations involved. The moment equation of the sphere about its geometric centre is:

$$\sum_{i=1}^{3} \vec{f}_i \times \vec{R}_i - \sum_{i=1}^{3} \vec{T}_{r_i} - \sum_{i=1}^{3} \vec{T}_{s_i} \;=\; [I_s]\,\dot{\vec{\Omega}} + \vec{\Omega} \times [I_s]\,\vec{\Omega} \quad . \tag{3.40}$$

The equations for the elastic effects at the contact points, derived using the model presented in Figure 3.2 are:

$$M_s(\ddot{\vec{R}}_l \cdot \hat{r}_{w_i} + \ddot{\Delta}_i + \ddot{\delta}_i) + C_i\dot{\delta}_i + K_i\delta_i + K_i'(\Delta_i + \delta_i) \;=\; K_i'(r_{w_i} - Z_c) - M_s\ddot{r}_{w_i} \tag{3.41}$$

and

$$m_i\ddot{\Delta}_i - C_i\dot{\delta}_i + c_i\dot{\Delta}_i - K_i\delta_i + k_i\Delta_i \;=\; 0 \quad , \tag{3.42}$$

where δ_i is defined in Figure 3.2 as the distance between the centre of the sphere to contact point i, and Δ_i is defined in Figure 3.2 as the distance between the centre of omnidirectional wheel i to its mounting point on the translational platform. Finally, from the kinematics we have Equation 2.20

$$\dot{\vec{\Omega}} = J\{\dot{\omega}\} \quad , \tag{3.43}$$

and the quaternionic differential equation 2.21

$$\dot{q} = \frac{1}{2}\Omega \circ q \quad . \tag{3.44}$$

It is essential to understand that a deviation of the centre of mass from the geometric centre will not result in coupling of the linear and rotational motions due to the fact that the motion of the omnidirectional wheels is controlled, and setting the moment applied to them is the only means to cause rotational motion in the system. Thus, as long as the friction limit at the contact points is not exceeded, the only effect would be that of increasing the reaction forces at the contact points. Since it is desired to obtain a slip-free system, the required external force $\vec{F}_{ext}$ that would yield zero kinetic slip needs to be determined. Obtaining this is done by assuming the friction limit is exactly reached while still maintaining the kinematic no-slip condition, that is, $f_i = \mu_i N_i$, and $\dot{\vec{\Omega}} = J\{\dot{\omega}\}$. The result is the minimum required external force to assure the no-slip condition. In our case, we obtain

$$\begin{aligned} \vec{F}_{ext} = & \frac{M_s}{M_T - M_s} \cdot \\ & \left(\frac{M_s}{M_T}\vec{P} - R^2 \left([v] - [\mu]^{-1} [R_i] \right) \left([I_w] [r_w]^{-1} [I_s]^{-1} [\Omega]^T [\Omega] + [r_w] \right)^{-1} \{T\} \right) \quad , \end{aligned} \tag{3.45}$$

and

$$\{N\} = \left([I_w]\, R^2\, [r_w]^{-1}\, [I_s]^{-1}\, [\Omega]^T\, [\Omega]\, [\mu] + [r_w]\, [\mu] \right)^{-1} \{T\} \qquad , \tag{3.46}$$

where, $[I_w]$ is a diagonal matrix containing the moments of inertia of the omnidirectional wheels, $[I_s]$ is the inertia tensor of the sphere, and $[\mu]$ is a diagonal matrix with μ_i as its elements. In addition, $[R_i]$ is a matrix with $\hat{R}_i$ as its columns, $[v]$ is a matrix with $\hat{v}_i$ as its columns, and $[r_w]$ is a matrix with r_{w_i} as its columns. This set of equations is a combination of differential equations and algebraic equations. Thus, the differential equations need to be integrated while the algebraic equations need to be solved at each integration step simultaneously. Integration was performed utilizing the basic 4^{th} order Runge-Kutta method (Ode45 solver) in a Matlab program.

Several steps were performed during each integration iteration. First, the orientation of each omnidirectional wheel is translated into the input function for the vibration equations utilizing Equations 3.11. Then the actual current omnidirectional wheel radii (r_{w_i}) and its time derivatives are evaluated. Next, the contact forces N_i are evaluated algebraically. Finally, the differential equations are evaluated and the required external force calculated. At the end of the integration step, constraints are checked and enforced.

3.2.1 Verification and Validation

A Matlab program was developed to simulate the dynamics. To verify the program and equations the orthogonal case presented in Chapter 2 was considered. The goal of this exercise was to qualitatively validate the program by introducing scenarios with predictable results before delving into analyses of more realistic and complex behaviours.

First, a scenario where all bodies are rigid and the omnidirectional wheels are perfectly round is examined as a baseline. Here, the expectation is to obtain the pure ideal motion

of a sphere rolling without sliding on actuating omnidirectional wheels. The translation should show parabolic motion as a result of a constant driving force. The rotational motion is expected to behave similarly driven by constant torques, which is to be indicated in the Euler parameters behaving in a sinusoidal manner. The resulting magnitudes of the angular velocity vector components of the sphere are expected to develop linearly. No perturbatory motion is expected is such an ideal system, meaning zero vibration. The program demonstrates the behaviour mentioned above for the rigid body case as the first part of the verification.

Second, to ensure that the non-ideal shape of the omnidirectional wheels affects the simulation results, a basic set of examples with varying values of roundness ratio are introduced. The expectation is to observe vibrational motion superimposed on the ideal motion. The frequencies are expected to reflect the number of rollers and angular velocity of each omnidirectional wheel. The orthogonal configuration would be used so that the three axes would be independent of one another, thus each axis should represent the effects of a single omnidirectional wheel.

Finally, to show the effects of a non-rigid sphere, an effective spring coefficient would be considered along with imperfect omnidirectional wheels to show the vibration isolation effects of the model. The expectation is to observe a reduction in the maximal magnitude that was observed when a similar omnidirectional wheel was used combined with a rigid sphere.

The baseline configuration is a sphere with radius $R = 1.22$ m and mass $M_s = 5$ kg. The low mass for the sphere is selected to enhance any vibrational motion. The linear platform's mass is $M_l = 5$ kg. The three identical wheels have a mass of $m_1 = m_2 = m_3 = 0.25$ kg and nominal radii of $r_{w_1} = r_{w_2} = r_{w_3} = 7.58$ cm. The coefficient of friction at the contact points was taken as a representative $\mu = 0.9$ [89].

"Perfect World"

The most basic results presented are for the "perfect world" case, where all bodies are rigid and the omnidirectional wheels are perfectly round ($\eta = 0$). This case is used for basic verification of the program. Figure 3.3 shows the development of the angular velocity vector components of the sphere. Both the linear behaviour and the magnitudes behave as predicted since there is no resisting moment acting on the sphere, and the actuating moment is constant.

The components of the quaternion representing the orientation of the sphere are shown in Figure 3.4. The harmonic plots represent motion about a constant axis, and the increasing frequency indicates an increasing angular velocity as one would expect. The linear portion of the motion, indicated by the position of the centre of mass of the linear platform, is presented in Figure 3.5. It is expected to develop in a parabolic fashion as there are no resisting forces to oppose the constant applied force $\vec{P}$. It is also clear that there is no indication of coupling between the angular degrees-of-freedom and the linear ones. The details of the driving forces used for the validation were taken to be step functions, where the magnitudes of the steps are $P_x = 0.1$ N, $P_y = 0.2$ N, $P_z = 0.3$ N and $T_1 = 0.1$ N $\cdot$ m, $T_2 = 0.2$ N $\cdot$ m, $T_3 = 0.3$ N $\cdot$ m.

All other components remain zero as expected. That is, there is no relative linear motion between the sphere and the linear platform.

Imperfect Omnidirectional Wheels

Here, the omnidirectional wheels are no longer assumed perfectly round. However, all system components are still maintained rigid. The goal here is to observe whether the rigid system reacts to the shape input of the wheels within the rigid constraints. It is expected that observeable relative motion will occur between the centre of the sphere and the linear platform which is of the same magnitude as the input signal, that is, the shape of the omnidirectional

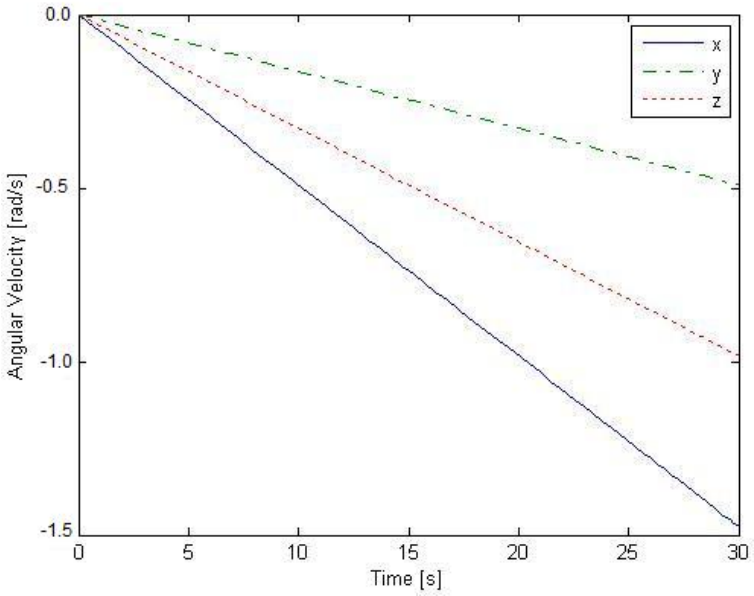

Figure 3.3: $\vec{\Omega}$ as a function of time for the orthogonal case.

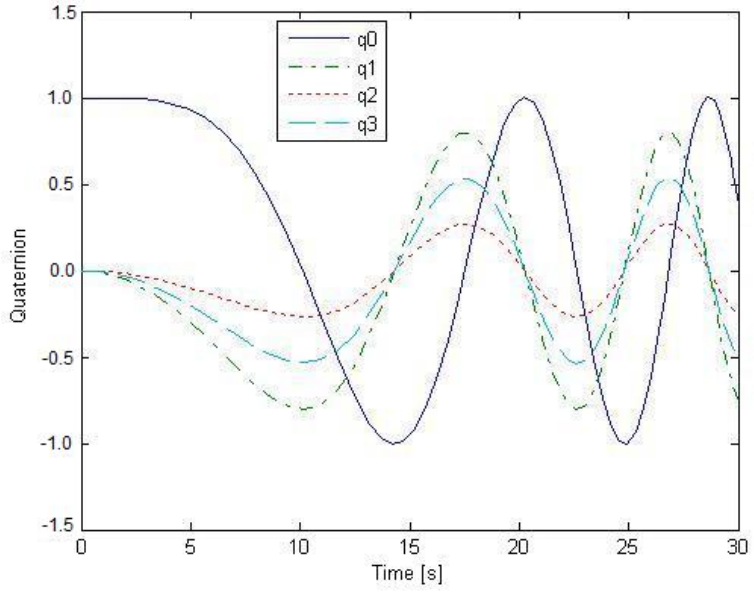

Figure 3.4: The quaternion as a function of time for the orthogonal case.

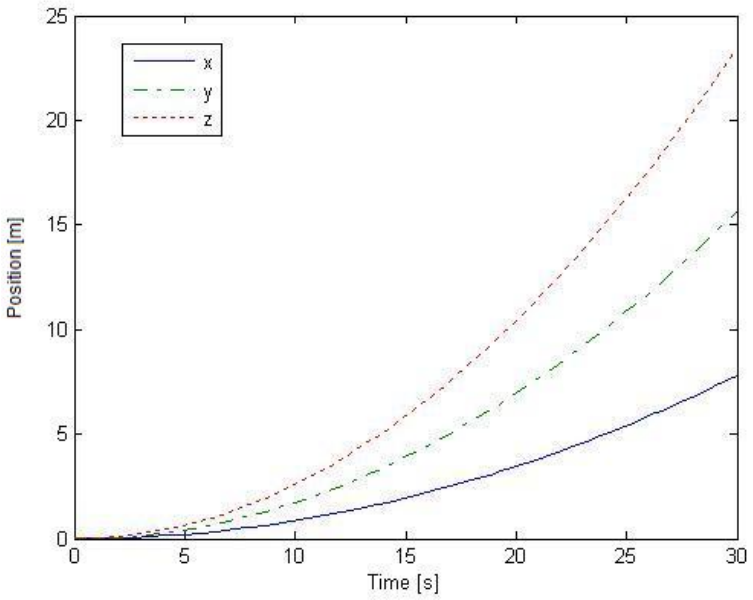

Figure 3.5: $\vec{R}_l$ as a function of time for the orthogonal case.

wheel. Results show the vibration caused by the gaps between the rollers. Presented in Figures 3.6 through 3.9 is the motion of the centre of the sphere for sample roundness ratios.

The omnidirectional wheels currently in use on the Atlas demonstrator have 14 rollers, and a roundness ratio of $\eta = 0.4485$. The figures present the motion of the centre of the sphere relative to the linear platform, in the inertial x, y, and z directions, along with the magnitude of the vector. All figures present a magnification of the graph showing the first 1.5 s of the results. From Figures 3.6 through 3.9 it is observed that the lower the roundness ratio, the smoother the motion, as the magnitude grows with the roundness ratio as presented in more detail in Figure 3.10. Looking at the plots reveals also that there is no change in the frequency of the peaks observed in the plots. These results are expected as suggested by Equations 3.6 and 3.8, where reducing θ_{s_i} and θ_{R_i} reduces Δr_{w_i} thereby reducing the magnitude of the input perturbation function.

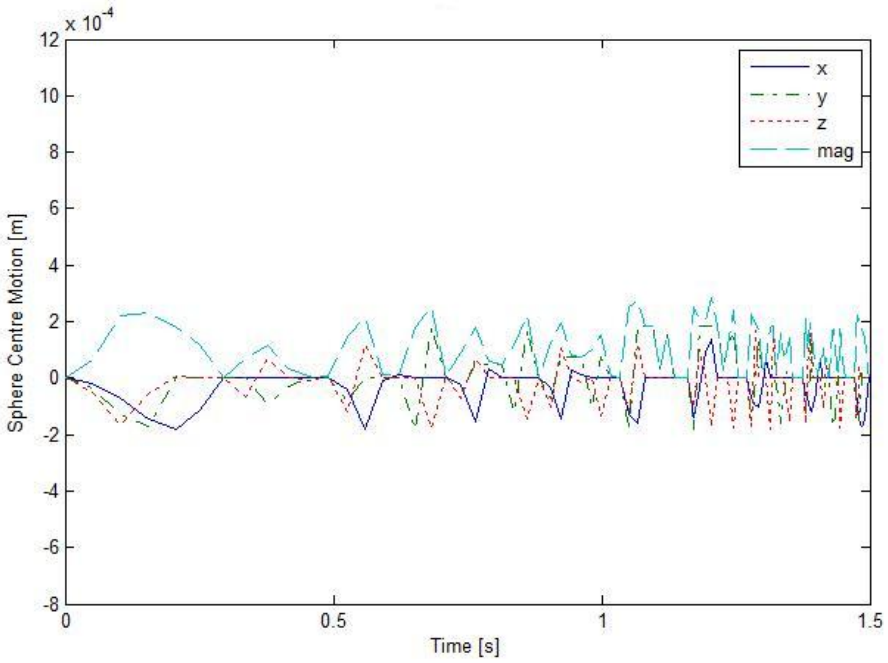

Figure 3.6: $\Delta\vec{R}$ as a function of time for the orthogonal case $\eta = 0.3$.

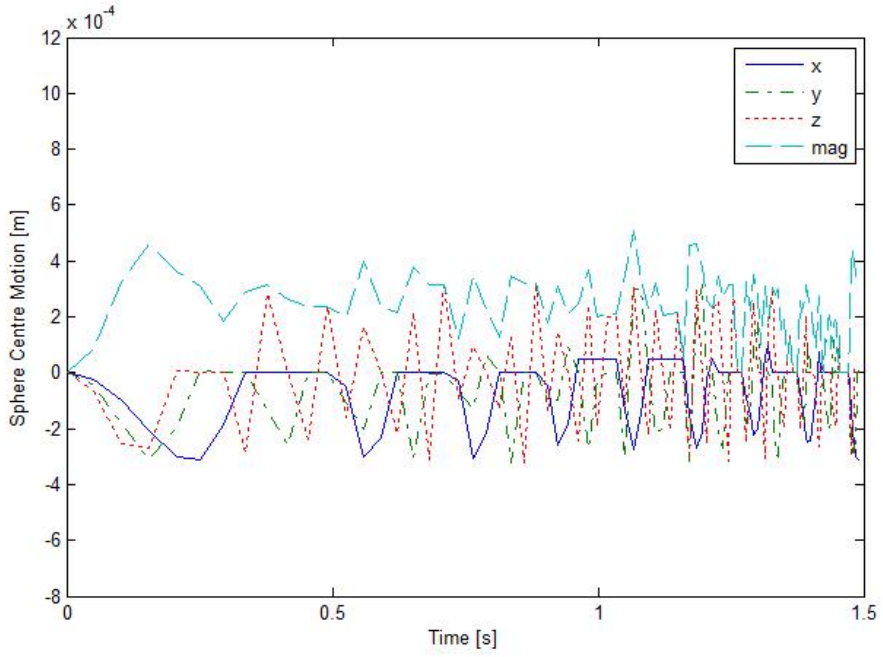

Figure 3.7: $\Delta\vec{R}$ as a function of time for the orthogonal case $\eta = 0.4$.

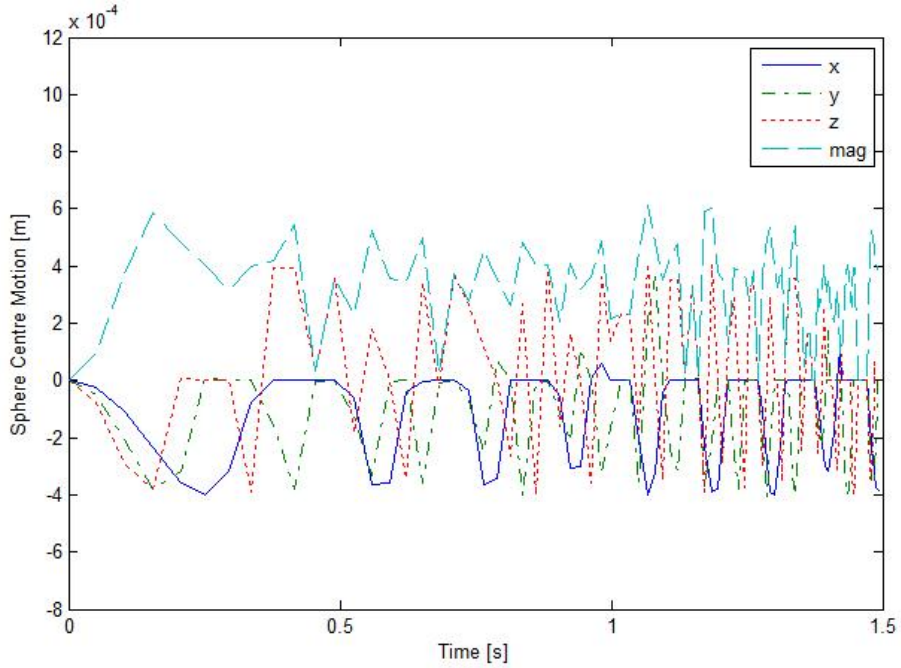

Figure 3.8: $\Delta\vec{R}$ as a function of time for the orthogonal case $\eta = 0.4485$.

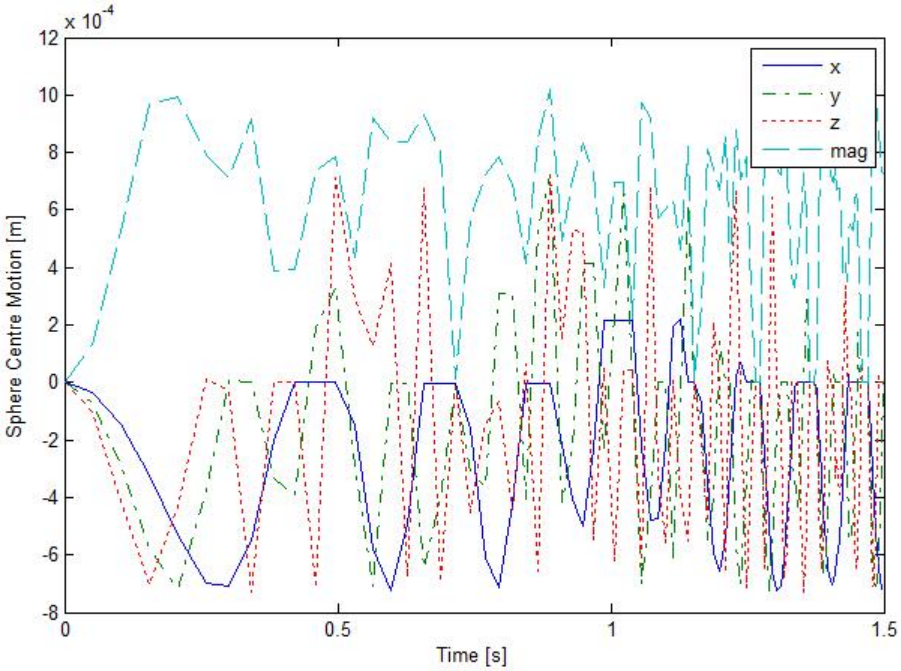

Figure 3.9: $\Delta\vec{R}$ as a function of time for the orthogonal case $\eta = 0.6$.

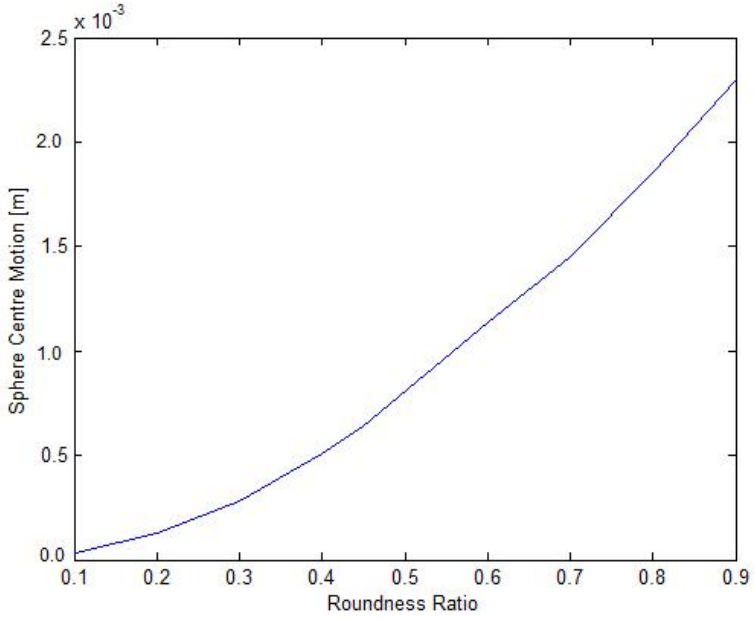

Figure 3.10: Maximum magnitude of $\Delta\vec{R}$ as a function of η for the orthogonal case.

Non-rigid Sphere

When considering a non-rigid sphere, the stiffness of the contact point is considered. In this case, as an example, this coefficient was selected to be $K_i = 188208$ N/m which is the measured stiffness of the sphere of the Atlas demonstrator. The effects of changes to this number will be presented in the next chapter. Figure 3.11 shows the response for constant angular speed values of $\omega_1 = 0.1$ rad/s, $\omega_2 = 1.2$ rad/s, $\omega_3 = 0.3$ rad/s for the case where the roundness ratio is $\eta = 0.4485$, but with the stiffness coefficient above. Comparing with the previous examples that had a completely rigid sphere, we can see that the magnitude of the vibration is orders of magnitude lower than that of the rigid system.

Figure 3.12 presents the result for the same system but with a damping coefficient of $C_i = 8500$ N $\cdot$ s/m, while in Figure 3.13 the damping coefficient is $C_i = 20000$ N $\cdot$ s/m. Thus, adding damping to the system, shows a noticeable but very slight reduction in the magnitude of the vibration. It does appear, however to dampen the secondary higher frequency vibration. Thus, the importance of the stiffness of the sphere is highlighted and is

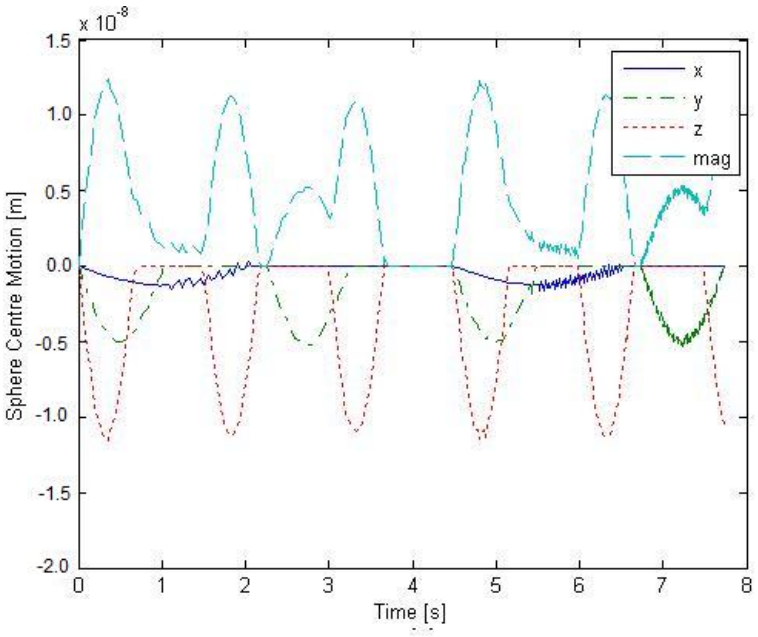

Figure 3.11: $\Delta\vec{R}$ as a function of time for the orthogonal case $\eta = 0.4485$, $K_i = 188208$ N/m.

worth further examination, but damping coefficient effects seem to be only secondary.

Discussion

The purpose of presenting the simulation results in this chapter was validation and verification of the simulation program so that results for more complex cases will be considered reliable. The expected results were stated for the ideal case and the simulation results obtained indeed agreed with expectations. The introduction of non-ideal shape parameters for the omnidirectional wheels added vibrations to the system and it was shown, as expected, that increasing the roundness ratio increases the maximal magnitude of the vibratory motion of the centre of the sphere. Removing the rigid body assumption from the sphere, introduced vibration isolation effects, and a significant reduction of the maximal magnitude and frequency of the sphere's position was observed. Adding damping to the system indeed smoothed the plots more without affecting the magnitude of the vibration. All these results

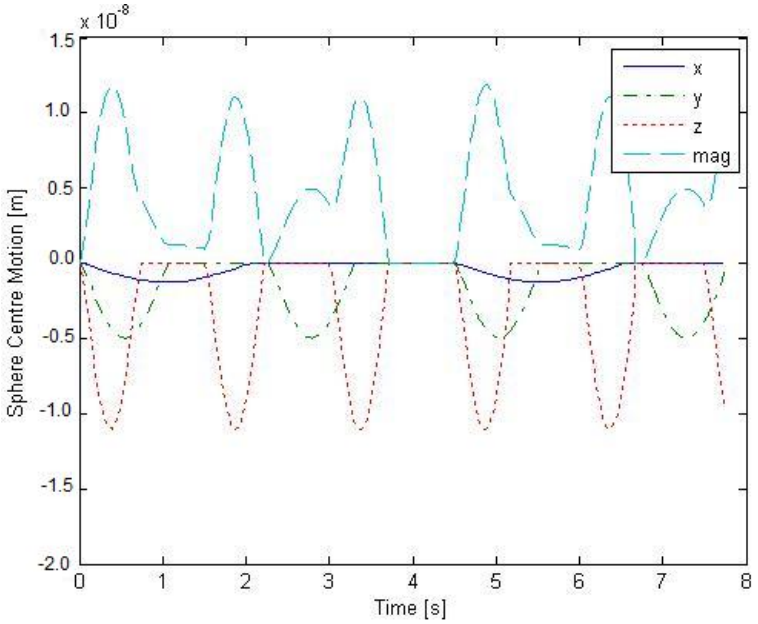

Figure 3.12: $\Delta\vec{R}$ as a function of time for the orthogonal case $\eta = 0.4485$ $K_i = 188208$ N/m $C_i = 8500$ N $\cdot$ s/m.

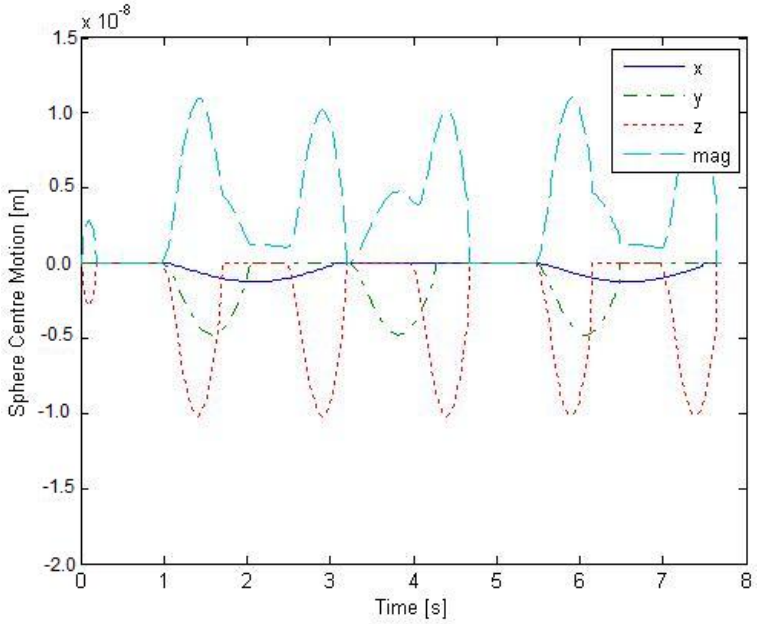

Figure 3.13: $\Delta\vec{R}$ as a function of time for the orthogonal case $\eta = 0.4485$ $K_i = 188208$ N/m $C_i = 20000$ N $\cdot$ s/m.

were predicted prior to running the simulation program and presented earlier in this chapter, thus verifying and validating the program for use in more complex scenarios.

A more detailed analysis and comparison will be performed in the next chapter. The purpose of the presentation here was for demonstration using relatively-simple examples and will serve as a starting point for more representative cases considered in the following chapter. However, it is quite clear from the results that the roundness ratio and the stiffness of the sphere significantly affect the motion of the sphere, as expected and presented in Figures 3.10 and 3.11, while the equivalent damping coefficient at the contact point has a less significant role in the resulting motion of the centre of the sphere. Attention should be paid to the fact that using the orthogonal case, there is a direct mapping between axes and omnidirectional wheel as shown when the orthogonal case was originally presented in Chapter 3. This allows us to examine the results in an easier fashion since the three omnidirectional wheels are orthogonal to each other, thus, making it easy to observe the effects of each individual omnidirectional wheel.

Chapter 4

Application and Analysis

The kinematics and dynamics of the system have been presented and demonstrated in Chapters 1 through 3. In this chapter, as a sample application of the formulation and engineering analysis of the simulation developed, the results are used to compare the performance of two different sets of omnidirectional wheels in the Atlas motion platform configuration. First, the effectiveness of the transmission is examined; then, the induced vibrations are compared. This application is a demonstration of the utility of the tools developed in Chapters 2 and 3 from the standpoint of the ability to investigate various architectures for the design of a motion platform based on a sphere actuated by omnidirectional wheels. The application selected compares two omnidirectional wheel sets. One comprises three standard omnidirectional wheels with fourteen rollers as illustrated in Figure 4.1. The other is a set of three Mecanum wheels with the same diameter but with sixteen rollers, as shown in Figure 4.2.

4.1 Mecanum Wheel Geometric Model

While the geometric model of the standard omnidirectional wheel was presented in Chapter 3, Mecanum wheels were only presented in the definition of the roundness ratio, η, stating that

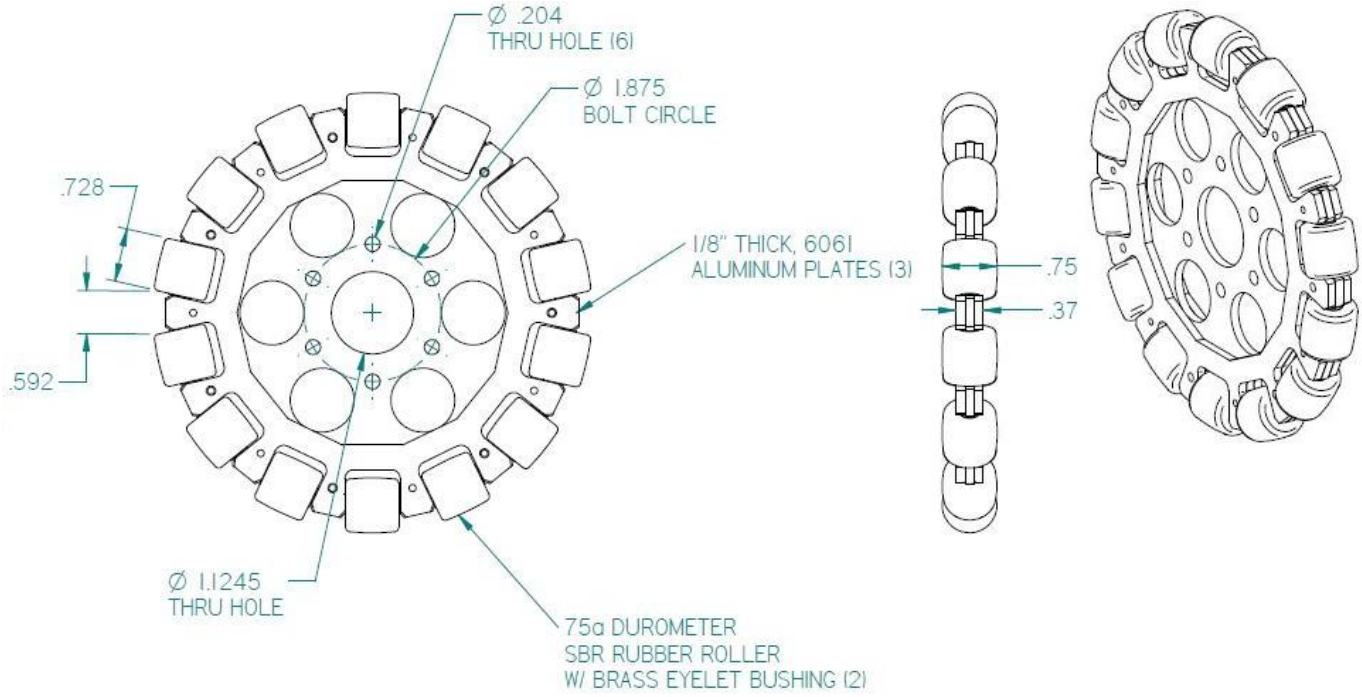

Figure 4.1: Standard omnidirectional wheel considered in this chapter [89].

for Mecanum wheels, $\eta = 1$. While this is indeed the case, the basic shape of the Mecanum wheel varies from that of the standard omnidirectional wheel. In a standard omnidirectional wheel the deviation from perfect roundness is due to gaps between the rollers. In the case of Mecanum wheels, gaps between rollers are not present because the cylindrical shape of the rollers combined with their orientation results in a series of ellipses touching each other, as shown in Figure 4.3, when looking in a cross-section at the contact line on the perimeter of the omnidirectional wheel.

For an orientation angle $\alpha = 45°$, the parameters for the ellipse become:

$$\begin{aligned} a &= \sqrt{2} r_r \quad , \\ b &= r_r \quad , \end{aligned} \tag{4.1}$$

where r_r is the radius of the roller. The state where the centre of the sphere is closest to the

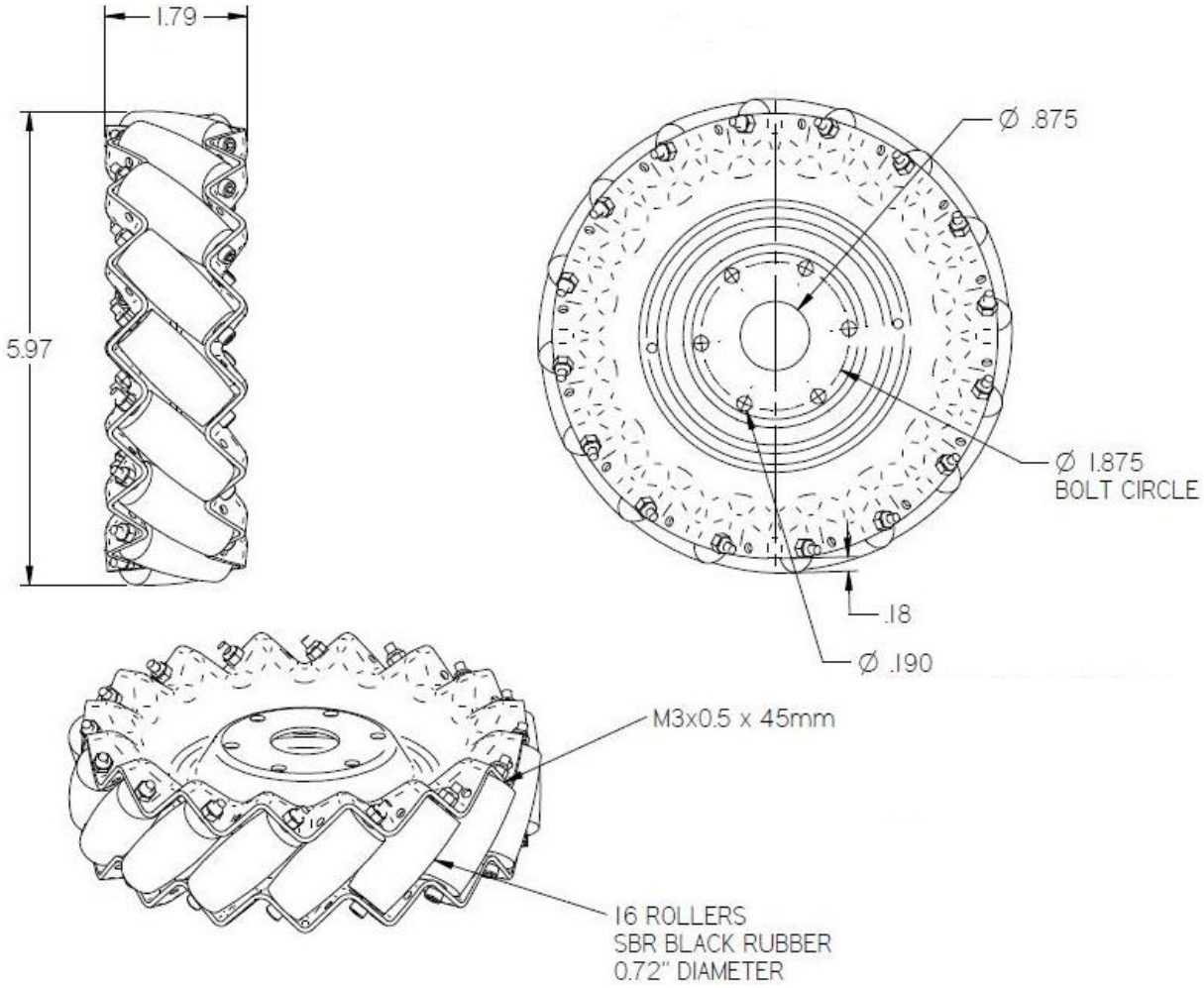

Figure 4.2: Mecanum wheel considered in this chapter [90].

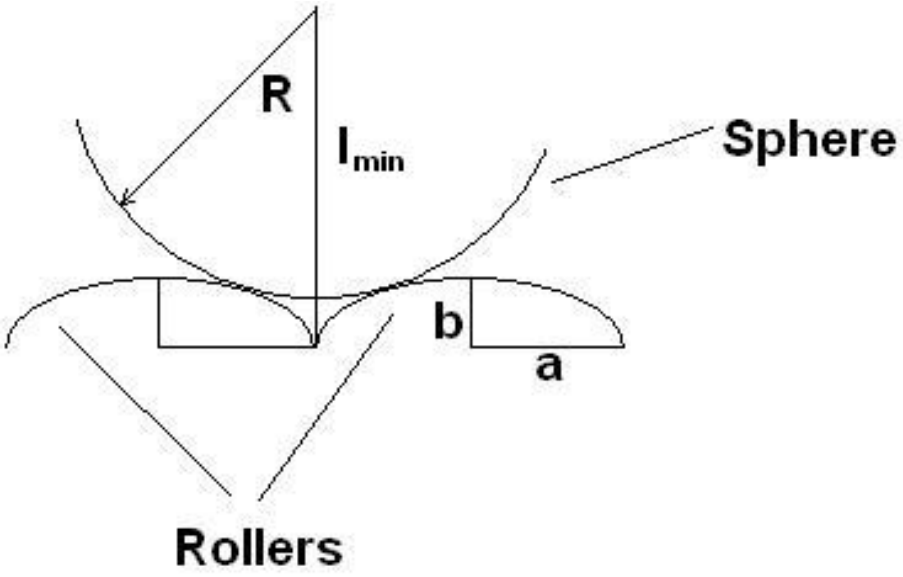

Figure 4.3: Contact area cross-section for Mecanum wheels.

centre of the omnidirectional wheel corresponds to:

$$l_{min}^2 = (R + r_r)^2 - r_r^2 \tag{4.2}$$

and the furthest state is:

$$l_{max} = R + r_r \quad . \tag{4.3}$$

Thus, in the Mecanum wheel case:

$$\Delta r_{w_i} = R_i + r_{r_i} - \sqrt{R_i(R_i + 2r_{r_i})} \quad , \tag{4.4}$$

where Δr_{w_i} is defined by the relation

$$r_{w_i} = r_{b_i} - \Delta r_{w_i} \quad . \tag{4.5}$$

Finally, similar to the way the standard omnidirectional wheels were treated in Chapter 3, the continuous function for the distance from the centre of the Mecanum wheel to the contact point becomes

$$r_{w_i} = r_{b_i} - \Delta r_{w_i} \sin\left(N_i \theta_i\right) \qquad . \tag{4.6}$$

The plots shown in Figures 4.4 - 4.6 illustrate the differences between the two wheel types in terms of position, velocity, and acceleration, respectively, for unit angular velocity of the wheels. The dimensions of the two omnidirectional wheels are presented in Figures 4.1 and 4.2.

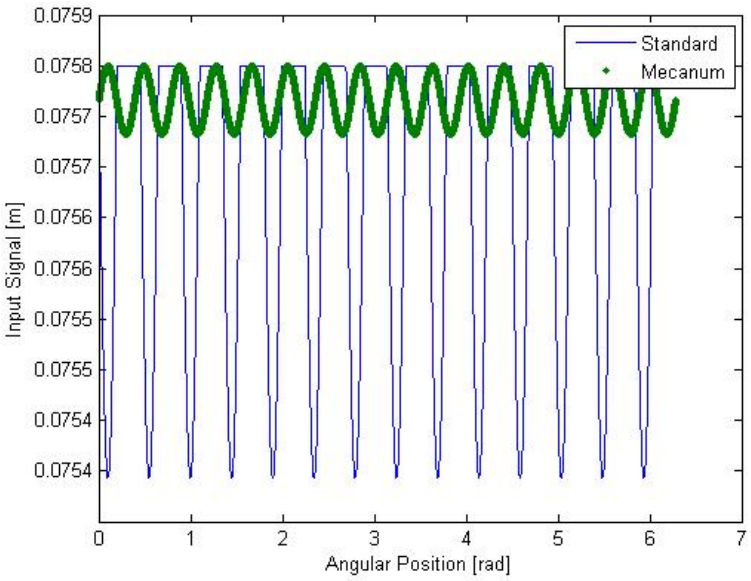

Figure 4.4: Positional excitation comparison between standard and Mecanum omnidirectional wheels.

The motivation for checking the Mecanum wheel option is quite clear from the figures. The excitation magnitudes resulting from the shape of the Mecanum wheels are significantly lower than the excitation magnitudes resulting from the shape of the standard omnidirectional wheels. The drawback is that the excitation frequency is slightly higher due to the

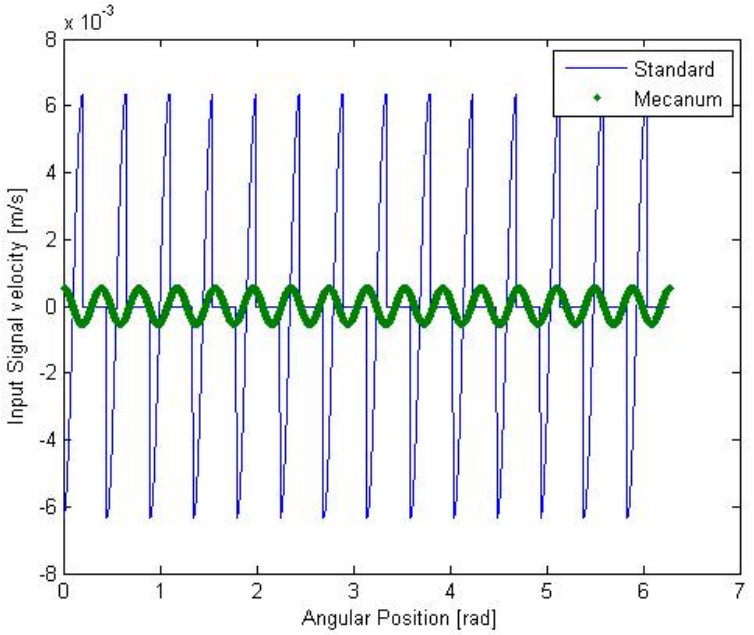

Figure 4.5: Velocity excitation comparison between standard and Mecanum omnidirectional wheels.

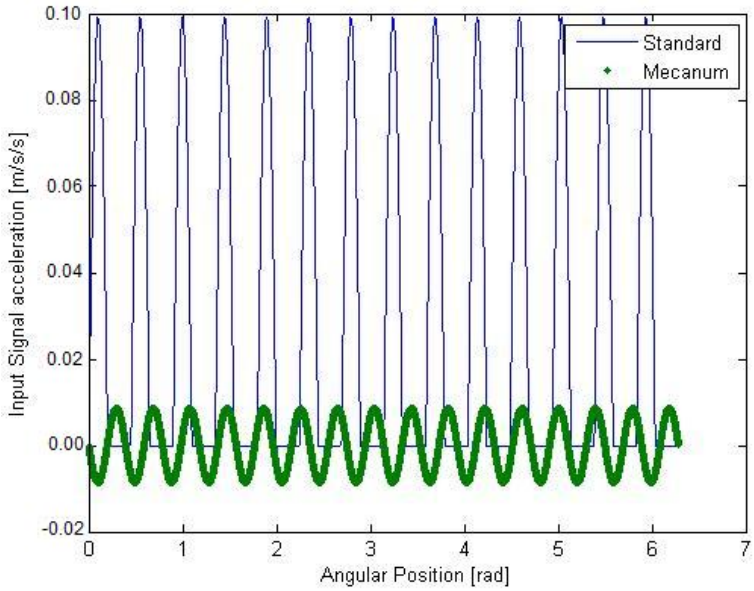

Figure 4.6: Acceleration excitation comparison between standard and Mecanum omnidirectional wheels.

fact that one may fit more rollers on the circumference of a Mecanum wheel.

4.2 Transmission Effectiveness

The first parameter to be examined is the effectiveness of the transmission. While the Jacobian developed in Chapter 2 exists for both types of wheels, it is clear that the direction of the resultant angular velocity vector is, generally, different. However, less obvious is the difference in the magnitude of the sphere angular velocities generated by the two types of wheels. In this section, the difference between the angular velocity vector magnitude of the sphere induced by Standard omnidirectional wheels and by Mecanum wheels is examined.

In order to examine the effectiveness of the transmission, a parameter similar to the traditional one degree-of-freedom transfer ratio is defined:

$$\iota = \frac{|\vec{\Omega}|}{|\vec{\omega}|} \tag{4.7}$$

where ι is the equivalent transfer ratio of the rotational subsystem. Since the system is assumed to be slip-free, the differences in the transmission effectiveness are due to different distribution of the angular velocity between the sphere itself and the rollers on the omnidirectional wheels. That is, loss of transmission effectiveness is a result of the rollers absorbing the slip instead of the sphere gaining the full magnitude possible from the actuating omnidirectional wheels. A better tool to compare the transmission effectiveness would remove the dependence on the radii of the sphere and omnidirectional wheels. Thus, for omnidirectional wheels with radius r, and a sphere with radius R, we define the transmission effectiveness:

$$\xi = \frac{R}{r}\iota = \frac{R}{r}\frac{|\vec{\Omega}|}{|\vec{\omega}|} \quad . \tag{4.8}$$

Greater values of ξ mean greater transmission effectiveness, thus allowing comparison of

various configurations and wheels. In this case, the comparison is made for identical configurations using two types of wheels - standard omnidirectional wheels and Mecanum wheels - with similar radii and the same sphere. The results for combinations of values for ω_1, ω_2, and ω_3 varying between $0-2.5$ rad/s are presented in Figure 4.7. Figure 4.7 presents the transfer ratio and the transmission effectiveness of regular and Mecanum omnidirectional wheels as a function of the norm of the input angular velocities column matrix, and clearly shows that regular omnidirectional wheels, i.e., with $\alpha = 90^\circ$ consistently have higher transmission ratio and transmission effectiveness, where the worst results for regular omnidirectional wheels are the upper limit for the Mecanum wheels.

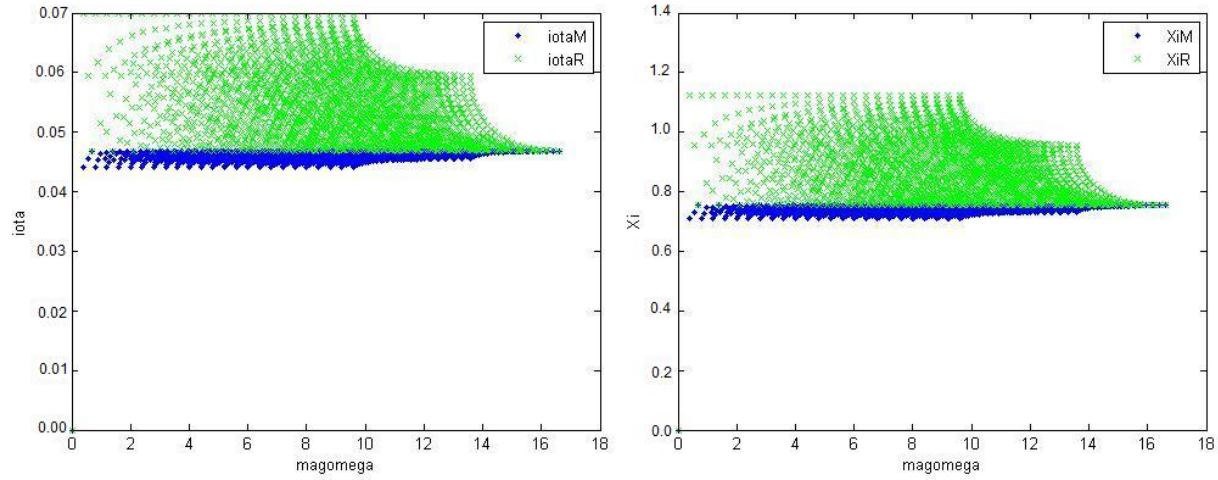

Figure 4.7: Comparing ι (left) and ξ (right) for regular (x) and Mecanum (+) omnidirectional wheels

4.3 Vibration

The major reason for examining Mecanum wheels is their relatively smooth circular profile, resulting in a smoother input function into the sphere in terms of vibration. The expectation is to find the Mecanum wheels advantageous in that regard simply because the noise input level has lower magnitude and has a smoother shape (lower magnitude of the derivatives).

Elastic properties of the sphere at the contact points, as well as elastic properties of the mounting of the omnidirectional wheels significantly affect the vibration response of the system. These effects, as well as damping effects, are investigated next.

4.3.1 Natural Frequency

The natural frequencies of the system are obtained from Equations 3.41 and 3.42, by resolving the coefficient determinant:

$$\begin{vmatrix} -M_s\omega_{n_i}^2 - K_i' & -M_s\omega_{n_i}^2 + K_i - K_i' \\ -m_i\omega_{n_i}^2 + k_i & -K_i \end{vmatrix} = 0 \quad i = 1, 2, 3 \tag{4.9}$$

for each contact point, where ω_{n_i} is the natural frequency for contact point i. Figure 4.8 illustrates the natural frequency as a function of K_i, illustrating the effects of changing the stiffness coefficient of the omnidirectional wheel mounting.

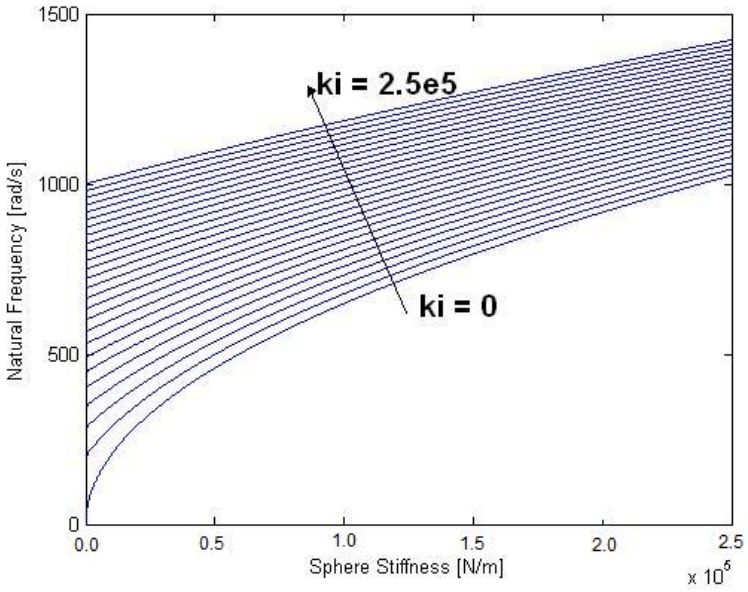

Figure 4.8: Natural frequency as a function of the stiffness of the sphere and the stiffness of the omnidirectional wheel mounting $K_i' = 0$

It is clear that increasing both these parameters increases the natural frequency of the system as shown in the plot. The effects of increasing the stiffness coefficient of the kinematic closure mounting K' are presented in Figure 4.9. Here, the effects of K' are negligible as seen

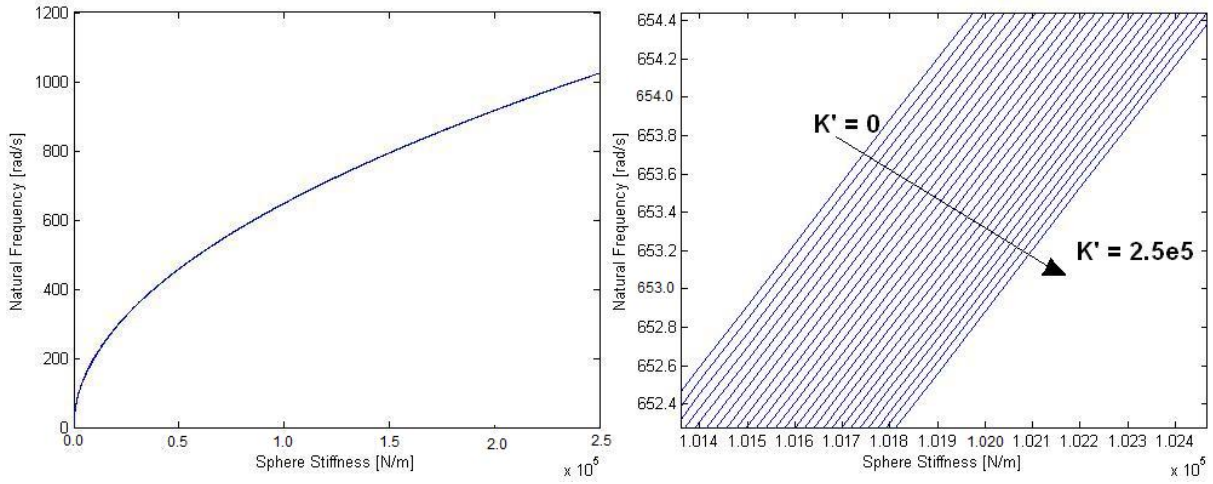

Figure 4.9: Natural frequency as a function of the stiffness of the sphere and the stiffness of the kinematic closure mounting, $k_i = 0$

in the left hand side of the figure and the overall relation is with the opposite effect, as is seen in the magnified area illustrated in the right hand side of the figure. That is, increasing K' decreases the natural frequency of the system.

4.3.2 Sphere Stiffness Effects

The stiffness of the sphere, as presented in section 3.2 plays a role in the dynamic behaviour of the sphere in isolating vibration. The vibration response, as well as the effects of the sphere's stiffness on the vibration magnitude are presented in this section, focusing on the comparison between the two omnidirectional wheels presented in the beginning of this chapter. Figure 4.10 shows the maximum magnitude of the motion of the sphere centre as a function of the stiffness coefficient of the sphere, K, comparing a standard omnidirectional wheel to a Mecanum wheel. The right hand side of the figure shows a magnification of the plot on

the left hand side to better highlight the differences. The results are for constant angular velocities of the omnidirectional wheels with values of $\omega_1 = 0.1$ rad/s, $\omega_2 = 1.2$ rad/s, and $\omega_3 = 0.9$ rad/s.

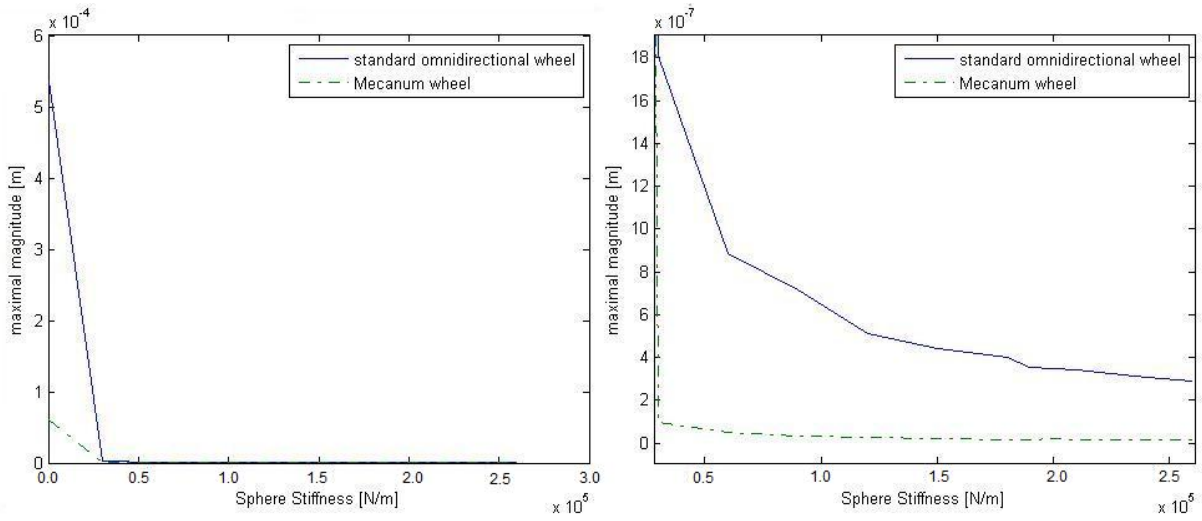

Figure 4.10: Maximum magnitude of sphere centre displacement as a function of K comparing standard and Mecanum omnidirectional wheels, $\omega_1 = 0.1$ rad/s, $\omega_2 = 1.2$ rad/s, and $\omega_3 = 0.9$ rad/s.

The rigid body case can be viewed at the $K = 0$ point on the left hand side plot and the significant reduction of the maximum magnitude for various stiffness coefficients for the sphere. The right hand side plot is a magnification of the plot on the left hand side that shows the differences between the two omnidirectional wheel types more clearly for non-zero values of K. The ratio between the maximal displacement magnitude resulting with the Mecanum wheel and a standard omnidirectional wheel is defined:

$$\kappa = \frac{|\Delta R_{s_{max}}|_{Mecanum}}{|\Delta R_{s_{max}}|_{Standard}} \quad . \tag{4.10}$$

The values for κ for this case, were all in the range of $0.04 < \kappa < 0.11$

To observe the effects of various combinations of input angular speeds, various combinations were used. Such an example, where another combination of input angular speeds was

used. The right hand side of the figure shows a magnification of the plot on the left hand side to better highlight the differences. The results are for constant angular velocities of the omnidirectional wheels with values of $\omega_1 = 2.0$ rad/s, $\omega_2 = 2.0$ rad/s, $\omega_3 = 2.0$ rad/s.

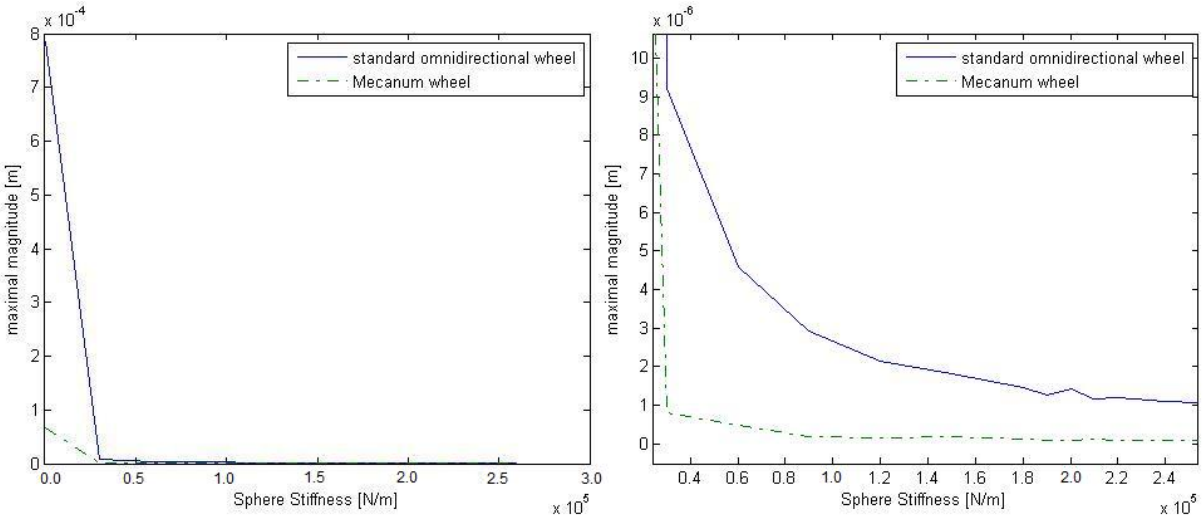

Figure 4.11: Maximum magnitude of sphere centre displacement as a function of K comparing standard and Mecanum omnidirectional wheels, $\omega_1 = 2.0$ rad/s, $\omega_2 = 2.0$ rad/s, $\omega_3 = 2.0$ rad/s. .

Similarly, the ratio κ for this case was in the range of $0.06 < \kappa < 0.12$.

A variety of input angular speeds was used with similar results where the input angular speed was in the range:

$$0 < \omega_i < 12 \text{ rad/s} \tag{4.11}$$

resulting in ratios in the range:

$$0.04 < \kappa < 0.12 \quad . \tag{4.12}$$

4.3.3 Omnidirectional Wheel Mounting Effects

While it is possible to affect the stiffness of the sphere, it may be done in a limited fashion. The omnidirectional wheel mounting may be affected by mounting the omnidirectional wheels onto the linear platform through spring-damper systems. However, this system is not directly affecting the sphere and its overall effects are expected to be small. Here, the effects of such mounting on the motion of the centre of the sphere is investigated. Figure 4.12 shows sample results for the case where $K = 190000$ N/m.

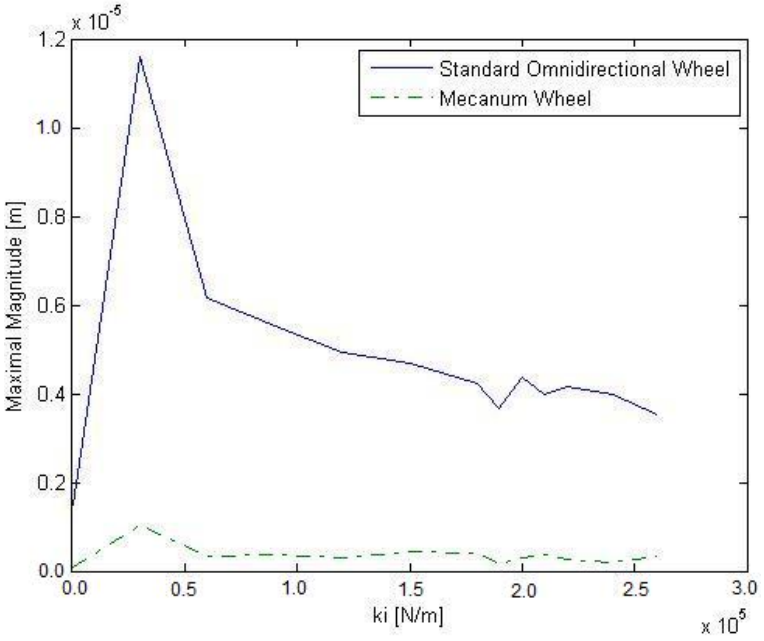

Figure 4.12: Maximal magnitude ratio as a function of k_i for $K = 190000$ N/m.

The results presented in Figure 4.12 clearly show that increasing k_i increases the maximum magnitude of the sphere centre motion; yet, once again, it stands out that the maximum magnitude for the Mecanum wheel is significantly lower than that of the standard omnidirectional wheel. This effect may be explained by the fact that the magnitude of the vibration increases with the natural frequency, and it was observed in the natural frequency section of this chapter that increasing k_i increases the natural frequency of the system.

4.3.4 Kinematic Closure Mounting Effects

Since the results obtained examining the effects of the omnidirectional wheel mounting showed little to no effect on the sphere vibration magnitude, the remaining location for vibration isolation is by controlling the stiffness of the kinematic closure mechanism, K'.

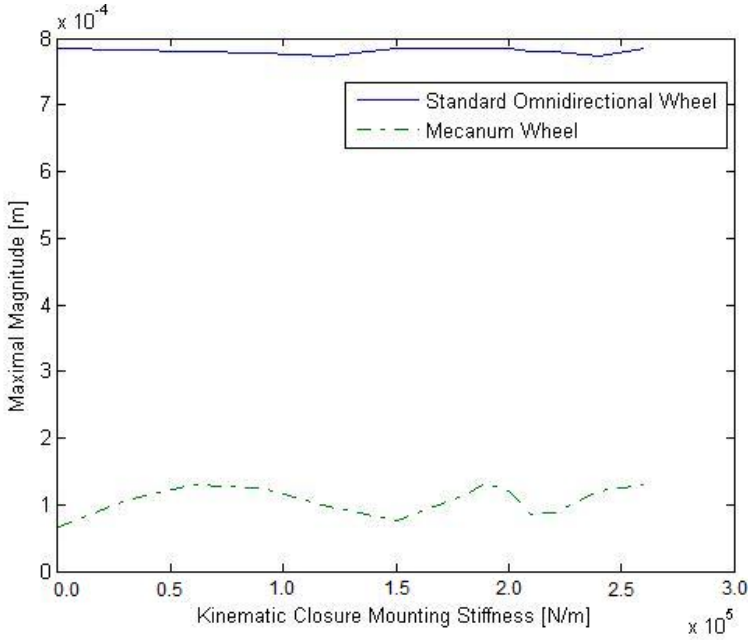

Figure 4.13: Maximum magnitude ratio as a function of k' for $K = 0$ N/m, $\omega_1 = 2.0$ rad/s, $\omega_2 = 2.0$ rad/s, $\omega_3 = 2.0$ rad/s.

Figure 4.13 shows that the effects of the kinematic closure mounting stiffness are insignificant, as the maximum magnitude of the vibration of the centre of the sphere remains the same, regardless of the value of K' and regardless of the omnidirectional wheel type. While the results presented in Figure 4.13 were obtained for the case where the angular velocities of the omnidirectional wheels with values of $\omega_1 = 2.0$ rad/s, $\omega_2 = 2.0$ rad/s, $\omega_3 = 2.0$ rad/s, similar results were obtained for other values of angular velocities, another such example is presented in Figure 4.14 for angular velocities values of $\omega_1 = 0.1$ rad/s, $\omega_2 = 1.2$ rad/s, $\omega_3 = 0.9$ rad/s.

Investigating the effects of k' on the results showed little to no effect of the parameter

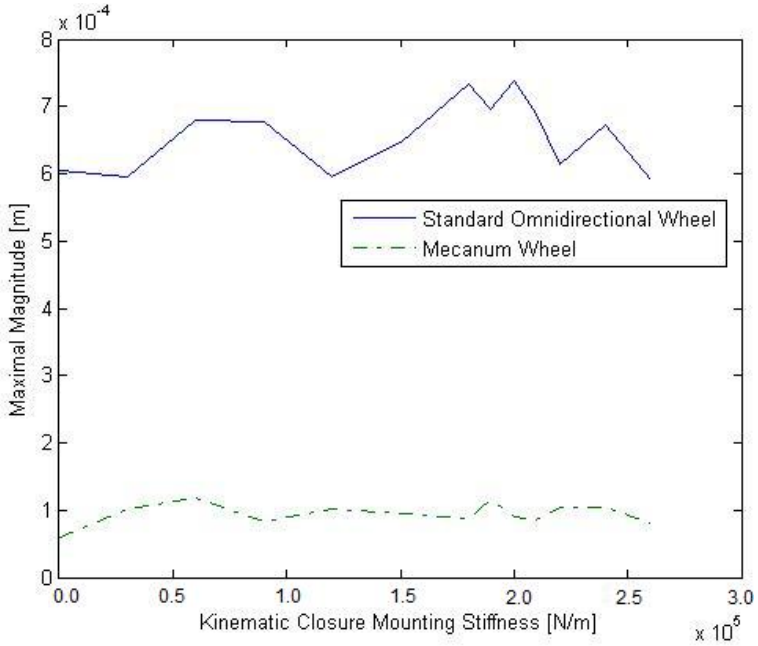

Figure 4.14: Maximum magnitude ratio as a function of k' for $K = 0$ N/m, $\omega_1 = 0.1$ rad/s, $\omega_2 = 1.2$ rad/s, $\omega_3 = 0.9$ rad/s.

on the resulting magnitude of the vibration of the sphere's centre. A sample demonstration where the sphere was not assumed rigid is presented in Figure 4.15, for angular velocity values of $\omega_1 = 0.1$ rad/s, $\omega_2 = 1.2$ rad/s, $\omega_3 = 0.9$ rad/s, and sphere stiffness of $K = 170000$ N/m.

Thus, it is concluded that the effects of the kinematic closure mounting are minor.

4.3.5 Standard Versus Mecanum Omnidirectional Wheel Potential

While the previous subsections focused on the comparison of two specific omnidirectional wheels - one a standard omnidirectional wheel and the other a Mecanum wheel, the comparison took place between two omnidirectional wheels that were picked for the purpose of construction of an Atlas demonstrator. Thus, major factors in the selection process were availability and comparable sizes. In this subsection, a more general comparison is made between standard and Mecanum omnidirectional wheels, from a vibration standpoint.

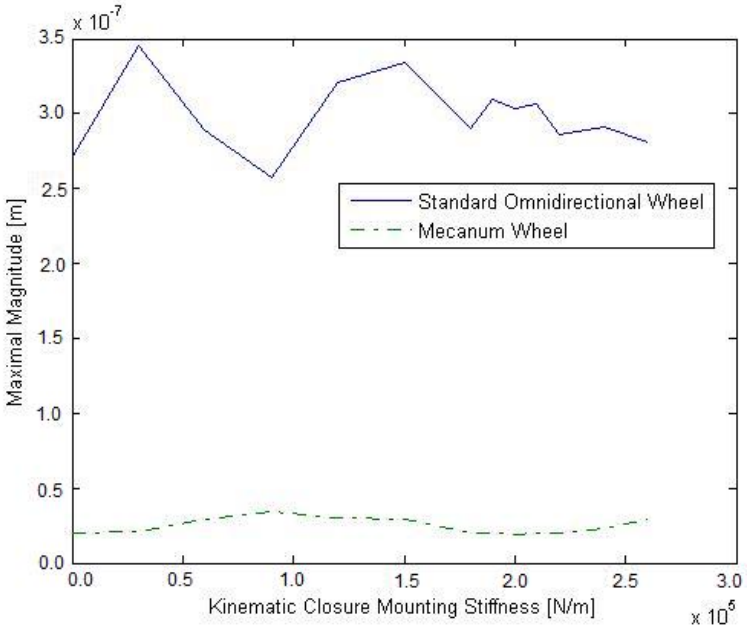

Figure 4.15: Maximum displacement magnitude ratio as a function of k' for $K = 1700000$ N/m.

The excitation levels of both omnidirectional wheel types are compared for both maximal magnitude, maximal velocity, and maximal acceleration. While it was clear from Figures 4.4 through 4.6 that the Mecanum wheel is far superior to the standard omnidirectional wheel, there may still be other standard omnidirectional wheels constructed, with the same diameter, that may show better levels of excitation. The same is true for Mecanum wheels. This subsection takes these omnidirectional wheels's improvements to the limits in order to compare the two wheel types's potential from the vibration standpoint.

In order to compare the two omnidirectional wheel types, a geometric descriptor needs to be selected as a parameter for the comparison. On the one hand, it seems like the number of rollers (for the same diameter wheel) may be a good choice. However, this is ignoring some of the advantages that the standard omnidirectional wheel may have with some clever design. The important parameter for the standard omnidirectional wheel is η, the roundness ratio. While increasing the number of rollers carries the potential to increase the roundness ratio,

there are some designs, presented in Chapter 1, such as conical rollers and variable diameter rollers, that significantly increase the roundness ratio and get very close to a smooth shape ($\eta = 0$). Thus a good parameter to describe the shape of a standard omnidirectional wheel is the roundness ratio, η. Mecanum wheels, on the other hand, possess a roundness ratio of $\eta = 1$, or very close to that. However, the roller orientation is the cause for vibration. In this case, the significant parameter is the roller diameter, which is representative of the number of rollers. Thus, comparison was performed using the roundness ratio for the standard omnidirectional wheels and the number of rollers for Mecanum wheels. The comparison was made for omnidirectional wheels with the same diameter as the wheels used in the Atlas demonstrator in the previous sections.

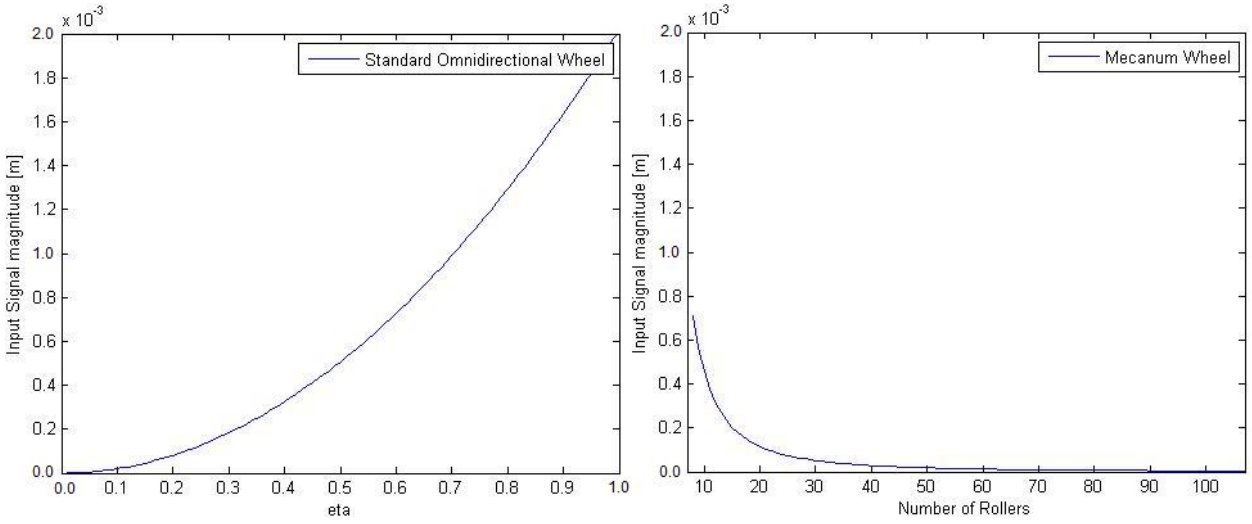

Figure 4.16: Maximum excitation magnitude comparison - standard omnidirectional wheel on the left, Mecanum wheel on the right.

Figure 4.16 shows a maximum excitation magnitude comparison between the two omnidirectional wheel types. While it is clear that in most cases, and specifically in the area that was investigated ($\eta = 0.4485$ for the standard omnidirectional wheel, $N = 16$ for the Mecanum wheel), the Mecanum wheel is superior to the standard omnidirectional wheel. One may observe from the plots presented in Figure 4.16 that for very low values of η, stan-

dard omnidirectional wheels have lower maximal excitation magnitudes than the best that Mecanum wheels can obtain even for a very large number of rollers ($N > 100$). In addition, a Mecanum wheel with such a large number of rollers would have a very low load capacity and would be extremely expensive to produce, whereas standard omnidirectional wheels may obtain very low values of η with a rather small number of rollers utilizing designs such as conical rollers or variable diameter rollers.

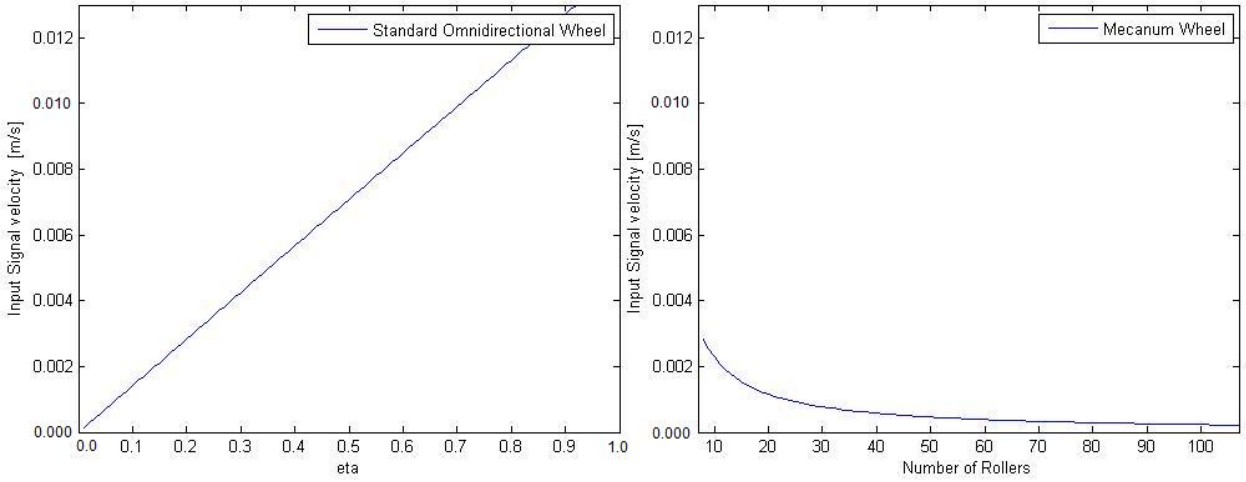

Figure 4.17: Maximum excitation velocity comparison - standard omnidirectional wheel on the left, Mecanum wheel on the right.

Similar observations may be obtained from Figure 4.17 regarding the velocity of the excitation, though less pronounced. The maximal excitation acceleration though shows a different picture, where it is clear that the Mecanum wheel is always superior to the standard omnidirectional wheel, as observed in Figure 4.18. This is likely due to the fact that the diameter changes that do occur in the standard omnidirectional wheel are abrupt and therefore produce large accelerations when transitioning between rollers.

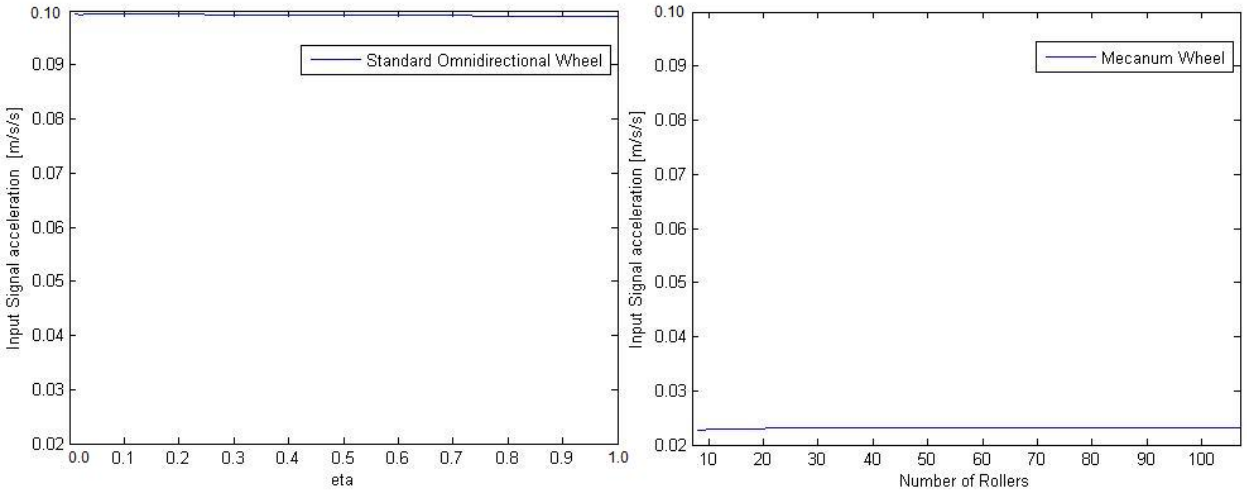

Figure 4.18: Maximum excitation acceleration comparison - standard omnidirectional wheel on the left, Mecanum wheel on the right.

4.4 Summary

In this chapter, standard and Mecanum omnidirectional wheels were compared using two specified omnidirectional wheel designs. It was observed that for the cases selected in this chapter Mecanum wheels show significantly less vibration than standard omnidirectional wheels. However, it was also shown that the equivalent transfer ratio of standard omnidirectional wheel is superior to that of the Mecanum wheels. Furthermore, extending and generalizing the geometric comparison between the two omnidirectional wheel types reveals that some standard omnidirectional wheel designs may perform even better than Mecanum wheels from the vibration standpoint.

In addition, it was also observed that the omnidirectional wheel mounts and the kinematic closure mounts play a very minor role when considering vibration, and the most significant factor in reducing vibration is the sphere-omnidirectional wheel interface.

Chapter 5

Conclusions and Future Work

The main goal of this thesis was the development of a comprehensive mathematical model for a sphere actuated by omnidirectional wheels, and in particular the kinematics and dynamics of a sphere actuated by three omnidirectional wheels. This work encompassed four main issues including:

1. Kinematics of a sphere actuated by n omnidirectional wheels of any type, size or shape, at any position and orientation;

2. The dynamics of a sphere actuated by omnidirectional wheels;

3. Vibration induced by omnidirectional wheels on an actuated sphere; and

4. A comparison between two major classes of omnidirectional wheels - standard omnidirectional wheels, and Mecanum wheels.

The development of the kinematics of a sphere actuated by omnidirectional wheels served as a basis for the dynamics of the system. Yet, the development of the kinematics has some merits on its own, since it was derived in a general manner and produced a tool to derive the kinematics of any system including a sphere actuated by any type of omnidirectional

wheel. The kinematics model also yields a set of conditions that must be met in order to obtain a system that is free of singularities and has zero kinematic slip. Satisfying these conditions it should be a first step in the design process of any such system, and to perform first qualification of a given architecture. In addition, the kinematics serve as a foundation for the dynamics of the system, and, in its inverse form, as the basis for feedback control. The kinematic model for the system was developed in stages, originating from the zero-slip concept applied to a basic three perfect wheels problem that resulted in the basic Jacobian portrayed in Equation 2.19.

To enhance the extent of the solution and obtain a more powerful tool, the concept was generalized to include any number of omnidirectional wheels. Furthermore, in order to make the results more applicable to real world problems, the imperfect nature of the omnidirectional wheel design was considered. Various omnidirectional wheel design concepts were treated as geometrical anomalies to the basic single-race perfectly round shaped omnidirectional wheels. Thus, dual-race omnidirectional wheels were treated as a combination of two alternating single-race omnidirectional wheels where the point of contact with the sphere shifts. This extension of the basic problem yielded a set of eight different Jacobians for the three wheels case, and a simple algorithm that selects the proper Jacobian for each instant. Sample results showed a correction of up to 4% and 3° in the magnitude and direction of the resulting angular velocity vector respectively, compared with using the single-race Jacobian. Thus, the modified set of Jacobians can be used as an error estimate if the single-race Jacobian is used to determine the kinematics of the system. Alternatively, the modified set of Jacobians can be used to determine the kinematics of the system more accurately, which would require either more computing power, or more sensors to determine the exact orientation of each omnidirectional wheel.

Next, triple-race omnidirectional wheels were treated as a combination of dual-race wheels from the standpoint of shifting contact points and $2n$ omnidirectional wheels, where each

set of two wheels was constrained to move with the same angular velocity. While the idea behind the design was to create an equivalent single contact point with the sphere, thus avoiding the errors/corrections of the dual-race Jacobian, the results showed conclusively that this is not the case, and singularity-free no-slip conditions cannot be obtained at all using triple-race omnidirectional wheels.

After that, Mecanum type wheels were considered, where the rollers are aligned at a 45° angle to the actuation axis of the wheel, instead of the standard 90° orientation. The appropriate Jacobian for this case was derived using a generalization of the basic method used for developing the kinematics for the standard omnidirectional wheel case. Finally, the inclination angle of the rollers was treated as a parameter, and the kinematics were generalized further to include any inclination angle for the rollers, where the Mecanum wheels become a special case where the inclination angle is 45°, and standard omnidirectional wheels are a special case with an inclination angle of 90°.

During the development and presentation process throughout Chapter 2, benchmark examples were used along with specific examples that illustrate and highlight important cases and ideas. These were used to demonstrate the approach and the differences between the various kinematic architectures and the omnidirectional wheel types. The kinematics showed that from the standpoint of slip, single-race and Mecanum omnidirectional wheels are superior to their multi-race counterparts. In addition, it was shown that an architecture comprising three omnidirectional wheels is superior to architectures comprising more or less omnidirectional wheels, with the exception of some special cases such as the example of six omnidirectional wheels with three wheels enslaved to the other three, as shown in Chapter 2.

Once the kinematics of a system are in place, deriving the equations of motion, assuming all bodies are rigid, is a relatively straightforward process. However, no system is completely rigid. Specifically with the Atlas platform it was observed that the sphere-roller interface experiences significant deflections (associated with the low mass design objective and the

soft castor rollers material). Thus, it was assumed that the interfaces between the sphere and the omnidirectional wheels are non-rigid. In addition, other connection points were assumed flexible. Most interesting is the non-rigid interface at the force transfer points; that is, the contact points between the sphere and the actuating omnidirectional wheels. The deflection at the sphere-roller interface causes the contact points to become contact patches with distributed normal and tangential forces. These, in turn, create moments resisting the driving moments in the form of spin resistance and rolling resistance. These moments were modelled in Chapter 3 as a product of a moment arm and a force. This idea for modelling allowed for the investigation of the effects of the moment arm length on the resisting moments regardless of the model selected to evaluate them. A detailed analysis using the classic Hertzian model for the contact forces was performed to demonstrate the approach. However, due to the Hertzian basic assumption that the contact patch is symmetric, rolling resistance vanished. This demonstrated the power of the modelling approach of a moment arm that can be varied to investigate its effect. The results showed only negligible effects of both spin resistance, and especially rolling resistance. The effects of elastic contact on the vibration of the centre of the sphere were, though, dominant when compared to a rigid sphere, but varied little with changes of the effective spring coefficient of the contact.

Modelling for vibration assumed that the contact points between the sphere and the omnidirectional wheels act like spring-damper systems that are independent of one another, since the actual centre of the sphere is not necessarily connected to the contact points. The shape of the omnidirectional wheels was taken as positional excitation. Similarly, the mounting of the omnidirectional wheels onto the linear platform and the contact between the sphere and kinematic closure mounting points were taken as non-rigid. The most significant effect on vibration by far was that of the stiffness of the sphere-wheel contact. It was evident that the effective spring coefficient of this interface is the dominant factor when it comes to natural frequency and maximum vibration magnitude of the centre of the sphere's

position. The omnidirectional wheels's mounting stiffness had a minor impact on the natural frequency of the system, but not much on the maximal magnitude. The damping coefficient's contribution was also minor.

The performance of two omnidirectional wheel types were compared and contrasted with the Atlas demonstrator. Comparing the two wheel types required developing a geometric model for the interface between their perimeter and a sphere. It was observed that the Mecanum wheel's perimeter, when it comes in contact with the sphere has a much smoother excitation function shape, as well as much smaller excitation function magnitude, compared with its standard omnidirectional wheel counterpart. Once this fact was established mathematically, it was no surprise to observe significant differences in the resulting motion of the centre of the sphere.

While initially it appeared that Mecanum wheels have the advantage over the standard omnidirectional wheels from the standpoint of vibration. A closer look at the differences between the two omnidirectional wheel designs exposed a more interesting conclusion. While most currently available omnidirectional wheels demonstrate the same kind of differences (i.e., smaller vibration magnitudes for the Mecanum wheels), Mecanum wheels are more limited in terms of potential. This means that comparing the best Mecanum wheel design to the best standard omnidirectional wheel design, the standard omnidirectional wheels would actually show a lower vibration magnitude than that of the Mecanum wheel. However, the acceleration would still be higher than that of the Mecanum wheel, which is significant if the application calls for something sensitive to accelerations inside the sphere (such as a human being).

Another observation derived directly from the kinematics of both omnidirectional wheels was that of the transmission ratio. It was demonstrated that for the same angular velocity input levels, the magnitude of the angular velocity of the sphere in the system comprising standard omnidirectional wheels would be higher than its counterpart comprising Mecanum

wheels.

Based on the conducted study, the contributions of this thesis with respect to existing systems, investigations, and approaches is summarized below:

- The development and application of general kinematic and dynamic formulations for the motion of a sphere actuated by any omnidirectional wheel type.

  There are no studies that attempt to obtain a general kinematic formulation to a system comprising a sphere actuated by omnidirectional wheels. The only studies that involve friction actuation using omnidirectional or Mecanum wheels deal with planar motion of a mobile robot. It is concluded that the proposed formulations and their applications are not only new, but also involve a different approach pertaining to the spatial nature of the problem.

- The development of a method for determining the angular velocity vector of a sphere based on partial information of velocities of points on the sphere.

  The proposed method was developed for the purpose of determining the kinematics of the sphere actuated by three omnidirectional wheels. In this case, only partial information is known about the velocities of the contact points between the sphere and the omnidirectional or Mecanum wheels. There are cited studies that derive the angular velocity vector of a rigid body providing the full information on the velocities of three points on the body are known. The method developed for the purpose of resolving the kinematics of this system is therefore new and utilized a different approach to the existing studies.

- The detailed treatment of the effects of omnidirectional wheel design on the kinematics of the system.

  While kinematics of systems comprising omnidirectional wheels was treated in previous

studies, most of which relate to mobile robots moving on a plane, the wheels themselves were always treated as perfectly-round-single-race wheels from the standpoint of kinematics. This thesis differentiates between omnidirectional wheels designed with a single race of rollers and designs with two and three races of rollers at the kinematics level, and shows differences too significant to ignore when dealing with these variations between omnidirectional wheel designs. This thesis analyzes the kinematics of the dual-race omnidirectional wheel design, suggests correction matrices, and estimates the error of the single-race assumption. In addition, the treatment of the triple-race omnidirectional wheel design shows major drawbacks and slip issues when using such wheels, all of which are ignored completely in previous studies of systems comprising omnidirectional wheels.

- The development of a general kinematic model for a sphere actuated by any number of omnidirectional wheels of any type, including slip estimation, and the concept of equivalent points.

  The theoretical expansion of the basic concept of actuating a sphere with three omnidirectional wheels to N omnidirectional wheels resulted in a robust tool for examining any desired architecture from the standpoint of slip and workspace singularities. This mathematical tool is novel and allows for the evaluation of a design at an early stage, prior to dealing with dynamics and detailed design of the system. The work performed in this thesis yields the Jacobian for any such system.

- The development of dynamics and vibration models for a 6 DOF system comprising a sphere actuated by omnidirectional or Mecanum wheels as its rotational subsystem.

  This 6 DOF system is a natural but novel expansion of the aforementioned 3 DOF counterpart. It demonstrates a unique system where the rotational degrees-of-freedom are uncoupled from the translational ones, at the input level. That is the control of

the translational motion is done using separate controls from the ones controlling the rotational motion. While some 6 DOF parallel motion platforms achieve the ability to perform translational-only and rotational-only motions, they must still employ all six controls at the input level to accomplish the task. This thesis also performs an analysis of the vibration induced by the actuating omnidirectional or Mecanum wheels on the actuated sphere.

- The application of the suggested models for the purpose of analyzing and comparing two similar systems with different omnidirectional wheel types from the standpoint of vibration.

  Two otherwise identical systems with similar sizes of Mecanum wheels and standard omnidirectional wheels were compared from the standpoint of vibration. Various system parameters, such as stiffness of certain points of the system were varied to obtain a broad picture of the differences between the two wheel types. This is the first time these two wheel types were compared directly in this regard.

- The general comparison between Mecanum and omnidirectional wheels actuation induced vibration.

  The two omnidirectional wheel types vibration excitation levels when in contact with a sphere were compared geometrically. The comparison was performed in a general manner such that their specific design were parameterized and taken into account to obtain their excitation levels. Both wheel types potential was compared and pushed to the limits. Such parametric mathematical comparison is done here for the first time.

5.1 Future Work

It is clear that the study conducted within this thesis has reached the objective set by the motivation to develop a general mathematical model of a sphere actuated by omnidirectional wheels, comparing various omnidirectional wheel types, and investigating vibration induced by omnidirectional wheels. Yet, there is still a lot to investigate with respect to all the issues of this thesis, as discussed in the following:

- While the effects of various parameters on the vibration of the system were investigated, some parameters were left for future work. Such parameters were the friction coefficients between the omnidirectional wheels and the sphere, the position and orientation of the omnidirectional wheels with respect to the sphere, the masses of the sphere and the linear platform, the radii ratio between the omnidirectional wheels and the sphere, and more. The tools to obtain these effects were developed in this thesis and their use was demonstrated.

- An experimental system that would allow for experiments to be conducted needs to be constructed and used to obtain experimental results that would allow for refining the results obtained in this thesis. This system would allow varying the omnidirectional wheel types, sizes, positions, and orientations, as well as controlling the Force closure that forces the no-slip condition.

- While the effects of varying effective spring coefficients for the sphere-omnidirectional wheel interface were investigated, design and strength of materials considerations would not allow for much flexibility in the selection of this parameter. Thus, a less constrained way for vibration isolation should be selected. Such a way would be application dependent, but would comprise a spring-damper subsystem that should be located between the excitation source (the omnidirectional wheels) and the sphere, probably inside the

sphere.

- Common anticipated applications, such as a flight simulator motion platform, should have their design requirements defined and, utilizing the mathematical model presented in this thesis, should be optimized. This stage would call for multi-objective optimization, followed by the design of a control system.

The scope of this thesis is wide. It introduces a mathematical formulation for the kinematics and dynamics of the Atlas platform using new and general approaches. It then applies these formulations to several benchmark designs. The ideas introduced in this thesis are general in nature, and as such, are applicable to any system with the basic configuration of a sphere actuated by omnidirectional wheels.

References

[1] D. Stewart. "A Platform with 6 Degrees of Freedom". *Proc. of the Institution of Mechanical Engineers*: (Part 1, 15): 371-386, 1965.

[2] V.E. Gough. "Contribution to Discussion of Papers on Research in Automobile Stability, Control and Tyre Performance". *1956-1957 Proc of Auto Div. Inst. Mech. Eng.*

[3] CAE Inc. "www.cae.com". Last visited on Spetember 22, 2010.

[4] M.J.D. Hayes, and R.G. Langlois. "A Novel Kinematic Architecture for Six DOF Motion Platforms". *2005 CCToMM Symposium on Machines, Mechanisms and Mechtronics,* Canadian Space Agency, On CD, May 26-27, 2005.

[5] J. Robinson, J.B. Holland, M.J.D. Hayes, and R.G. Langlois. "Velocity-level Kinematics of a Spherical Orienting Device Using Omni-directional Wheels". *2005 CCToMM Symposium on Machines, Mechanisms and Mechtronics,* Canadian Space Agency,On CD, May 26-27, 2005.

[6] J.P. Merlet. "Parallel Robots". *Boston, MA: Kluwer Academic Publishers, 2000.*

[7] S.K. Advani. "The Kinematic Design of Flight Simulator Motion-Bases". Ph.D. Thesis, *Delft University Press, 1998.*

[8] H.K. Hunt. "Structural kinematics of in parallel actuated robot arms". *J. of Mechanisms, Transmissions and Automation in Design*: 105:705–712, March 1983.

[9] H. McCallion, and D.T. Pham. "The Analysis of a six degrees of freedom work station for mechanized assembly". *Proc. 5th World Congress on Theory of Machines and Mechanisms*: pp 611–616, Montreal, July 1979.

[10] C. Innocenti, and V. Parenti-Castelli. "Direct kinematics of the 6-4 fully parallel manipulator with position and orientation uncoupled". *European Robotics and Intelligent Systems Conf.*: Corfu, June 23–28 1991.

[11] D. Bernier, J-M. Castelain, and X. Li. "A new parallel structure with six degree of freedom". *9th World Congress on the Theory of Machines and Mechanisms*: pp 8–12, Milan, August 30–September 2, 1995.

[12] S.P. Patarinski, and M. Uchiyama. "Position/Orientation decoupled parallel manipulator". *ICAR*: pp 153–158, Tokyo, November 1–2, 1993.

[13] D. Zlatanov, M.Q.. Dai, R.G. Fenton, and B. Benhabib. "Mechanical design and kinematics analysis of a three-legged six degree-of-freedom parallel manipulator". *22nd Biennial Mechanisms Conf.*: volume DE-45, pp 529–536, Scottsdale, September 13–16, 1992.

[14] K. Mianowski. "Dexterous fully parallel manipulator with six degrees of freedom". *7th International Conference on Control, Automation, and Vision*: 45–50, vol. 1 2002.

[15] G. Yang, W. Chen, and E.H.L. Ho. "Design and Kinematics of a modular hybrid parallel-serial manipulator". *12th RoManSy*: pp 253–260, Paris, July 6–9 1998.

[16] K.J. Waldron, M. Raghavan, and B. Roth. "Kinematics of a hybrid series-parallel manipulator". *Mechanism and Machine Theory*: 34:1037–1055, 1999.

[17] L. Romdhance. "Design and analysis of a hybrid serial-parallel manipulation system". *ASME Journal of Dynamic Systems, Measurements, and Control*: 111:211–221, June, 1989.

[18] S.A.A. Moosavian., A. Pourreza, and K. Alipour "Kinematicas and dynamics of a hybrid serial-parallel mobile robot". *2009 IEEE International Conference on Robotics and Automation*: Kobe, Japan, May 12–17, 2009.

[19] J. Yan, C. I-Ming, Y. Guilin. "Kinematic Design of a 6-DOF Parallel Manipulator with Decoupled Translation and Rotation". *IEEE Transactions on Robotics*: v112, n3, pages 331–336, 1990.

[20] J. Kim, J.C. Hwang, J.S. Jim, C.C. Iurascu, F.C. Park, Y.M. Cho. "Eclipse II: A New Parallel Mechanism Enabling Continuous 360-Degree Spinning Plus Three-Axis Translational Motions". *IEEE Transactions on Robotics and Automation*: v18, n3, pages 367–373, June 2002.

[21] W. Bles, and E. Groen. "The DESDEMONA motion facility: Applications for space research". *Microgravity Science and Technology*: v21, n4, pages 281–286, November, 2009.

[22] L. Ferriere, and B. Raucent. "ROLLMOBS, a New Universal Wheel Concept". *Proceedings of the 1998 IEEE International Conference on Robotics and Automation*: pages 1877–1882, May, 1998.

[23] M. Wada, and H.H. Asada. "Design and Control of a Variable Footprint Mechanism for Holonomic Omnidirectional Vehicles and its Application to Wheelchairs". *Proceedings of the 2001 IEEE International Conference on Robotics and Automation*, v 15, n 6: pages 978–989, December, 1999.

[24] M. West, and H. Asada. "Design and Control of Ball Wheel Omnidirectional Vehicles". *Proc. IEEE Int. Conf. Robot. Automat.*, pp. 1931–1938, May 1995.

[25] T.B. Lauwers, G.A. Kantor, R.L. Hollis. "One is Enough!". *Proceedings of 2005 International Symposium of Robotics Research, October 2005*

[26] G.S. Chirikjian, and D. Stein. "Kinematic design and commutation of a spherical stepper motor". *IEEE/ASME Transactions on Mechatronics*: v 4, n 4, pages 342–353, December 1999.

[27] D. Stein, E.R. Scheinerman, and G.S. Chirikjian. "Mathematical models of binary spherical-motion encoders". *IEEE/ASME Transactions on Mechatronics*: v 8, n 2, pages 234–244, June 2003.

[28] K.M. Lee, and C.K. Kwang. "Design concept of a spherical stepper for robotic applications". *IEEE Transactions on Robotics and Automation*: v 7, n 1, pages 175–181, February 1991.

[29] S.L. Dickerson. "Control of an Omni-Directional Robotic Vehicle with Mecanum Wheels". *Proceedings of the 1991 IEEE International Conference on Robotics and Automation*: pages 323–328, 1991.

[30] P. Viboonchaicheep, A. Shimada, and Y. Kosaka. "Position Rectification Control for Mecanum Wheeled Omni-directional Vehicles". *IECON Proceedings (Industrial Electronics Conference)*, v 1, 2003: pages 854–859.

[31] K.L. Han, O.K. Choi, I. Lee, I. Hwang, J.S. Lee and S. Choi. "Design and control of omni-directional mobile robot for mobile haptic interface". *International Conference on Control, Automation and Systems 2008*, October 14–17, 2008, Seoul, Korea: pages 1290–1295.

[32] O. Diegel, A. Badve, G. Bright, J. Potgieter, and S. Tlale. "Improved mecanum wheel design for omni-directional robots". *Proceedings of the 2002 Australian Conference on Robotics and Automation*,Auckland, November 27–29, 2002: pages 117–121.

[33] J.B. Song, and K.S. Byun. "Design and Control of a Four Wheeled Omnidirectional Mobile Robot with Steerable Omnidirectional Wheels". *Journal of Robotic Systems*, v 21, n 4: pages 193–208, April, 2004.

[34] J.C. Alexaner, and J.H. Maddocks. "On the Kinematics of Wheeled Mobile Robots". *The International Journal of Robotics Research*, v8, n5, pp. 15–27, 1989.

[35] K.H. Low, and Y.P. Leow. "Kinematic Modeling, Mobility Analysis and Design of Wheeled Mobile Robots". *Advanced Robotics*, v19, pp. 73–99, 2005.

[36] H. Yu, S. Dubowsky, and A. Skwersky. "Omni-directional Mobility Using Active Split Offset Castors". *Proceedings of the 26th Biennial Mechanisms and Robotics Conf of the 2000 ASME Design Engineering Technical Conferences*, Sep 2000.

[37] R. Williams, D. Carter, P. Gallina, and G. Rosati. "Dynamics Model with Slip for Wheeled Omni-Directional Robots". *IEEE Transactions on Robotic and Automation*, v 18, n 3: pages 285–293, 2002.

[38] K. Saha, J. Angeles, and J. Darcovich. "The Design of Kinematically Isotropic Rolling Robots with Omnidirectional Wheels". *Mechanism and Machine Theory*, v30, n8, pp. 1127–1137, 1995.

[39] Y.P. Leow, K.H. Low, W.K Loh. "Kinematic Modelling and Analysis of Mobile Robots with Omni-Directional Wheels". *Proceedings of the 7th International Conference on Control, Automation, Robotics and Vision, ICARCV 2002*: pages 820–825, 2002.

[40] W.K Loh, K.H. Low, Y.P. Leow. "Mechatronics Design and Kinematics Modelling of a Singularityless Omni-Directional Wheeled Mobile Robot". *Proceedings - IEEE International Conference on Robotics and Automation*, v 3: pages 3237–3242, 2003.

[41] H. Asama, M. Sato, L. Bogoni, H. Kaetsu, A. Matsumoto, I. Endo. "Development of an Omni-Directional Mobile Robot with 3 DOF Decoupling Drive Mechanism". *Proceedings - IEEE International Conference on Robotics and Automation*: pages 1925–1930, 1995.

[42] R. Damoto, W. Cheng, and S. Hirose. "Holonomic Omni-Directional Vehicle with New Omni-Wheel Mechanism". *Proceedings of the 2001 IEEE International Conference on Robotics and Automation*: pages 773–778, May, 2001.

[43] N. Hushimi, M. Yamamoto, A. Mohri. "Two Wheels Caster Type Odometer for Omni-directional Vehicles". *Proceedings of the 2003 IEEE International Conference on Robotics and Automation*: pages 497–502, 2003.

[44] B.E. Ilon. "Wheels for a Course Stable Selfpropelling Vehicle Movable in any Desired Direction on the Ground or Some Other Base". *U.S. Patent and Trademark Office*: patent 3876255, 1975.

[45] J. Efendi, M. Salih, M. Rizon, S. Yaacob, A. Adom, M.R. Mamat. "Designing Omni-Directional Mobile Robot with Mecanum Wheel". *American Journal of Applied Sciences*, v3, n5, pages 1831–1835, 2006.

[46] A. Gfrerrer. "Geometry and Kinematics of the Mecanum Wheel". *Computer Aided Geometric Design*, v25, pages 748–791, 2008.

[47] N. Tlale, M. de Villiers. "Kinematics and Dynamics Modelling of a Mecanum Wheeled Mobile Robot". *15th International Conference on Mechatronics and Machine Vision in Practice*, pages 657–662, 2–4 Dec 2008.

[48] A. Shimada, S. Yajima, P. Viboonchaicheep, K. Samura. "Mecanum-wheel Vehicle Systems Based Position Corrective Control". *32nd Annual Conference of IEEE Industrial Electronics Society 2005*: pages 2077–2082, 2005.

[49] X. Gao, K. Li, Y. Wang, G. Men, D. Zhou, K. Kikuchi. "A Floor Cleaning Robot Using Swedish Wheels". *Proceedings of the 2007 IEEE International Conference on Robotics and Biomimetics* pages 2069–2073, Dec 15–18, 2007.

[50] X. Gao, Y. Wang, D. Zhou, K. Kikuchi. "Floor Cleaning Robot Using Omni-directional Wheels". *Industrial Robot: An Internationanl Journal*, v36, n2, pages 157–164, 2009.

[51] G. Indiveri. "Swedish Wheeled Omnidirectional Mobile Robots: Kinematics Analysis and Control". *IEEE Transactions on Robotics*, v25, n1, pages 164–171, Feb 2009.

[52] J. Angeles. "Fundamentals of Robotic Mechanical Systems: Theory, Methods, and Algorithms". *2nd ed. New York: Springer-Verlag, 2003.*

[53] J. Angeles. "Rational Kinematics". *New York: Springer-Verlag, 1988.*

[54] M. Stock, K. Miller. "Optimal Kinematic Design of Spatial Parallel Manipulators: Application to Linear Delta Robot". *Trans. of the ASME Journal of Mechanical Design*, v 125, n 2: pages 292–301, June 2003.

[55] A. Fattah, S.K. Agrawal. "On the Design of Cable-Suspended Planar Parallel Robots". *Trans. of the ASME Journal of Mechanical Design*, v 127, n 5: pages 1021–1028, September 2005.

[56] J.P. Merlet. "Jacobian, Manipulability, Condition Number, and Accuracy of Parallel Robots". *Trans. of the ASME Journal of Mechanical Design*, v 128, n 1: pages 199–206, January 2006.

[57] J. Denavit, and R. Hartenberg. "A kinematic notation for lower pair mechanisms based on matrices". *Journal of Applied Mechanics*: 22, pages 215–221, 1955.

[58] M.L. Husty. "An algorithm for solving the direct kinematics of general Stewart-Gough platforms". *Mechanisms and Machine Theory*: v31, n4, pages 365–380, 1996.

[59] M.J.D. Hayes, P.J. Zsombor-Murray, C. Chen. "Unified kinematic analysis of general planar parallel manipulators". *ASME Journal of Mechanical Design*: v26, n5, pages 866–874, 2004.

[60] C. Gosselin. "Determination of the Workspace of 6-DOF Parallel Manipulators". *ASME Journal of Mechanical Design*: v22, n3, pages 545–551, June 2006.

[61] G. Campion, G. Bastin, B. D'Andrea-Novel. "Structural properties and classification of kinematic and dynamic models of wheeled mobile robots". *IEEE Transactions on Robotics and Automation*, v 12, n 1: pages 47–62, 1993.

[62] A. Betourne, A. Fournier. "Kinematics, dynamics and control of a conventional wheeled omnidirectional mobile robot". *Conference Proceedings. 1993 International Conference on Systems, Man and Cybernetics. System Engineering in the Service of Humans*: v 2, pages 276–281, February, 1996.

[63] B.J. Yi, and W.K. Kim. "The Kinematics for redundantly actuated omnidirectional mobile robots". *Journal of Robotic Systems*: v 19, n 6, pages 255–267, June 2002.

[64] K. Kanjanawanishkul, and A. Zell. "Path following for an omnidirectional mobile robot based on model predictive control". *Proceedings - IEEE International Conference on Robotics and Automation*: Kobe, Japan, pages 3341–3346, May 12–17, 2009.

[65] K.S. Byun, S.J. Kim, and J.B. Song. "Design of a four-wheeled omnidirectional mobile robot with variable wheel arrangement mechanism". *Proceedings of the 2002 International Conference on Robotics and Automation*, Washington, DC, May, 2002.

[66] J.H. Ginsberg. "Advanced Engineering Dynamics". *New York: Harper & Row, 1988.*

[67] H. Baruh. "Analytical Dynamics". *McGraw-Hill, 1999.*

[68] D.T. Greenwood. "Principles of Dynamics". *2nd ed. Englewood Cliffs, NJ: Prentice-Hall, 1988.*

[69] J.I. Neimark, N.A. Fufaev. "Dynamics of Nonholonomic Systems". *Providemce, RI: American Mathematical Society, 1972.*

[70] A. Weiss, R.G. Langlois, and M.J.D. Hayes. "A Comparative Survey of the Dynamics of a Cylindrical Orienting Device Using an Omni-Directional Wheel". *Carleton University Applied Dynamics Lab Report ADL-10-AW-1, 2005.*

[71] R. Balakrishna, and A. Ghosal. "Modeling of Slip for Wheeled Mobile Robots". *IEEE International Transactions on Robotics and Automation*, v 11, n 1,: pages 126–132, Feb, 1995.

[72] S.S. Rao. "Mechanical Vibrations". *4th ed. Upper Saddle River, NJ: Pearson Prentice Hall, 2004.*

[73] A.A. Shabana. "Theory of Vibration - An Introduction". *2nd ed. New York: Springer-Verlag, 1996.*

[74] A.A. Shabana. "Vibration of Discrete and Continuous Systems". *2nd ed. New York: Springer-Verlag, 1997.*

[75] A.H. Nayfeh, D.T. Mook. "Nonlinear Oscillations". *New York: John Wiley & Sons, 1979.*

[76] K.L. Johnson. "Contact Mechanics". *New York: Cambridge University Press, 1985.*

[77] H. Hertz. "On the contact of elastic solids". *J. reine und angewandte Mathematik, 92*: pages 156–171, 1882.

[78] AirTrax Inc. "Airtrax". "www.airtrax.com". Last visited on Spetember 16, 2010.

[79] M. Wada. "Omnidirectional control of a four-wheeled drive mobile base for wheelchairs". *2005 IEEE Workshop on Advanced Robotics and its Social Impacts*: v2005, Pages 196–201, 2005.

[80] A.L. Schwab, and J.P. Meijaard. "How to Draw Euler Angles and Utilize Euler Parameters". *Proceedings of ASME IDETC/CIE 2006*: September 10-13, 2006.

[81] A. Weiss, R.G. Langlois, and M.J.D. Hayes. "The Effects of Dual-Row Omnidirectional Wheels on the Kinematics of the Atlas Spherical Motion Platform". *Journal of Mechanism and Machine Theory*, v 44, n 2: pages 349–358 February 2009.

[82] M.J.D. Hayes, R.G. Langlois, and A. Weiss. "Atlas Motion Platform Generalized Kinematic Model". *Meccanica*, accepted 2010.

[83] M.J.D. Hayes, R.G. Langlois, and A. Weiss. "Atlas Motion Platform Generalized Kinematic Model". *Proceedings of the Second International Workshop on Fundamental Issues and Future Research Directions for Parallel Mechanisms and Manipulators*, September 21–22 2008, Montpellier, France.

[84] A. Weiss, M.J.D. Hayes, and R.G. Langlois. "Kinematics of an Atlas Platform with Redundant Contact Points". *2008 CSME Symposium on Machines, Mechanisms and Mechatronics*, on CD, Ottawa, Canada, June 2008.

[85] A. Weiss, R.G. Langlois, and M.J.D. Hayes. "Unified Treatment of the Kinematic Interface Between a Sphere and Omnidirectional Wheel Actuators". *ASME Journal of Robotics*, conditionally accepted, 2009.

[86] J.B. Holland, M.J.D. Hayes, and R.G. Langlois. "A Slip Model for the Spherical Actuation of the Atlas Motion Platform". *2005 CSME Symposium on Machines, Mechanisms and Mechtronics,* Canadian Space Agency, On CD, May 26-27, 2005.

[87] J. Arnada, A. Grau and J. Climent. "Control Architecture for a Three-wheeled Roller Robot". *International Workshop on Advanced Motion Control*, AMC, 1998: pages 518–523.

[88] H. Yu, M. Spenko, and S. Dubowsky. "Omni-Directional Mobility Using Active Split Offset Castors". *Journal of Mechanical Design, Transactions of the ASME*, v 126, n 5, September, 2004: pages 822–829.

[89] AndyMark Inc. "http://lib.store.yahoo.net/lib/yhst-33833170891817/6-alum-omni-asm.pdf". Last visited on September 16, 2010.

[90] AndyMark Inc. "http://lib.store.yahoo.net/lib/yhst-33833170891817/6-mecanum-asm.pdf". Last visited on September 16, 2010.